THE UNIVERSITY OF CHICAGO

DEFINING ANTIBODY IMMUNODOMINANCE TO PANDEMIC-THREAT VIRUSES IN HUMANS

A DISSERTATION SUBMITTED TO
THE FACULTY OF THE DIVISION OF THE BIOLOGICAL SCIENCES
AND THE PRITZKER SCHOOL OF MEDICINE
IN CANDIDACY FOR THE DEGREE OF
DOCTOR OF PHILOSOPHY

COMMITTEE ON IMMUNOLOGY

BY
HALEY DUGAN

CHICAGO, ILLINOIS
JUNE 2021

CONTENTS

LIST OF FIGURES

LIST OF TABLES

ABSTRACT

B cell immunodominance is defined as the hierarchical antibody response to distinct antigenic proteins found in pathogens. Various factors shape the preference of antibody targeting to certain viral epitopes over others, including preexisting immunity, age, sex, and disease severity. Our understanding of human antibody immunodominance to conserved antigenic sites of viruses is limited, despite its importance for developing universal vaccines that protect against pandemic-threat viruses such as influenza and SARS-CoV-2. The ability of these viruses to rapidly mutate, re-circulate seasonally, and pose the threat of future deadly pandemics necessitates a better understanding of human antibody immunodominance to conserved and protective antigenic sites. In this work, we utilized monoclonal antibody (mAb) technology, single-cell RNA sequencing approaches, and *in vivo* infection challenge studies to dissect human antibody immunodominance and protective responses to influenza and SARS-CoV-2 viruses. We reveal that natural infection induces a considerable antibody response to non-neutralizing viral targets, shaped by factors such as age, preexisting immunity, and disease severity. This work has implications for epitope-guided universal vaccine design for two distinct viruses, one century-old and the other completely novel. Finally, our study stresses the importance of considering host-intrinsic factors such as preexisting immunity and age in the design of next generation vaccination strategies.

CHAPTER 1

INTRODUCTION

1.1 Human antibody responses to viruses

Antibodies serve as a critical arsenal against viral infection. Antibodies simultaneously alert the immune system to the presence of invading pathogens and directly interfere with viral entry into host cells. In individuals who are capable of mounting successful immune responses, anti-viral antibodies can provide highly specific and long-lasting protection from future viral insults. Our understanding of antibodies and their ability to protect against pathogens has been continually evolving and improving since the late 1800s, when it was first discovered that serum from infected animals could be used to prevent infection in other animals(*1*).

Despite a long history of technological and intellectual advances in antibody and vaccine science, effective vaccines for persistent viral threats such as influenza virus are still needed. Recently, the emergence of pandemic coronavirus SARS-CoV-2 and recent variants that escape vaccine-mediated immunity have further emphasized the importance of investigating barriers to protective humoral immunity. In order to understand challenges facing the development of effective anti-viral vaccines and therapeutics against influenza virus and SARS-CoV-2, one must first understand factors that shape the generation of B cell responses to complex pathogens.

1.1.1 Generation of antigen-specific B cell memory

One of the hallmarks of our immune system is the ability to generate long-lived pathogen-specific memory cells, including memory B cells (MBC) and plasma cells (PC). In essence, memory cells formed upon infection or vaccination should provide protection from future infection with the same pathogen. The success of vaccine platforms is dependent on the generation of durable memory cells with high affinity and neutralizing activity against

pathogens. As a result, understanding the generation and maintenance of B cell memory is a key area of focus for the vaccine research community.

MBCs, PCs, and short-lived antibody secreting cells (ASC) with high specificity for pathogens are the product of antigen activation and affinity maturation in the germinal center (GC; Figure 1.1)(*2*). The GC is a specialized microanatomical structure that forms in secondary lymphoid tissues upon infection or vaccination. It is divided into two distinct compartments: the dark zone, which is the site of B cell proliferation and somatic hypermutation (SHM), and the light zone, where B cells capture antigen presented on follicular dendritic cells (FDC) for presentation to T follicular helper cells (T_{FH}) in order to undergo selection. The process of SHM allows B cells to generate mutations in their variable heavy and light chain genes, producing high affinity B cell receptors (BCR) specific to the pathogen in question. Only B cells with sufficient affinity will be selected to exit the GC as MBCs, PCs, or ASCs.

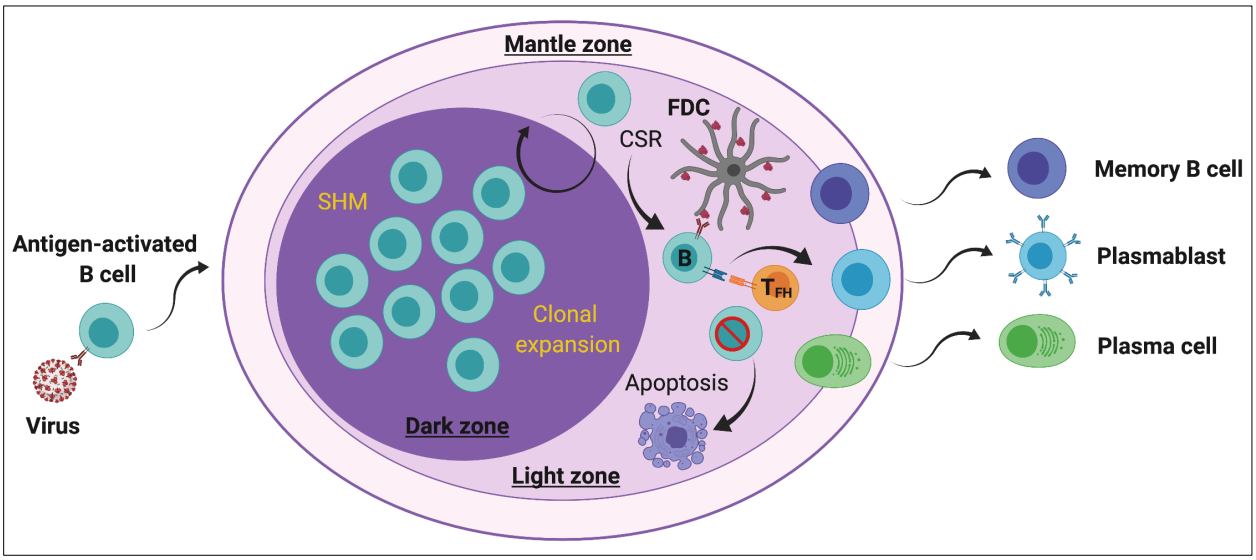

Figure 1.1. The germinal center reaction. Antigen-activated naïve B cells initiate the germinal center (GC) reaction, where they differentiate into centroblasts and undergo clonal expansion and somatic hypermutation (SHM) in the dark zone. The process of SHM increases antibody affinity for antigen by introducing base-pair changes into the variable region of the immunoglobulin heavy and light chain genes. Centroblasts then differentiate into centrocytes and move to the light zone, where the modified antigen receptor is tested for affinity with help from T follicular helper (T_{FH}) cells and follicular dendritic cells (FDC). B cells bearing low affinity or autoreactive receptors undergo apoptosis. B cells then continue to undergo iterative rounds of SHM in the dark zone and selection in the light zone, whereby the highest affinity contenders can then exit the GC as memory B cells or plasma cells. Within the light zone, a subset of B cells can undergo class-switch recombination (CSR) to generate receptor isotypes that can interact with immune cells in different inflammatory contexts. Created with BioRender.com.

The decision of a GC B cell to commit to the MBC, PC, or ASC fate is contingent upon multiple factors: precursor affinity, transcription factor expression, strength of interaction with T_{FH}, and immunoglobulin (Ig) isotype(*3*). Well-appreciated in the field, newly activated B cells with high affinity for pathogen are poised to differentiate into short-lived extrafollicular ASCs(*4*). Similarly, preexisting high affinity MBCs can rapidly differentiate into ASCs upon pathogen re-encounter, independent of GC re-entry. B cells with lower affinity are more prone to differentiate into MBCs, and high affinity B cells in the GC often differentiate into ASCs or PCs(*5, 6*).

The characterization of transcription factors governing distinct MBC subsets in humans has not been completely elucidated, and much of what is understood regarding B cell subset identity is derived from studies in mice. However, previous work has defined putative transcriptional regulators of MBC fate, including CD27, ZBTB32, KLF2, ABF-1, STAT5, BACH2, and POU2AF1(*7-15*). Master transcription factors that regulate PC fate are clearer, including IRF4, Blimp-1, and CD38 (*2, 16, 17*). It is also well-established that Ig isotype can regulate the MBC versus PC fate. B cells that have class-switched to IgG, IgE, or IgA are more likely to differentiate to PCs than MBCs, and distinct subsets of somatically mutated IgM MBCs also exist in humans(*18-24*). Finally, high affinity B cells display enhanced endocytosis and presentation of antigen, resulting in stronger and longer interactions with T_{FH}. This ultimately leads to an increase in IRF4 expression and generation of PC precursors over the MBC fate(*25*).

In summary, MBCs, PCs, and ASCs are highly specialized to provide protective re-call responses to previously encountered pathogens and are thus key to the success of vaccination platforms. Much remains to be discovered regarding the generation of protective B cell subsets to distinct pathogens in humans, and how diverse antigen-specific BCR repertoires can protect against infection. The studies on B cell responses to SARS-CoV-2 infection herein provide a unique opportunity to gain insight into these issues, as we delineate B cell subsets induced by a completely novel viral infection in humans.

1.1.2 B cell immunodominance to viruses

The generation of the antigen-specific BCR repertoire is a highly efficient process; yet is limited by various factors shaping B cell immunodominance. Immunodominance describes the hierarchical landscape of viral epitopes that can be preferentially targeted by antibodies, and is shaped by antigen accessibility, precursor frequency, preexisting immunity, genetics, microbiome, and age (Figure 1.2)(*26*). Understanding B cell immunodominance to pathogens that pose a significant global health threat, including influenza and SARS-CoV-2 virus, is critical for designing vaccines that induce antibody responses to evolutionarily conserved and protective antigenic sites.

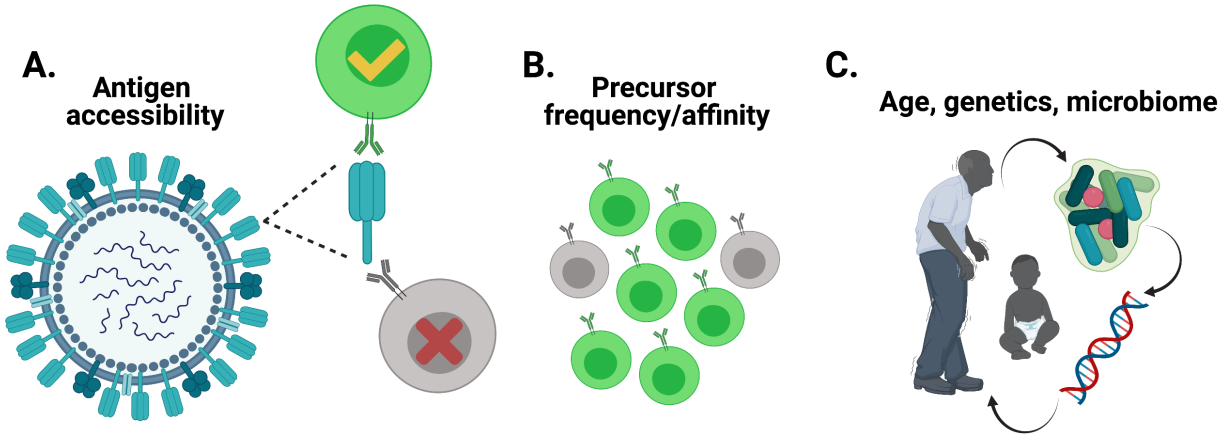

Figure 1.2. Proposed factors shaping B cell immunodominance to viruses. Immunodominant phenotypes are shown in green and subdominant phenotypes are shown in gray. (**A**) Immunodominance is favored by accessibility of surface-exposed viral epitopes, and unfavored when viral epitopes are sterically inaccessible (i.e.; membrane-embedded). (**B**) Immunodominance is favored by high naïve B cell precursor frequency and affinity, which allows for selective activation and increased antigen presentation to T follicular helper cells to obtain maximal help. Precursor frequency itself can be shaped by various factors, including preexisting immunity and individual variation in B cell repertoire. (C) Lastly, immunodominance can be shaped by other factors such as age, microbiome, and genetics. Created with BioRender.com.

For rapidly evolving pathogens such as influenza virus, antigenically variable viral epitopes on major surface glycoproteins are typically the most immunodominant targets of antibodies. This is largely owed to their surface accessibility, a major prerequisite for effective antibody targeting. Unfortunately, these epitopes are under constant immune pressure to rapidly mutate and escape host immunity, resulting in a continual arms race between human antibody responses and viruses. The development of universal vaccines and therapeutics

therefore relies on the discovery of conserved viral epitopes, particularly antigenic regions that are both neutralizing and feasible targets for antibodies.

Discouragingly, many conserved viral epitopes of viruses are immunosubdominant, such as the membrane-embedded stalk region of the influenza virus hemagglutinin (HA) and the stem of the SARS-CoV-2 spike protein (S2 domain). Immunosubdominance of these regions is predominantly shaped by inaccessibility, steric restraints imposed on antibodies to access them, or poor immunogenicity (*27, 28*). In addition, previous exposures to viruses may result in circulating serum antibodies that can bind to and mask available epitopes on current challenging strains (*29-31*). Antibody responses to conserved yet immunosubdominant regions can be boosted in humans upon secondary exposure to antigenically distinct viruses that are of the same family and that bear a high degree of homology. For example, antibody responses to conserved epitopes in the SARS-CoV-2 S2 domain are boosted in subjects that were exposed to SARS-CoV-1, and several reports suggest preexisting immunity to endemic common cold coronaviruses (HCoV) results in cross-reactive antibody responses upon SARS-CoV-2 infection (*32-34*). Similarly, preexisting immunity to influenza H1N1 resulted in the expansion of HA stalk-specific B cells upon exposure to the novel 2009 H1N1 pandemic virus(*35-38*). Current universal vaccination and therapeutic platforms for influenza are aimed at investigating antibody generation against conserved, neutralizing viral epitopes, particularly on the HA head and stalk(*33, 39-43*).

Dissecting how factors such as age and preexisting immunity shape antibody immunodominance to these epitopes is therefore a high priority for designing effective universal vaccines and therapies. Such interventions would be capable of protecting against antigenically variable and pandemic-threat pathogens such as influenza virus and SARS-CoV-2, which have had devastating global impacts over the last century. In this work, we dissect B cell immunodominance to influenza and SARS-CoV-2 viruses, providing key insights into how distinct host factors shape protective antibody responses in humans.

1.1.3 Epitope-guided design of vaccines and antibody therapeutics

Investigating viral epitope targeting by recombinant monoclonal antibody (mAb) technology represents a promising avenue for informing the design of vaccines and therapeutics. MAbs are monovalent proteins expressed by B cells that can precisely target 3-dimensional epitopes, and can be generated *in vitro* from single B cells(*44*). MAbs have revolutionized modern healthcare by providing precision medicine against many diseases, and there are currently over 70 Food and Drug Administration-approved mAb-based drugs. MAbs can target specific immunological pathways to help eliminate cancer (*45, 46*), and limit aberrant immune responses during autoimmunity and transplantation (*47-49*). Additionally, mAbs have prophylactic and therapeutic potential for preventing and limiting infection with highly variable pathogens such as human immunodeficiency virus (HIV-1), influenza virus, and coronavirus, and importantly, can guide rational vaccine design (*50-55*).

The concept that antibodies can guide vaccine design has been deemed "reverse vaccinology", or "epitope-focused vaccinology"(*56, 57*). Advances in the characterization of mAbs against various pathogens have led to the identification of promising vaccine antigens, and reciprocally, a deeper understanding of desirable antibody responses elicited by vaccination(*58-60*). In particular, the identification of broadly neutralizing antibodies (bnAbs) against conserved viral epitopes has set the stage for investigating vaccine candidates that induce robust antibody responses to these epitopes.

In the case of rapidly evolving and persistent pathogens such as influenza and SARS-CoV-2 viruses, understanding factors that shape antibody immunodominance to conserved epitopes will be paramount for informing effective vaccination strategies. In this work, two approaches are presented that dissect human antibody immunodominance patterns to influenza (Chapter 2) and SARS-CoV-2 (Chapter 3) viruses. In both studies, we utilize recombinant mAb technology to understand viral epitope targeting by antibodies, and how specificity correlates with antibody neutralization and protection from infection.

1.2 Influenza Viruses

1.2.1 Antibody responses to influenza viruses

Influenza viruses are enveloped, single-stranded RNA viruses responsible for over 5 million severe cases of respiratory tract infection and 650,000 deaths globally each year (*61*) (Figure 1.3). In the United States alone, influenza imposes an annual economic burden of over 11 billion dollars(*62*), and the emergence of another pandemic could cost up to 45 billion dollars(*63*). Due to the massive global health and economic burdens imposed by influenza viruses, it is a high priority to develop effective vaccines.

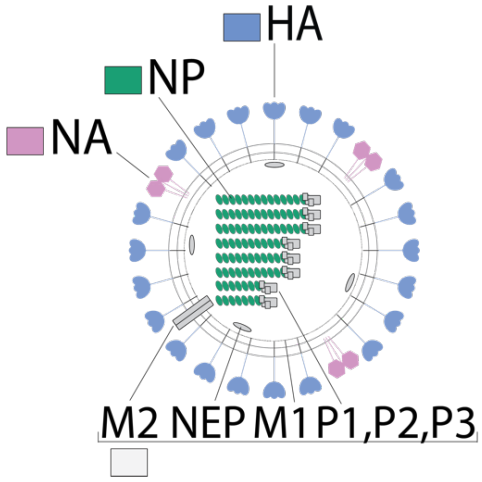

Figure 1.3 Influenza virion.

There are three types of influenza viruses capable of infecting humans: influenza A, B, and C, which are categorized based on their highly conserved internal proteins: matrix protein 1 (M1), membrane matrix protein (M2), and nucleoprotein (NP). Influenza also harbors other conserved structural and accessory proteins, including nuclear export protein (NEP) and polymerase proteins 1–3 (P1–P3). Influenza A and B viruses currently circulate and are responsible for causing seasonal epidemics. Influenza A viruses (IAV) are further divided into subtypes based on the amino acid sequence of the major surface glycoproteins hemagglutinin (HA) and neuraminidase (NA). Influenza subtypes are classified into two groups: group 1 and group 2, and the primary group 1 and group 2 viruses that infect humans each year are H1N1 and H3N2, respectively. Influenza B viruses are not divided into subtypes, and are rather divided into two distinct lineages, B/Yamagata and B/Victoria(*64*).

The HA and NA proteins of influenza are highly immunogenic and are the key targets of current vaccination platforms(*64*). HA is a trimeric glycoprotein divided into two domains: the head and the stalk. The immunodominant globular head region of the HA protein enables the virus to enter host cells through the binding of sialic acids on epithelial cells of the respiratory tract. The sialic acid receptor binding site (RBS) on the HA head is highly

conserved, though most other regions on the globular head are poorly conserved(*65, 66*). Antibodies elicited against the HA head inhibit receptor binding to sialic acid, referred to as hemagglutination inhibition (HAI)(*65, 67*). The highly conserved but immunosubdominant HA stalk functions to mediate viral membrane fusion and cell entry, and antibodies against the stalk limit viral membrane fusion(*68, 69*). The conservation of the HA stalk domain is likely the result of its importance to viral fitness, and the fact that antibody responses against it are more rare. Therefore, there is less immune pressure on the HA stalk domain to mutate.

NA is a tetrameric glycoprotein responsible for cleaving sialic acids on host cells, allowing viral particles to bud from and infect neighboring cells(*70*). The active site of NA and regions within close proximity to it are highly conserved, while other epitopes undergo antigenic drift albeit at a slower and more discordant rate than HA(*71-73*). Antibodies specific for NA limit the spread of viral infection to neighboring host cells and are important for preventing disease severity and transmission(*74, 75*). Neutralizing antibodies targeting NA are primarily induced by natural infection, and current seasonal vaccines fail to elicit protective NA-specific antibodies due to insufficient antigen quality and quantity(*50, 70, 76*).

Finally, antibody responses to influenza virus NP are also prevalent upon infection, and to a lesser extent, vaccination(*77, 78*). NP is a highly abundant conserved internal protein that encapsulates the viral RNA genome. Because NP is an internal viral protein, it is unclear whether antibodies against it neutralize or provide protection from infection. Some studies have shown that anti-NP antibodies possess Fc receptor-dependent functions, including antibody-dependent cellular cytotoxicity (ADCC)(*79*). However, future studies are warranted to fully understand whether and how anti-NP antibodies provide protection from influenza.

While anti-HA and anti-NA antibodies are known to be protective, the HA and NA antigens are also more susceptible to mutation. The gradual mutation of HA and NA epitopes that occurs seasonally is referred to as antigenic drift, which results from immune pressure and point mutations introduced by the error prone viral RNA-dependent RNA polymerase(*80, 81*). Drift allows the virus to escape the host immune response and is responsible for seasonal epidemics, as humans have no preexisting immunity to these drifted

influenza variants. The genetic re-assortment of different influenza viruses causes antigenic shift, which results in the generation of completely novel viruses responsible for pandemics(*82*). Immunity to drifted and shifted influenza strains relies strongly on antigen-specific B cells, which have the ability to rapidly mutate their BCRs to generate high affinity antibodies against influenza antigens(*83*). Thus, a key goal of current influenza vaccination strategies is to elicit high affinity HA- and NA-specific antibodies that can neutralize and clear virus.

1.2.2 Current influenza virus vaccination platforms

Due to the vast diversity of influenza viruses and their ability to rapidly mutate, new seasonal vaccines must be generated each year to help protect susceptible individuals from infection. According to the Centers for Disease Control and Prevention, adults 65 years of age and older, children under 5 years of age, and immunocompromised individuals are most susceptible to infection, however, thousands of healthy young adults are infected each year.

A primary goal of seasonal influenza virus vaccination is to induce antibodies capable of rapid clearance and neutralization of the virus upon exposure. Seasonal vaccines are composed of either inactivated or live-attenuated viruses, and are predominantly formulated to be quadrivalent with one H1N1 strain, one H3N2 strain, and two influenza B lineage strains. Influenza vaccines can either be produced in eggs or in insect cells, but recent research suggests that vaccines grown in eggs may acquire mutations that impact antibody binding (*84*). While seasonal vaccination decreases influenza virus infection burdens, vaccine effectiveness is low at an estimated 45% for the 2019–2020 season. Notably, vaccine effectiveness varies by influenza type, and is typically most effective for influenza B viruses, followed by H1N1 IAV, and finally, H3N2 IAV (*85*). Current annual vaccination largely induces strain-specific antibody responses toward the HA head with little cross-reactivity to drifted viruses, which is of major concern due to the high likelihood of false predictions of seasonally circulating strains(*86, 87*). It is consequently a high priority to develop a universal influenza vaccine that is capable of providing protection against all drifted influenza viruses

an individual may encounter. Such a vaccine could prevent the need for annually updating and administering seasonal vaccines, and provide protection against newly emerging pandemic viruses.

One avenue of universal vaccine development is aimed at eliciting neutralizing antibody responses against conserved regions of viral proteins(*88-90*). In particular, recent universal influenza vaccine trial initiatives have focused on inducing antibody responses to the conserved HA stalk region through headless HA stem constructs or chimeric HA antigens (*39, 40, 91*). Unfortunately, antibody responses to the HA stalk region are immunosubdominant, posing a challenge for vaccination in inducing protective levels of HA stalk antibodies(*27, 92*). Other conserved epitopes of the HA head represent potently neutralizing targets, such as the RBS and lateral patch(*93-96*). Further characterization of broadly neutralizing viral epitopes of influenza viruses and factors enabling or hindering antibody responses against them will be imperative for informing future universal influenza virus vaccination strategies.

1.2.3 Impact of preexisting immunity and age on antibody responses to influenza

One of the greatest factors shaping protective antibody responses to conserved influenza virus epitopes in humans is preexisting immunity. Adults are exposed to influenza viruses repeatedly over the course of a lifetime, and therefore the majority of B cells activated in response to seasonal infection and vaccination are largely derived from preexisting immune memory (*35-37, 97-104*). As a result, *de novo* generation of antibodies specific for drifted antigens on influenza viruses is limited by the preexisting immune memory bias of the individual. Through a process called epitope masking, high preexisting serological antibody levels against strains from prior exposures can mask or prevent access to protective surface accessible epitopes on HA and NA, further limiting the generation of antibodies specific for drifted epitopes(*31*). Moreover, the response kinetics of preexisting high affinity MBCs outcompetes that of naïve B cells due to their comparatively lower activation threshold, further hindering *de novo* B cell responses to drifted epitopes(*105-107*).

The ability of an individual's first influenza virus exposure to bias the response during subsequent exposures was first described in the 1950s and coined, 'original antigenic sin' (OAS; Figure 1.4)(*97*). This observation was based on antibody patterns observed in baseline sera collected from cohorts of different age groups, as well as age-associated differences in antibody responses to vaccination. It was discovered that individuals had high serum titers to influenza strains that circulated during childhood, and that later in life vaccination elicited cross-reactive antibodies to childhood strains.

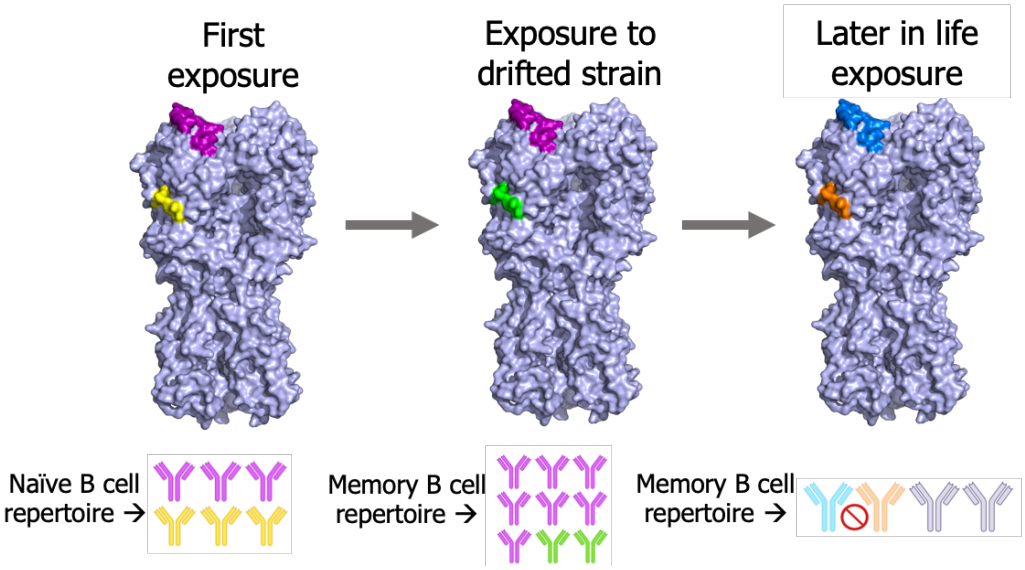

Figure 1.4. Effects of original antigenic sin on antibody adaptability. Influenza virus hemagglutinin proteins are depicted, with the colored regions representing antigenically variable viral epitopes. First exposure to influenza virus in childhood (strain 1) results in a *de novo* antibody response to unique epitopes presented in strain 1 (pink and yellow). Upon secondary exposure to a drifted strain in a following year, whereby the yellow epitope has mutated to green, the antibody response will derive from preexisting memory to the pink epitope conserved with strain 1. In a third exposure to strain 3 later in life, if both epitopes have now mutated, the individual will further rely on preexisting immunity to various shared epitopes across strains from past exposures (gray). Protective outcome will be determined by whether the conserved (gray) epitopes are neutralizing.

The phenomenon of OAS was assigned the negative interpretation as 'sin', because it was expected that protective antibody responses against subsequent encounters to antigenically drifted strains would be suppressed. However, several studies that followed have challenged this notion and confirmed that secondary exposures boost cross-reactive

responses to epitopes shared with strains previously encountered, but are not necessarily strongest to or specific for strains encountered in childhood(*35-38, 99, 102*). Studies have since more accurately described the theory of OAS as 'antigenic imprinting', or 'seniority', which accounts for the effects of cumulative exposures by infection and vaccination on driving the generation of cross-reactive antibodies (*108, 109*) Antigenic imprinting posits that primary exposures are indeed important for generating an individual's first MBC lineages against influenza, but that those MBCs can undergo continued affinity maturation upon re-call by subsequent exposures. Consequently, a hierarchy of influenza antigen exposures over time will shape MBC specificity, contradicting the idea that B cells specific for early childhood strains will always dominate later in life. In support of this, it was shown that individuals born in 1957 were more likely to be infected with a drifted seasonal variant of H1N1 in 2013 due to preexisting immunity to seasonal H1N1 strains that circulated after 1977, which were not experienced until around the age of 20(*101*).

This revised concept of imprinting also accounts for both the positive and negative effects of past exposures on protective immune responses to influenza. For example, studies suggest that imprinting can be protective when individuals are exposed to the same subtype as they first encountered in childhood(*98, 99, 103, 109*). Older adults who did not succumb to infection during the 2009 pandemic had preexisting cross-reactive antibody titers against the 2009 pandemic H1N1 virus, presumably because H1N1 was the only IAV subtype in circulation between 1918 and 1957(*98, 99*). More recently, population cohort studies using computational modeling approaches have identified that childhood imprinting subtype predicts susceptibility to avian influenza as well as H1N1 and H3N2(*103, 109*). Although a mechanism has never been fully addressed, the boosting of antibodies specific for conserved non-protective viral epitopes may explain susceptibility to infection with subtypes that differ from the original imprinting strain. Conversely, the boosting of antibodies to conserved protective viral epitopes may underlie protective imprinting responses.

To understand how effective targeting of conserved neutralizing viral epitopes of influenza can be achieved, understanding mechanisms of imprinting responses in influenza

naïve populations and populations with prior exposure will be paramount. In this study, we assessed how influenza virus infection and vaccination differentially recall preexisting MBCs in adults, providing an in-depth assessment of how preexisting immunity shapes antibody immunodominance patterns upon different routes of viral exposure.

1.3 Severe acute respiratory syndrome coronavirus 2

1.3.1 Emergence of the COVID-19 pandemic

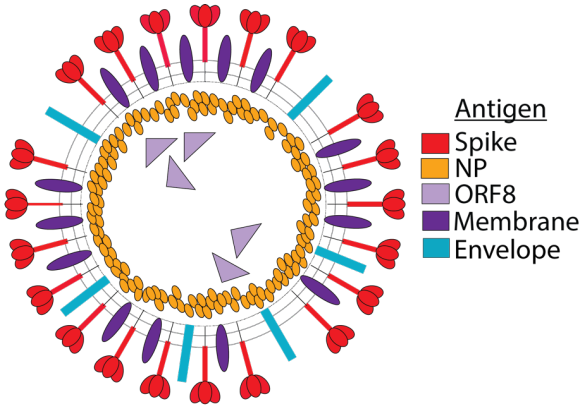

Figure 1.5 SARS-CoV-2 virion.

Coronaviruses are enveloped non-segmented single stranded RNA viruses belonging to the family *Coronaviridae* and circulate broadly amongst humans and other mammals(*110*). Over the past two decades, two betacoronaviruses, severe acute respiratory syndrome coronavirus 1 (SARS-CoV-1) and Middle East respiratory syndrome coronavirus (MERS-CoV), were responsible for over 10,000 cases of infection. The mortality rate of SARS-CoV-1 was 10% with 29 countries affected, and the mortality rate of MERS-CoV was 35% with 27 countries affected globally(*111*). As a result, the emergence of novel coronaviruses has become a major concern in the 21st century(*110*).

In December of 2019, a novel coronavirus (SARS-CoV-2) was discovered through deep sequencing analysis after a series of pneumonia cases were reported in Wuhan, Hubei, China with unknown viral origin (Figure 1.5)(*112*). Several independent studies have since confirmed that the novel virus originated from exposures in a Wuhan seafood market, and have dubbed SARS-CoV-2 as the causative agent of 'COVID-19' disease(*113*). Extremely transmissible, the World Health Organization has reported 160 million COVID-19 infections worldwide, and spread to almost every global country in the course of one year. Even more threatening, SARS-CoV-2 has been mutating since it was first sequenced, and there are currently four substrains and eleven prominently circulating mutated variants in the

United States(*114*). Several characterized mAbs with potent neutralization activity against the Wuhan variant have lost binding and neutralizing ability against circulating variants, emphasizing the ability of SARS-CoV-2 to undergo rapid viral escape(*115-117*). In the face of persistent antigenic evolution, the development of pan-coronavirus vaccines and mAb therapeutics targeting conserved viral epitopes is critical.

Since the identification of SARS-CoV-2, the scientific community has led the development of over 60 vaccination platforms in Phase III clinical trials(*118*). Currently, mRNA- and adenovirus vector-based vaccines designed to induce neutralizing antibody responses against the SARS-CoV-2 spike glycoprotein are approved and being mass-administered to the general population(*119-123*). The receptor binding domain (RBD) of the spike glycoprotein is the major target of current vaccination platforms, as it is the key region responsible for binding the ACE2 receptor on epithelial cells, serving as the primary step for viral entry(*124, 125*). In addition to the development of vaccines, multiple groups have utilized mAb technology for the development of therapeutics and diagnostics(*41, 126-128*). Despite these advances, our understanding of the human immune response to SARS-CoV-2 remains extremely limited. Moreover, it remains unclear whether current vaccines will provide sufficient protection against SARS-CoV-2 variants. The characterization of MBC responses, antibody immunodominance patterns, and conserved protective viral epitopes is thus vital for the design of vaccines and therapies that can end the COVID-19 pandemic and prevent future coronavirus pandemics on the horizon.

1.3.2 Antibody responses to SARS-CoV-2

Since the beginning of the COVID-19 pandemic, there have been massive strides in our understanding of protective B cell-mediated immunity to SARS-CoV-2. Early in the pandemic, initial studies characterizing serum antibody responses to SARS-CoV-2 revealed that serum titers waned over time in infected individuals, raising the concern that durable immunity would be difficult to achieve(*129-131*). Several studies that followed identified the generation of durable MBCs against the spike protein, which persist and evolve over a time

period of at least 6–8 months(*132-135*). While promising, several reports suggest that serum antibody responses to distinct targets including the spike protein, internal nucleocapsid protein (NP), and open reading frame protein 8 (ORF8) correlate with increased disease severity, and it remains unclear how antibody specificity and quantity directly relate to disease pathogenesis (*136-141*). In addition, some studies report atypical MBC responses and impaired GC formation in severe SARS-CoV-2, and it is poorly understood how these responses contribute to protection (*142-144*). Finally, several reports suggest that factors such as preexisting immunity, age, and biological sex impact protective responses to SARS-CoV-2, which are highlighted below.

1.3.3 Impact of host factors on the antibody response to SARS-CoV-2

Like influenza, preexisting immunity also shapes antibody responses to SARS-CoV-2. The phenomenon of original antigenic sin has been described for viruses that are endemic and cause recurrent infections, most notably influenza virus and dengue virus (*108, 145-148*). As data continue to accumulate on characterization of SARS-CoV-2 T and B cell responses in humans, it has been identified that humans possess preexisting immunity to SARS-CoV-2 due to prior exposures to SARS-CoV-1 or other endemic HCoV(*33, 149-153*).

HCoV re-circulate seasonally and cause the common cold, and include betacoronaviruses HKU1 and OC43 and the alphacoronaviruses 229E and NL63(*154*). SARS-CoV-2 is classified as a betacoronavirus and shares more homology with HKU1 and OC43 than to alphacoronaviruses(*154, 155*). It remains unclear whether previous HCoV immunity can prevent or alter the course of SARS-CoV-2 infection, though some reports suggest that cross-reactive antibodies are not associated with protection (*149*). Moreover, some studies have identified that antibodies cross-reactive with SARS-CoV-1 and SARS-CoV-2 are predominantly non-neutralizing, suggesting they target conserved but non-protective antigenic sites. It is currently unknown whether cross-reactive original antigenic sin-like antibodies induced by SARS-CoV-2 infection lead can lead to antibody dependent enhancement of disease, which has been described in the case of dengue and Zika virus

infections(*148, 156*). Finally, there are conflicting results on whether age and birth year impact SARS-CoV-2 immunity based on prior HCoV exposure. One study suggested there are no major differences in serum antibody titers to HCoV strains based on age (*157*). While this group saw no differences, children generally experience higher rates of HCoV infections and other studies suggest that children are more likely to possess cross-reactive antibodies as a result(*152*). It remains unknown whether this directly impacts the distribution of SARS-CoV-2 cases by age.

Beyond preexisting immunity, age is likely to have a profound impact on the generation of protective immune responses to SARS-CoV-2 due to immunosenescence. Immunosenescence is defined as the progressive deterioration of the immune system with aging. Immunosenescence stifles the generation of protective B and T cell-mediated adaptive immunity in response to various pathogens, resulting in increased disease susceptibility and severity in the elderly population(*158*). Elderly individuals greater than sixty years of age have been disproportionately affected by COVID-19, with high rates of both morbidity and mortality in this group (*159*). Aged individuals are at higher risk for co-morbidities, which have been tied to increased incidence and severity of COVID-19. Moreover, immunosenescence results in thymic involution and reduced output of mature T cells, reduced B cell adaptation, reduced germinal center formation, and increased pro-inflammatory responses to pathogens(*160*). To date, little is known regarding the impact of aging on B cell responses to SARS-CoV-2. Preliminary reports suggest that elderly individuals possess increased serum antibody titers to spike as well as non-neutralizing internal targets such as NP (*136, 161*). These results are consistent with studies of influenza in the elderly, who mount antibody responses to internal targets and fail to adapt their B cell responses efficiently with age(*72*). Further studies are required to address differences in B cell specificities and subsets with age in COVID-19.

Finally, there are several reported effects of biological sex on the generation of antibody responses to SARS-CoV-2. Men have been identified to have more severe infection and higher antibody titers than women (*136, 161*). However, antibody titers have been

observed to decline more rapidly in men than in women (*162*). Mechanisms of sex-based differences in antibody responses to SARS-CoV-2 and how they impact susceptibility and severity remain to be addressed.

In summary, several factors can shape protective antibody responses to both influenza and SARS-CoV-2 viruses. In this work, we aimed to address how factors such as preexisting immunity, age, and sex impact B cell immunodominance and protective antibody responses to influenza (Chapter 2) and SARS-CoV-2 (Chapter 3) through the characterization of mAbs and MBCs in distinct infection and vaccination cohorts.

CHAPTER 2

PREEXISTING IMMUNITY SHAPES DISTINCT ANTIBODY LANDSCAPES AFTER INFLUENZA VIRUS INFECTION AND VACCINATION IN HUMANS

Haley L. Dugan[1,†], Jenna J. Guthmiller[2,†], Philip Arevalo[3], Min Huang[2], Yao-Qing Chen[2], Karlynn E. Neu[1], Carole Henry[2,#a], Nai-Ying Zheng[2], Linda Yu-Ling Lan[1], Micah E. Tepora[2], Olivia Stovicek[2], Dalia Bitar[2], Anna-Karin E. Palm[2], Christopher T. Stamper[1], Siriruk Changrob[2], Henry A. Utset[2], Lynda Coughlan[4,#b], Florian Krammer[4], Sarah Cobey[3], Patrick C. Wilson[1,2*]

[1]Committee on Immunology, University of Chicago, Chicago, IL 60637, USA.

[2]Department of Medicine, Section of Rheumatology, University of Chicago, Chicago, IL 60637, USA.

[3]Department of Ecology and Evolution, University of Chicago, Chicago, IL 60637, USA.

[4]Department of Microbiology, Icahn School of Medicine at Mount Sinai, New York, NY 10029, USA.

[†]These authors contributed equally.

[#a]Current address: Moderna Inc., Cambridge, MA 02139, USA.

[#b]Current address: University of Maryland School of Medicine, Department of Microbiology and Immunology and Center for Vaccine Development and Global Health, Baltimore, MD 21201, USA.

[*]Corresponding author. E-mail: wilsonp@uchicago.edu

2.1 ABSTRACT

Humans are repeatedly exposed to variants of influenza virus throughout their lifetime. As a result, preexisting influenza-specific memory B cells can dominate the response following infection or vaccination. Memory B cells recalled by adulthood exposure are largely reactive to conserved viral epitopes present in childhood strains, posing unclear consequences on the ability of B cells to adapt to and neutralize newly-emerged strains. We sought to investigate

the impact of preexisting immunity on generation of protective antibody responses to conserved viral epitopes upon influenza virus infection and vaccination in humans. We accomplished this by characterizing monoclonal antibodies (mAbs) from plasmablasts, which are predominantly derived from preexisting memory B cells. We found that, while some influenza infection-induced mAbs bound conserved and neutralizing epitopes on the hemagglutinin (HA) stalk domain or neuraminidase, the majority of mAbs elicited by infection targeted non-neutralizing epitopes on nucleoprotein and other unknown antigens. Furthermore, most infection-induced mAbs had equal or stronger affinity to childhood strains, indicating recall of memory B cells from childhood exposures. Vaccination-induced mAbs were similarly induced from past exposures and exhibited substantial breadth of viral binding, though in contrast to infection-induced mAbs they targeted neutralizing HA head epitopes. Finally, cocktails of infection-induced mAbs displayed reduced protective ability in mice compared to vaccination-induced mAbs. These findings reveal that both preexisting immunity and exposure type shape protective antibody responses to conserved influenza virus epitopes in humans. In particular, natural infection largely recalls cross-reactive memory B cells against non-neutralizing epitopes, while vaccination harnesses preexisting immunity to target protective HA epitopes.

2.2 One sentence summary: Antibody immunodominance to conserved influenza virus epitopes is impacted by both preexisting B cell memory and route of exposure.

Published in Science Translational Medicine 09 Dec 2020:Vol. 12, Issue 573 [entire article presented herein](163)

2.3 INTRODUCTION

Influenza viruses are responsible for more than five million severe cases of respiratory tract infection and up to 650,000 deaths globally each year (*61*). Current influenza vaccine effectiveness is low (*85*), partly due to rapid antigenic evolution of the major surface glycoproteins of influenza virus: hemagglutinin (HA) and neuraminidase (NA) (*164*). Influenza vaccination platforms focus on eliciting protective antibody responses against HA, the most abundant and immunodominant viral glycoprotein (*165*). Antibodies against the HA head domain are potently neutralizing and inhibit receptor binding to sialic acid on epithelial cells. This is measured in vitro as the ability of an antibody to inhibit agglutination of red blood cells, referred to as hemagglutination inhibition (HAI) (*67*). Antibodies against HA are capable of limiting infection, and serum HAI titers have been used as the primary correlate of vaccine-induced protection against influenza for nearly 50 years (*67, 166*). However, the HA head is highly variable and easily mutates to evade host immunity (*167-170*), leading to seasonal epidemics and necessitating frequent reformulation of seasonal influenza vaccines.

In addition to rapid antigenic evolution, preexisting immunity profoundly affects protective immune responses upon exposure to novel influenza viruses or viruses that exhibit antigenic drift, the accumulation of mutations in viral surface glycoproteins (*38, 103, 171*). Original antigenic sin, also called imprinting, suggests that an individual's first encountered strain takes a senior antigenic position in the memory B cell (MBC) repertoire (*97, 108, 172*). As a result, subsequent exposure to influenza viruses later in life leads to the recall of MBCs specific to epitopes present in strains from an individual's childhood. Several reports have proposed beneficial and detrimental effects of imprinting on antibody responses to influenza viruses, depending on the context (*99, 101, 173*). It was recently suggested that the first HA group 1 or HA group 2 virus an individual was exposed to predicts protection against avian influenza viruses belonging to the same group and susceptibility to avian influenza viruses of the other group (*103*). Furthermore, the age distribution of seasonal influenza virus cases can be predicted by the likely subtype of first infection for each birth cohort (*174, 175*). The

boosting of antibodies reactive to conserved protective or non-protective viral epitopes may therefore play a major role in shaping influenza virus susceptibility or protective outcomes upon exposure.

To date, few studies have addressed the role of preexisting immunity in shaping the reactivity of antibodies elicited by natural influenza virus infection compared to vaccination at the single B cell level. Our current understanding of antibody immunodominance to influenza viruses in humans is largely limited to an understanding of vaccination-induced responses derived from serology studies, which fail to resolve the full spectrum of epitope targeting. It is well-established that vaccination induces HA head-specific responses due to enrichment of HA during vaccine manufacturing (*50, 176*), but it is unclear how preexisting immunity shapes the targeting of conserved HA epitopes upon vaccination. Furthermore, past studies have suggested that viral antigens such as the HA stalk, NA, and internal nucleoprotein (NP) are frequently targeted upon infection, as these antigens are in high abundance (*50, 177, 178*). However, the frequencies by which conserved antigens are targeted by B cells upon natural infection remain to be determined. We hypothesized that plasmablasts that are induced early after natural infection would target conserved, yet less protective, viral epitopes on the HA stalk domain, NA, and NP, rather than antigenically drifted epitopes on the HA head, as only conserved epitopes will be recognized by the preexisting MBC repertoire. By contrast, we hypothesized that vaccination may draw upon preexisting immunity to boost HA head-specific responses.

In this study, we characterized monoclonal antibodies (mAbs) cloned from plasmablasts induced early after IAV infection and seasonal vaccination. Plasmablasts are a useful model as they are predominantly derived from the MBC compartment and typically express highly somatically-mutated variable genes despite their rapid activation (5–14 days) after antigen exposure (*38, 179*). In addition, they are readily found to have clonal relationships with B cells activated by previously encountered influenza virus strains (*38*). By characterizing antigen reactivity, cross-reactivity toward historical and contemporary influenza virus strains, in vitro virus neutralization, and in vivo protective ability of human

mAbs, we discovered key differences in how natural infection and seasonal vaccination rely on preexisting B cell memory to induce early protective antibody-mediated immunity. Our data demonstrate that preexisting immunity largely biases the early antibody response after infection toward conserved yet less protective viral epitopes, with only a small percentage of infection-induced mAbs targeting the HA head. Conversely, vaccination can draw upon preexisting immunity to boost cross-reactive and neutralizing responses against the HA head, likely resulting in superior protection when circulating strains are well-matched to vaccine strains. This study emphasizes the necessity of understanding mechanisms of immune memory bias such as original antigenic sin in shaping protective antibody responses to influenza viruses, as harnessing or surmounting preexisting immunity is likely the most effective path toward universal vaccination.

2.4 RESULTS

2.4.1 A minority of antibodies induced early after influenza virus infection recognize the HA head

To examine how preexisting immunity shapes the antibody response following natural influenza virus infection and vaccination, we generated mAbs from single plasmablasts obtained from human participants after H1N1 or H3N2 virus infection (Table 2.1) and from healthy individuals after seasonal vaccination (Table 2.2). H1N1-infected individuals were recruited during the 2015–2016 flu season, and H3N2-infected individuals were recruited during the 2014–2015 flu season. Vaccinated individuals were studied after receipt of the northern hemisphere trivalent influenza vaccine in the 2010–2011 flu season or the quadrivalent influenza vaccine in the 2014–2015 flu season. Notably, the vaccine strains received by the vaccination cohort were distinct from infecting strains circulating during the time of sample isolation from the infection cohort (Table 2.1, Table 2.2). Samples were collected at day 7 post-vaccination and estimated days 7–11 post-infection. All mAbs generated were initially screened for reactivity to influenza viruses (indicated in Table 2.1 and Table 2.2) and only included in the study if they exhibited specific binding.

Table 2.1. Participant characteristics for influenza virus infection cohorts. Likely infecting strains for the specified influenza seasons are referenced (*180, 181*). Vaccination history represents any known history within three years prior to the current sampling time. Sampling time is estimated based on the total number of days participants had been experiencing symptoms of influenza illness at the time of the study visit. All participants were PCR-confirmed influenza positive. S: seasonal; Pan: pandemic; COPD: chronic obstructive pulmonary disease.

Participant ID	Season	Age	Sex	Influenza A Strain	Comorbidities	Vaccination History	Sampling time
228-14	2014–2015	34	M	S H3N2 A/Switzerland/9715293/2013	Asthma	2011–2012 2012–2013 2013–2014	D7
229-14	2014–2015	46	F	S H3N2 A/Switzerland/9715293/2013	COPD Asthma	2011–2012 2012–2013	D7
235-15	2014–2015	49	M	S H3N2 A/Switzerland/9715293/2013	Asthma	2009–2014	D7
294-16	2015–2016	23	M	Pan H1N1 A/California/7/2009	None	2015–2016	D7
296-16	2015–2016	26	M	Pan H1N1 A/California/7/2009	None	No History	D7
300-16	2015–2016	30	M	Pan H1N1 A/California/7/2009	None	No History	D11
301-16	2015–2016	46	F	Pan H1N1 A/California/7/2009	Asthma	2014–2015	D8

Table 2.2. Participant characteristics for influenza virus vaccination cohorts. Sampling time refers to day post vaccination with either the trivalent influenza vaccine (TIV) or quadrivalent influenza vaccine (QIV).

Participant ID	Season	Age	Sex	Vaccine	Influenza A Vaccine Strains	Vaccination History	Sampling time
008-10	2010–2011	26	F	TIV	A/California/7/2009 (H1N1) A/Perth/16/2009 (H3N2)	2009–2010	D7
009-10	2010–2011	25	F	TIV	A/California/7/2009 (H1N1) A/Perth/16/2009 (H3N2)	2009–2010	D7
011-10	2010–2011	30	---	TIV	A/California/7/2009 (H1N1) A/Perth/16/2009 (H3N2)	2009–2010	D7
014-10	2010–2011	27	M	TIV	A/California/7/2009 (H1N1) A/Perth/16/2009 (H3N2)	2009–2010	D7
017-10	2010–2011	24	M	TIV	A/California/7/2009 (H1N1) A/Perth/16/2009 (H3N2)	2009–2010	D7
019-10	2010–2011	23	F	TIV	A/California/7/2009 (H1N1) A/Perth/16/2009 (H3N2)	2009–2010	D7
028-10	2010–2011	32	---	TIV	A/California/7/2009 (H1N1) A/Perth/16/2009 (H3N2)	2009–2010	D7
034-10	2010–2011	40	F	TIV	A/California/7/2009 (H1N1) A/Perth/16/2009 (H3N2)	2009–2010	D7
039-10	2010–2011	25	M	TIV	A/California/7/2009 (H1N1) A/Perth/16/2009 (H3N2)	2009–2010	D7
051-10	2010–2011	43	M	TIV	A/California/7/2009 (H1N1) A/Perth/16/2009 (H3N2)	2009–2010	D7
217-14	2014–2015	31	M	QIV	A/California/7/2009 (H1N1) A/Texas/50/2012 (H3N2)	2013–2014	D7
220-14	2014–2015	24	F	QIV	A/California/7/2009 (H1N1) A/Texas/50/2012 (H3N2)	Unknown	D7
221-14	2014–2015	34	F	QIV	A/California/7/2009 (H1N1) A/Texas/50/2012 (H3N2)	No History	D7

Table 2.2. Participant characteristics for influenza virus vaccination cohorts, continued

236-15	2014–2015	32	F	QIV	A/California/7/2009 (H1N1) A/Texas/50/2012 (H3N2)	No History	D7
237-14	2014–2015	32	F	QIV	A/California/7/2009 (H1N1) A/Texas/50/2012 (H3N2)	No History	D7
240-15	2014–2015	28	M	QIV	A/California/7/2009 (H1N1) A/Texas/50/2012 (H3N2)	No History	D7
241-15	2014–2015	29	F	QIV	A/California/7/2009 (H1N1) A/Texas/50/2012 (H3N2)	No History	D7
244-15	2014–2015	29	M	QIV	A/California/7/2009 (H1N1) A/Texas/50/2012 (H3N2)	2013–2014	D7

Whereas greater than 90% of mAbs induced by vaccination recognized HA by Enzyme-Linked Immunosorbent Assay (ELISA) (Figure 2.1A), only 30% of mAbs induced by natural infection with either H1N1 or H3N2 were HA-reactive, including the HA head and stalk domain regions, with the majority recognizing other antigens such as NA and the highly conserved NP ($p < 0.0001$; Figure 2.1B). Nearly half of all H1N1 infection-induced mAbs were HA-reactive, although this was substantially less than the proportion of mAbs induced by seasonal vaccination (Figure 2.1B, bottom left panel). Furthermore, H3N2 infection-induced mAbs mostly targeted NA and NP, whereas only 18% bound HA (Figure 2.1B, bottom right panel). Because age-related factors likely affect antibody responses to conserved antigens (*72, 182, 183*), we next analyzed antigen reactivity in each individual within our infection cohort. Although there was variability in the proportion of antibodies targeting non-HA proteins per H3N2-infected individual, each individual mounted a non-HA-biased response overall, with roughly 80% of the response per individual directed toward non-HA antigens (Figure 2.2A). Similarly, for H1N1-infected individuals, a substantial fraction of all mAbs per person recognized non-HA antigens, although there was some degree of inter-individual variability (Figure 2.2B). Accordingly, we found that only 6% of all mAbs induced by infection had HAI activity compared to 59% induced by vaccination ($p < 0.0001$; Figure 2.1C), and the percentage of HAI^+ mAbs per infected individual was on average only 5.5% (Figure 2.1D).

Preexisting immunity is expected to impact antibody responses to conserved viral epitopes, so we next assessed whether antibodies induced by influenza virus infection

targeted typically more conserved and immunosubdominant viral epitopes. Of total HA-binding mAbs induced by vaccination, nearly two-thirds possessed HAI activity, reflective of their ability to target the HA head region (Figure 2.2C), compared to just 20% of HA-reactive infection-induced mAbs ($p < 0.0001$; Figure 2.2D). To determine mAbs binding epitopes on the stalk domain, we performed competition ELISAs with an anti-stalk mAb known to bind a well-characterized broadly neutralizing stalk epitope (mAb CR9114, (*184*)) as well as ELISA against a headless stalk construct (*60*) and chimeric HA constructs (cH5/1; cH7/3). Only 14% of vaccination-induced HA-reactive mAbs bound the HA stalk domain (Figure 2.2C), compared to 49% of all HA-reactive mAbs induced by infection ($p < 0.0001$; Figure 2.2D). Remarkably, 58% of all HA-reactive H1N1 infection-induced mAbs bound the stalk domain (Figure 2.2D, bottom left panel). Of all stalk domain-reactive antibodies induced by infection or vaccination, we did not see a difference in typical broadly neutralizing stalk epitopes bound (CR9114-competing), versus mAbs binding uncharacterized stalk epitopes (CR9114 non-competing, but positive for the headless stalk construct and chimeric HA constructs (cH5/1; cH7/3) (Figure 2.2E). Notably, we also identified HA-reactive mAbs induced by infection and vaccination that did not confer HAI activity and were ruled out against binding stalk domain epitopes by our assays (Figure 2.2C, D). These mAbs were categorized as HA^+ mAbs binding to "unknown" epitopes, potentially binding undefined HAI^- epitopes on the HA head or stalk. Altogether, these data reveal that the minority of infection-induced HA^+ mAbs bind HAI^+ head epitopes, and instead tend to bind HAI^- head and stalk epitopes.

Similar to HA, the head region of the influenza virus NA surface glycoprotein is susceptible to antigenic drift, although the active site and nearby epitopes are highly conserved (*72*). Because several infection-induced mAbs bound to NA, we asked whether NA-reactive mAbs bound to conserved sites. To address this, we used influenza neuraminidase inhibitor resistance detection (NA-STAR) and NA enzyme-linked lectin assays (ELLA), which can determine whether a mAb is binding conserved epitopes on the NA active site or regions within close proximity to it. In the NA-STAR assay, a small

chemiluminescent substrate is bound directly to the NA enzymatic site unless an antibody binds the active site and blocks access of the substrate. For ELLA, the sialic acid substrate is present in glycans of the fetuin glycoprotein, and an antibody that binds to NA at or near the enzymatic site can sterically block access to the enzymatic site. We found that more than half of all infection-induced NA-reactive mAbs were NA-STAR$^+$ or ELLA$^+$ (Figure 2.2F). There was no significant difference between the percentages of combined NA-STAR$^+$ and ELLA$^+$ mAbs elicited by H1N1 and H3N2 infection, with 70% induced by H1N1 infection and more than half induced by H3N2 infection (Figure 2.2F, bottom panel). Overall, these data suggest that natural infection recalls preexisting MBCs reactive to more conserved influenza virus antigens, a hallmark of original antigenic sin.

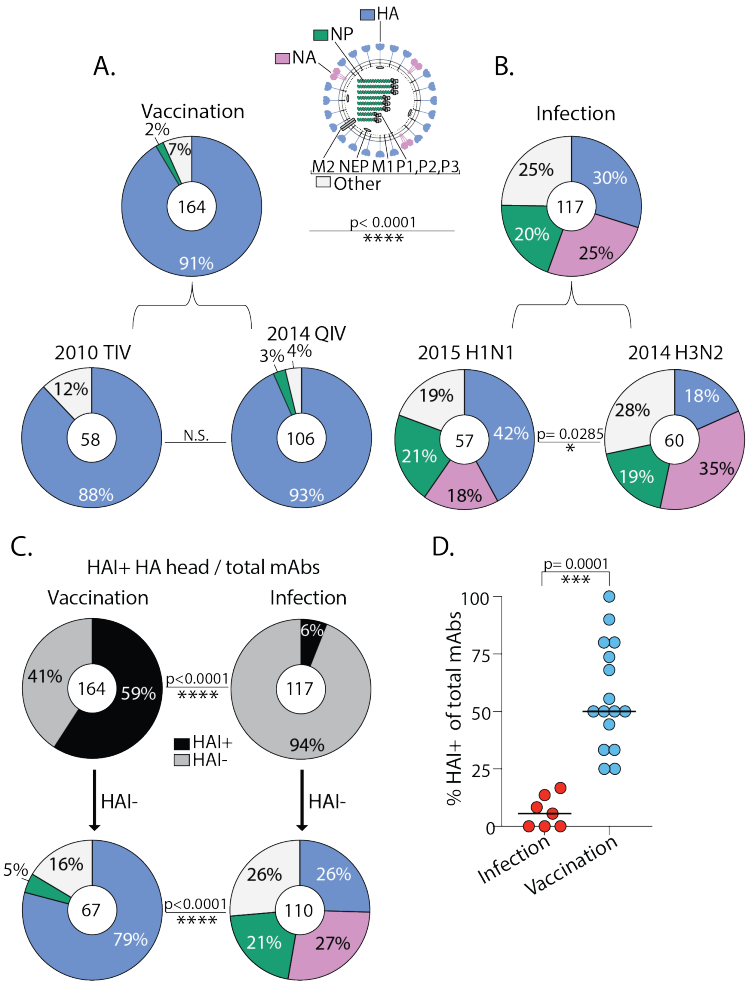

Figure 2.1. A minority of antibodies induced early after influenza virus infection recognize the HA head. (**A**) Pie charts show binding of 2010–2011 trivalent and 2014–2015 quadrivalent vaccination-induced mAbs to a panel of hemagglutinin (HA), neuraminidase (NA), and nucleoprotein (NP) recombinant proteins by ELISA. (**B**) Pie charts show binding of

Figure 2.1, continued
2015–2016 H1N1 and 2014–2015 H3N2 infection–induced mAbs to a panel of HA, NA, and NP recombinant proteins by ELISA. Recombinant proteins were chosen from the representative influenza A vaccine strains within each vaccine (table S2) or from viruses bearing resemblance to recently circulating strains during the year of mAb isolation from infected individuals (2014 H3N2: A/Switzerland/9715293/2013, A/Hong Kong/4801/2014; 2015 H1N1: A/California/7/2009, A/Michigan/45/2015). mAbs in the "Other" category bind virus, but not HA, NA, or NP, and likely bind other undetermined influenza virus antigens. **(C)** Pie charts demonstrate the percent of total isolated mAbs with HAI activity isolated from both cohorts (top) and the antigen reactivity of HAI−mAbs within each cohort (bottom panel). **(D)** The percentage of mAbs with HAI activity was compared in individuals from infected (n= 7) and vaccinated cohorts (n = 16). Numbers in the center of each pie chart indicate the number of mAbs tested. Statistical significance was determined by chi-square test (****P < 0.0001; *P = 0.0285) **(A–C)** and unpaired nonparametric Mann-Whitney test (***P=0.0001) **(D)**. Data are representative of two to three independent experiments performed in duplicate.

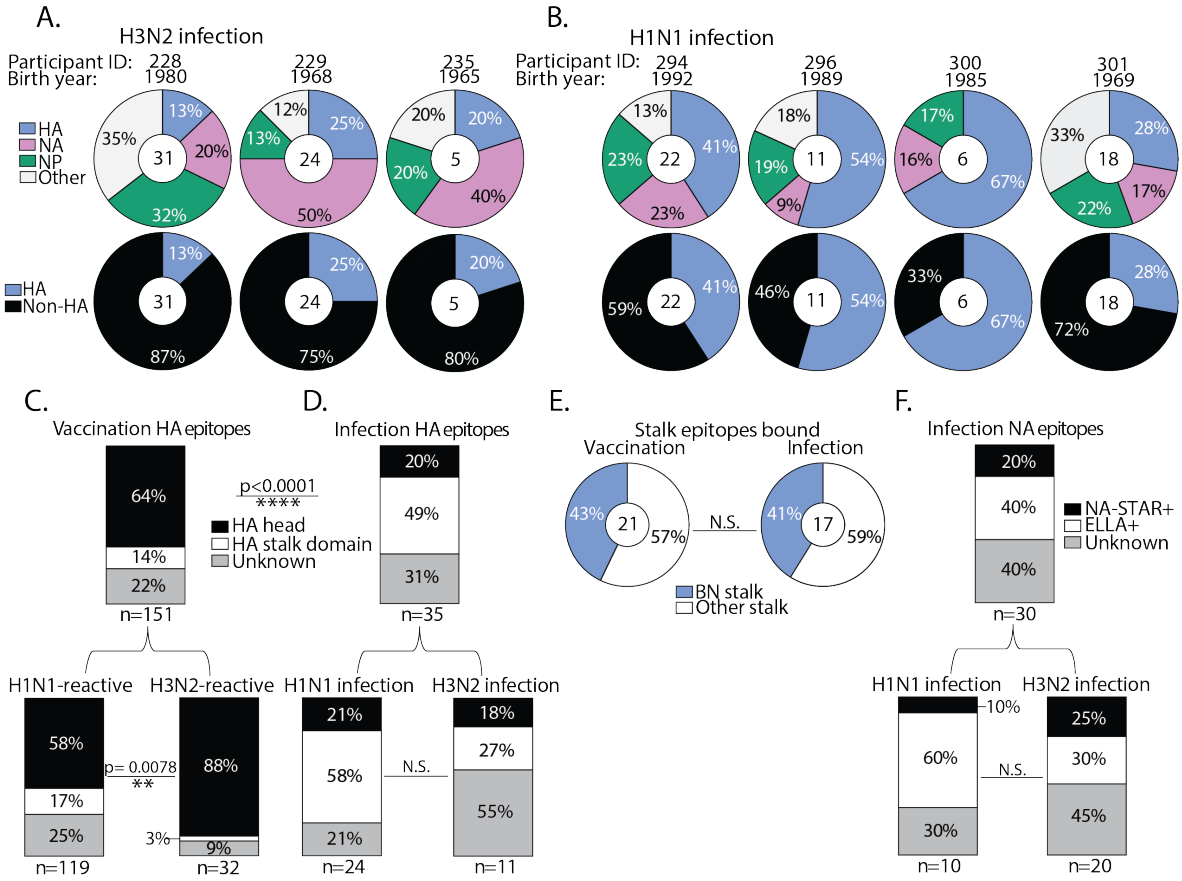

Figure 2.2. Reactivity of influenza virus infection-induced antibodies from individual participants and conserved epitope reactivity. (A, B) Pie charts show binding of 2014–2015 H3N2 infection-induced mAbs **(A)** and 2015–2016 H1N1 infection-induced mAbs **(B)** to a panel of hemagglutinin (HA), neuraminidase (NA), and nucleoprotein (NP) recombinant proteins by ELISA. Recombinant proteins were chosen from the relevant circulating strains during the time of mAb isolation from infected individuals. **(C, D)** Bar charts demonstrate influenza virus HA epitopes bound by vaccination-induced HA-reactive mAbs **(C)** and infection-induced HA-reactive mAbs **(D)**. **(E)** Pie charts demonstrate the percentage of distinct stalk epitopes bound by stalk domain-reactive mAbs. MAbs binding the broadly neutralizing stalk epitope were determined by CR9114 competition ELISA, and mAbs binding undefined stalk epitopes were determined by ELISA against a headless HA stalk construct and chimeric HA. **(F)** Bar charts display NA epitopes bound by NA-reactive infection-induced mAbs, determined by NA-STAR and ELLA assay. Numbers in the center of

Figure 2.2, continued
or below each chart indicate the number of mAbs tested. Statistical significance was determined by Fisher's exact test, ****p<0.0001; **p=0.0078 (**C–F**). Data are representative of 2–3 independent experiments performed in duplicate.

2.4.2 Infection-induced antibodies are predominantly non-neutralizing

Only 6% of early infection-induced mAbs possessed HAI activity (Figure 2.1C), which is the primary correlate of antibody-mediated protection against influenza. However, mAbs reactive to immunosubdominant and neutralizing regions such as the HA stalk and NA active site were also identified. These results led us to address whether these mAbs were neutralizing toward the inducing vaccinating and infecting strains. To do so, we determined the neutralization capacity of mAbs induced by infection or vaccination using an in vitro virus microneutralization assay or plaque reduction neutralization assay. Only 29% of infection-induced mAbs were neutralizing, relative to 80% of mAbs that were induced by seasonal vaccination ($p < 0.0001$; Figure 2.3A). Moreover, we observed that the overall neutralization potency of all infection-induced mAbs was markedly reduced compared to vaccination-induced mAbs ($p < 0.0001$; Figure 2.3B), and the potency was still reduced when non-neutralizing mAbs were not included in the analysis ($p = 0.0188$, H1N1; $p = 0.0024$, H3N2; Figure 2.3C).

We previously demonstrated that the distribution in antibody reactivity varied widely between H1N1 and H3N2 infections ($p = 0.0285$; Figure 2.1B). We therefore analyzed the distribution in reactivity of neutralizing and non-neutralizing infection-induced mAbs. Of H1N1 infection-induced mAbs, only 38% were neutralizing, of which 67% bound HA and 33% bound NA (Figure 2.3D and Figure 2.4A). The majority of stalk domain-reactive H1N1-induced mAbs were neutralizing, confirming the protective nature of mAbs against this region. Only 20% of all H3N2 infection-induced mAbs were neutralizing, and in sharp contrast to H1N1 infection, 70% of all H3N2 infection-induced neutralizing mAbs were NA-reactive, with the minority recognizing HA (Figure 2.3E and Figure 2.4B). All mAbs binding NP and other unknown antigens were non-neutralizing, with a substantial fraction of non-neutralizing HA- and NA-reactive mAbs detected in each group (Figure 2.3D, E).

We next addressed whether there were qualitative differences in the neutralization ability against distinct antigens between infection-induced and vaccination-induced mAbs. For both groups, the majority of neutralizing mAbs targeted the HA head and stalk domain regions (Figure 2.3F, G). Unique to infection-induced mAbs, a substantial portion of NA-reactive mAbs were neutralizing (Figure 2.3F). The majority of infection-induced mAbs targeting unknown regions of HA and other unknown antigens were non-neutralizing, in addition to several non-neutralizing NP-reactive mAbs isolated (Figure 2.3F, G). Notably, all mAbs isolated targeting the broadly neutralizing stalk epitope (CR9114-competing) were neutralizing, and several mAbs targeting other undefined stalk domain epitopes were also neutralizing (Figure 2.3H). Lastly, we identified that HA head-reactive mAbs were typically more potent than HA stalk domain-reactive mAbs (Figure 2.3I, J and Figure 2.4C, D), and NA-reactive mAbs were less potent than HA head- and stalk domain-reactive mAbs (Figure 2.3I). Together, these data demonstrate that the majority of mAbs isolated from infected individuals targeted conserved yet non-neutralizing targets, though some neutralizing mAbs reactive to immunosubdominant epitopes of the HA stalk domain and NA were identified.

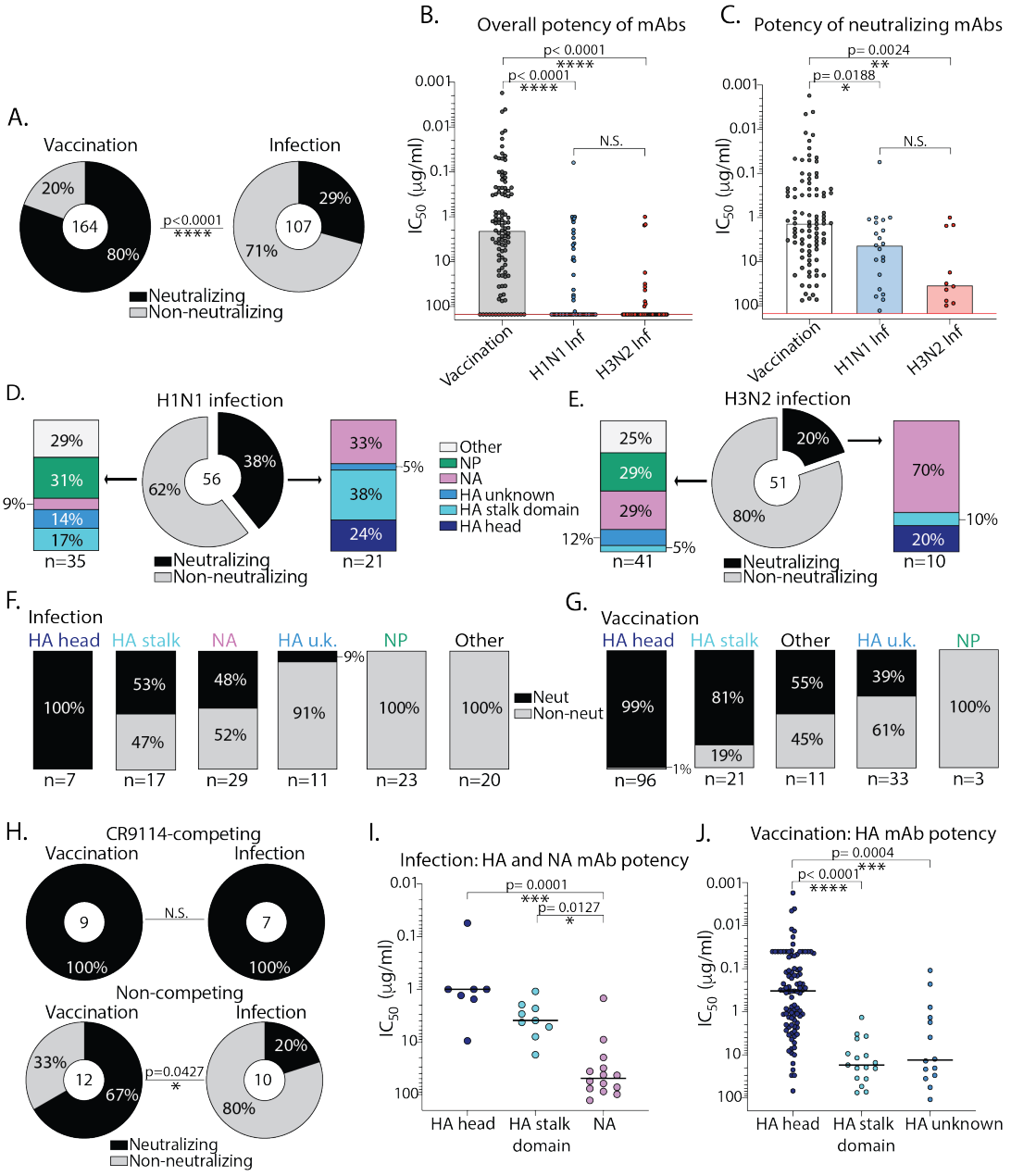

Figure 2.3. Influenza virus infection-induced antibodies are predominantly non-neutralizing in vitro compared to vaccination-induced antibodies. **(A)** Pie charts display percentages of all vaccination- and infection-induced mAbs with virus neutralization activity as assessed by microneutralization or plaque reduction assay using Madin-Darby canine kidney cell lines. **(B)** The overall potency of neutralizing and non-neutralizing vaccination-induced mAbs (n=164) was compared to infection-induced mAbs (H1N1 n=56; H3N2 n=51), depicted as microneutralization IC_{50} values. Non-neutralizing mAbs are displayed on the red line above the highest test concentration at 150 µg/ml. **(C)** The potency of all neutralizing mAbs induced by the quadrivalent vaccine (n=92) was compared to the potency of neutralizing infection-induced mAbs (H1N1 n= 21; H3N2 n=10), depicted as microneutralization IC_{50} values. **(D, E)** Bar charts show the antigen reactivity of neutralizing and non-neutralizing H1N1 **(D)** and H3N2 **(E)** infection-induced mAbs. **(F, G)** Bar charts display the percent of total neutralizing and non-neutralizing mAbs induced by infection **(F)** and vaccination **(G)**, subset by antigen-reactivity. **(H)** Pie charts demonstrate the percentage of neutralizing and non-neutralizing stalk domain-reactive mAbs binding a broadly neutralizing stalk epitope, as determined by a CR9114 competition ELISA (top panel),

Figure 2.3, continued
or mAbs binding undefined stalk epitopes, determined by ELISA against a headless HA stalk construct and chimeric HA (bottom panel). **(I, J)** The potency of HA- and NA-reactive mAbs induced by infection **(I)** was compared to the potency of HA-reactive mAbs induced by vaccination **(J)**. The numbers in the center of or below each chart indicate the number of mAbs tested. Statistical significance was determined by Chi-square test, ****p<0.0001 **(A)**, Fisher's exact test, *p=0.0427 **(H)**, or by unpaired non-parametric Kruskal-Wallis test with Dunn's correction for multiple comparisons **(B, C, I, J)**. Data are representative of two independent experiments performed in duplicate.

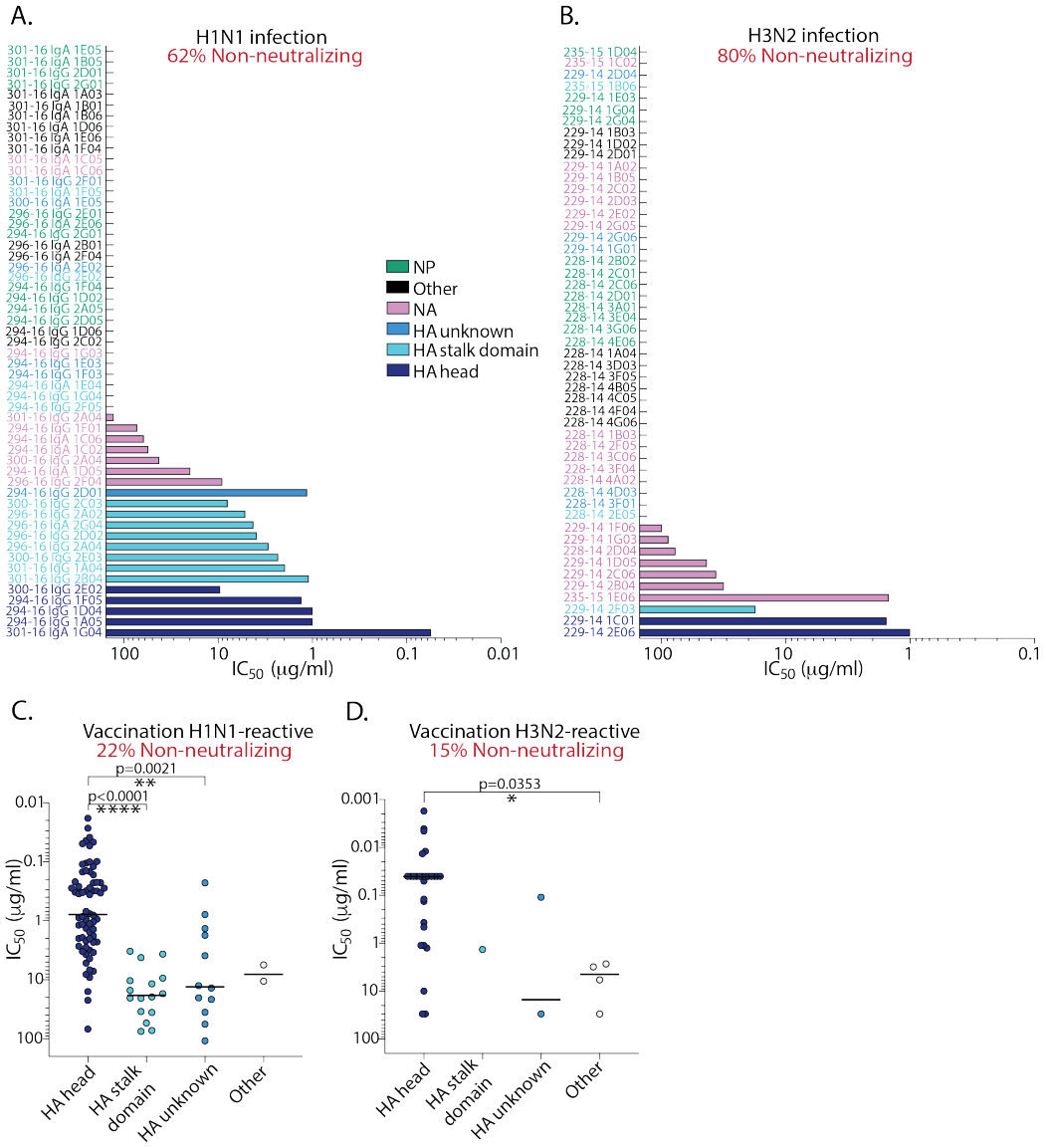

Figure 2.4. Neutralization potency of influenza virus infection- and vaccination-induced antibodies stratified by subtype reactivity. (A, B) Bar graphs display the potency of HA-reactive and NA-reactive neutralizing mAbs induced by H1N1 infection (n= 56) **(A)** and H3N2 infection (n= 51) **(B)**, expressed as microneutralization (MN) IC_{50} values. **(C, D)** The potency of vaccination-induced mAbs binding distinct epitopes was compared for H1N1-reactive (n=100) **(C)** and H3N2-reactive (n=39) mAbs **(D)**, depicted as MN IC_{50} values. Statistical significance was determined using an unpaired non-parametric Kruskal-Wallis test with Dunn's correction for multiple comparisons, ****p<0.0001; **p=0.0021; *p=0.0353 **(C–D)**. Data are representative of 2–3 independent experiments performed in duplicate.

2.4.3 The reactivity of influenza virus infection-induced antibodies is biased by original antigenic sin

The majority of vaccination-induced mAbs bound antigenically drifted viral epitopes on the HA head. In contrast, the majority of mAbs induced by infection bound to conserved epitopes, such as the HA stalk domain, NA active site, and NP (Figure 2.1B and Figure 2.2). Accordingly, the majority of these mAbs were non-neutralizing (Figure 2.3). To further investigate the role of original antigenic sin and previous immune history in shaping mAb reactivity, we assessed the cross-reactivity of mAbs induced by natural infection against heterosubtypic viral strains and past strains circulating during the lifetime of the individual. First, we tested each mAb against historical and contemporary H1N1 and H3N2 viral strains, which accounted for nearly 50 years of viral antigenic drift, to determine the degree of homosubtypic and heterosubtypic cross-reactivity within each infection and vaccination cohort. Consistent with the high prevalence of vaccination-induced mAbs that bound the HA head, the majority of vaccination-induced mAbs were homosubtypic (Figure 2.5A). Conversely, infection-induced mAbs displayed increased heterosubtypic cross-reactivity relative to vaccination-induced mAbs, regardless of the infecting subtype ($p = 0.0017$; Figure 2.5B). As expected, and likely due to differences in age, immune histories, and other factors, we observed variation in heterosubtypic cross-reactivity amongst individual donors (Figure 2.6A–C). Strikingly, 60% of all infection-induced mAbs displayed equal or stronger affinity for childhood viral strains than viral strains circulating at the time of infection (Figure 2.5C, Table 2.3), confirming a substantial role for original antigenic sin in shaping early antibody responses to natural infection. For vaccination-induced mAbs, this phenotype was also substantial, as 45% could bind with equal or stronger affinity to childhood strains as compared to viral strains circulating at the time of mAb isolation. As responses to influenza viruses are thought to be shaped not only by childhood exposures, but by any past exposures (*108*), we analyzed the percentage of mAbs induced by infection or vaccination that had equal or stronger affinity toward any past strain relative to the inducing strains. We identified that 60% of vaccination-induced mAbs had equal or stronger reactivity toward past strains,

compared to 80% for infection-induced mAbs ($p = 0.0012$; Figure 2.5D). We observed a greater effect for original antigenic sin by past exposures on mAbs that were H3N2-reactive versus H1N1-reactive, patterns that were consistent amongst infected individuals (Figure 2.5C, D, bottom and Figure 2.6D, E). Overall, we observed greater variation in both cross-reactivity and affinity toward past strains in vaccinated individuals (Figure 2.6C, F).

As the cross-reactivity of infection-induced mAbs appeared to be more influenced by past exposures, we addressed whether these mAbs possessed increased immunoglobulin heavy chain variable region (VH) somatic mutations relative to vaccination-induced mAbs, as these antibodies were likely derived from MBCs that were continually recalled into germinal centers during the lifetime of the individual. Infection-induced mAbs had a median of 22 VH gene somatic mutations, while vaccination-induced mAbs had a median of 14 VH gene mutations ($p < 0.0001$; Figure 2.5E). There was no difference in the number of somatic mutations between H1N1 and H3N2 infection-induced mAbs (Figure 2.5F). Together, these data suggest influenza virus infection recalls MBCs from long-past exposures, likely from childhood, supporting the original antigenic sin hypothesis. By contrast, vaccination may recall MBCs from more recent virus exposures, though the antibody response to vaccination is still largely biased by past exposures. Notably, mAbs derived from preexisting MBCs that bind with higher affinity to historical test strains relative to current test strains implies that those MBCs were originally generated upon exposure to a similar historical strain. However, recent exposures to divergent lineages similar to the historical test strain analyzed may also account for increased affinity.

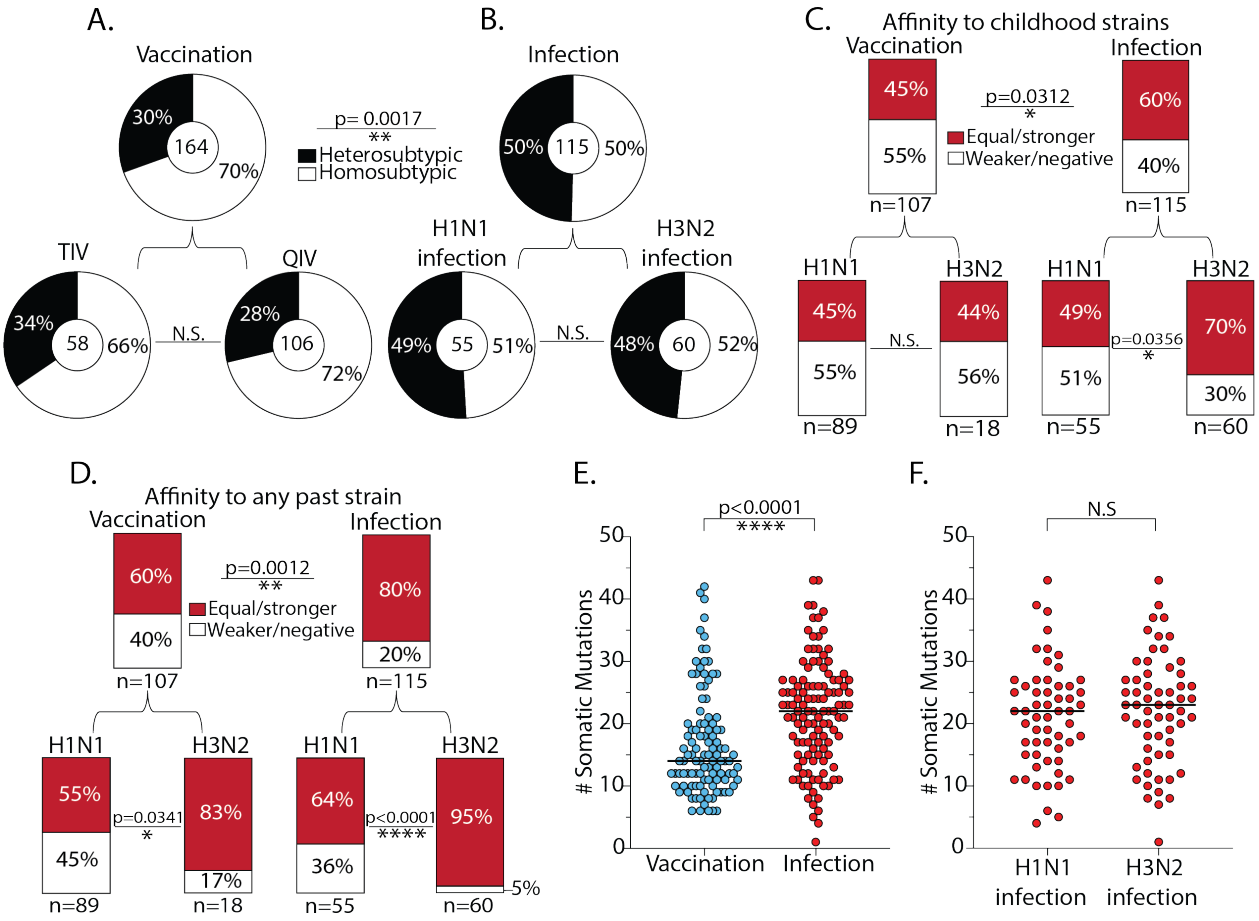

Figure 2.5. The cross-reactivity of influenza virus infection-induced antibodies is biased by original antigenic sin. (A, B) Pie charts demonstrate the cross-reactivity of vaccination-induced mAbs **(A)** and infection-induced mAbs **(B)**, which was inferred by ELISA binding to a panel of H1N1 and H3N2 viruses. Heterosubtypic cross-reactivity was defined based on the ability of a mAb to bind to at least one or more strains opposite of the inducing subtype, such as an H1N1-induced mAb binding to one or more H3N2 strains. **(C, D)** Bar charts represent the percentage of infection-induced mAbs with equal or greater binding affinity to childhood strains **(C)** or any past strains **(D)** relative to contemporary strains circulating during the time of mAb isolation. Past strains in **(D)** include all available strains tested that were circulating prior to the year of the inducing strain for each cohort (H1N1 infection n=5; H3N2 infection n=6; H1N1-reactive vaccination n=5; H3N2-reactive vaccination n=3 strains analyzed). **(E)** The number of somatic mutations in the immunoglobulin heavy chain variable region for 2014–2015 quadrivalent vaccine-induced mAbs (n=106) was compared to H1N1 and H3N2 infection-induced mAbs combined (n=117). **(F)** The number of somatic mutations in the immunoglobulin heavy chain variable region for H1N1 infection-induced mAbs (n=57) was compared to H3N2-infection induced mAbs (n=60). The numbers in the center of or below each chart indicate the number of mAbs tested. Statistical significance was determined by Chi-square or Fisher's exact test, $^{**}p=0.0017$; $^{*}p=0.0312$; $^{**}p=0.0012$ **(A–D)** and unpaired non-parametric Mann-Whitney test, $^{****}p<0.0001$ **(E, F**; bars indicate median). Data are representative of 2–3 independent experiments performed in duplicate.

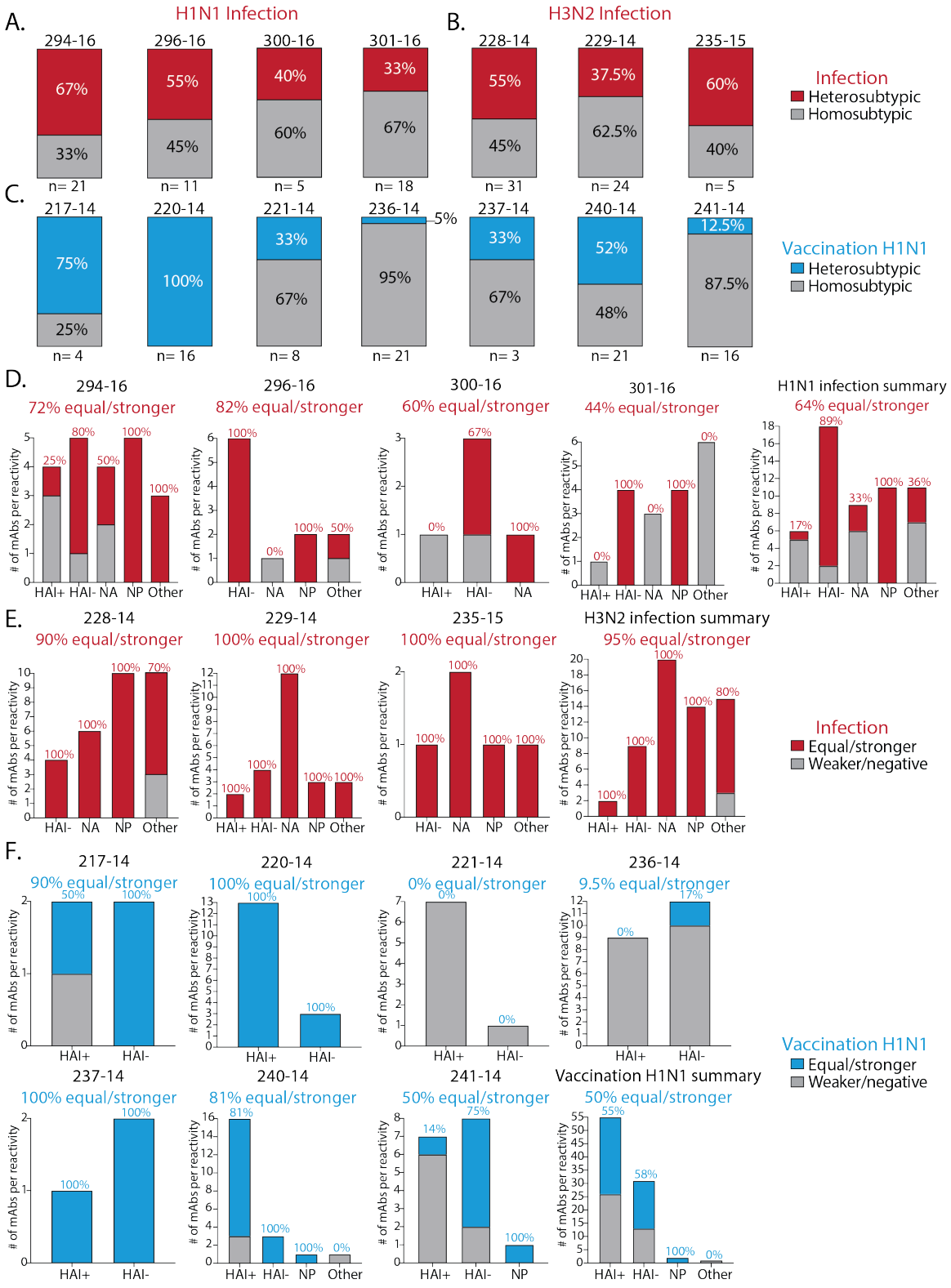

Figure 2.6. Antibody cross-reactivity and affinity toward past strains by individual participants. (A–C) Bar charts display heterosubtypic cross-reactivity for H1N1 infection-induced mAbs tested against H3N2 strains **(A)**, H3N2 infection-induced mAbs tested against H1N1 strains **(B)**, and H1N1-reactive quadrivalent influenza vaccine-induced mAbs tested

Figure 2.6, continued
against H3N2 strains (**C**). Heterosubtypic cross-reactivity was defined based on the ability of a mAb to bind to at least one or more strains opposite of the inducing subtype. (**D–F**) Bar graphs display mAbs from H1N1-infected individuals (**D**), H3N2-infected individuals (**E**), and vaccinated individuals (**F**; quadrivalent influenza vaccine, H1N1-reactive) exhibiting equal or stronger affinity to past viral strains relative to inducing strains. Data are broken down by individual mAb reactivities and summarized for each cohort in the last graph of each panel. Numbers below each bar chart indicate the number of mAbs tested per individual, and data are representative of 2–3 independent experiments performed in duplicate.

Table 2.3. Reference childhood strains used to characterize influenza virus infection-induced antibodies. Reference childhood strains were chosen based on available virus strains circulating within the first 10–15 years of the individual's life. A mAb was chosen as having equal or greater reactivity toward the reference viral strain if the affinity toward one or more of the indicated reference strains was within the same log molar range or greater than the affinity toward the contemporary inducing strain. QIV: Quadrivalent influenza vaccine.

Participant ID	Cohort	Year of Birth	Reference Childhood Strains
228-14	2014–2015 H3N2 Infection	1980	A/Philippines/2/1982 H3N2
229-14	2014–2015 H3N2 Infection	1968	A/Hong Kong/1/1968 H3N2; A/Philippines/2/1982 H3N2
235-15	2014–2015 H3N2 Infection	1965	A/Hong Kong/1/1968 H3N2; A/Philippines/1982 H3N2
294-16	2015–2016 H1N1 Infection	1992	A/Texas/36/1991 H1N1; A/New Caledonia/20/1999, A/Solomon Islands/2006
296-16	2015–2016 H1N1 Infection	1989	A/Texas/36/1991 H1N1; A/New Caledonia/20/1999
300-16	2015–2016 H1N1 Infection	1985	A/Texas/36/1991 H1N1; A/New Caledonia/20/1999
301-16	2015 H1N1 Infection	1969	A/Chile/1/1983
217-14	2014–2015 QIV	1983	A/Texas/36/1991 H1N1; A Philippines/2/1982 H3N2
220-14	2014–2015 QIV	1990	A/Texas/36/1991 H1N1; A/New Caledonia/20/1999; A Philippines/2/1982 H3N2
221-14	2014–2015 QIV	1980	A/Texas/36/1991 H1N1; A Philippines/2/1982 H3N2
236-15	2014–2015 QIV	1982	A/Texas/36/1991 H1N1; A Philippines/2/1982 H3N2
237-14	2014–2015 QIV	1982	A/Texas/36/1991 H1N1; A Philippines/2/1982 H3N2
240-15	2014–2015 QIV	1986	A/Texas/36/1991 H1N1; A/New Caledonia/20/1999 H1N1; A Philippines/2/1982 H3N2
241-15	2014–2015 QIV	1985	A/Texas/36/1991 H1N1; A/New Caledonia/20/1999 H1N1, A Philippines/2/1982 H3N2

2.4.4 Influenza virus antigen- and subtype-reactivity shape original antigenic sin-like antibody responses

Reactivity toward distinct antigens is expected to shape mAb cross-reactivity. To determine how antigen targeting and subtype reactivity impact cross-reactivity of infection- and vaccination-induced mAbs, we clustered mAbs by antigen bound in heatmaps based on their affinity (ELISA K_D) for several H1N1 and H3N2 virus strains. Based on patterns in reactivity, groups of mAbs predicted to bind similar epitopes could then be visualized based on cluster formation. For H1N1 infection-induced mAbs, HA stalk domain- and NP-reactive mAbs displayed the greatest breadth of cross-reactivity to H1N1 strains, generally binding to all seven influenza H1N1 strains tested (Figure 2.6D and Figure 2.7A, B). The majority of mAbs isolated from H1N1 infected individuals bound to the pandemic strains A/California/7/2009 and A/Michigan/45/2015, suggesting that those individuals were likely infected with an influenza virus variant most similar to these viral strains (Figure 2.7A, right). Regardless of epitope reactivity, most mAbs cross-reacted with several H1N1 viral strains dating back to 1983 (A/Chile/1/1983). A distinct pattern in reactivity was seen for H3N2 infection-induced mAbs, which exhibited a marked degree of homosubtypic cross-reactivity, regardless of the epitope bound (Figure 2.6E and Figure 2.7C, D). For both subtypes, heterosubtypic cross-reactivity was mainly observed for mAbs reactive to HA, NP, and other unknown antigens, while NA-reactive mAbs were largely homosubtypic. These results demonstrate both distinct and overlapping patterns in mAb breadth, dependent on the infecting subtype and viral epitopes targeted. Together, these results highlight the ability of H1N1 and H3N2 viruses to differentially induce antibodies to conserved viral epitopes.

The cross-reactivity of vaccination-induced mAbs was shaped by preexisting immunity, with H3N2-reactive mAbs characteristically having higher affinity toward past strains (Figure 2.7C, D). We therefore performed the same analyses with vaccination-induced mAbs to determine how antigen and subtype targeting impacted cross-reactivity. Vaccination-induced H1N1-reactive mAbs displayed vast viral binding breadth to several strains, despite these mAbs predominantly targeting the antigenically variable HA head

region (Figure 2.8A, B). Vaccination-induced H3N2-reactive mAbs were similarly cross-reactive and bound the majority of test strains analyzed (Figure 2.8C, D). We observed similar degrees of homosubtypic breadth compared to infection-induced mAbs for H1N1- and H3N2-reactive mAbs targeting the HA head, HA stalk domain, NP, or other regions on HA, with H3N2-reactive vaccination-induced mAbs typically exhibiting greater breadth regardless of epitope targeted (Figure 2.8C, D). Together, our results point to inherent differences in the ability of H1N1 and H3N2 viruses to draw upon preexisting immunity and induce cross-reactive antibody responses, regardless of exposure type, with the degree of cross-reactivity dependent on antigens targeted. Additionally, these results demonstrate the breadth of homosubtypic viral binding by HA head-reactive mAbs induced by seasonal vaccines, which are typically thought to elicit highly strain-specific responses.

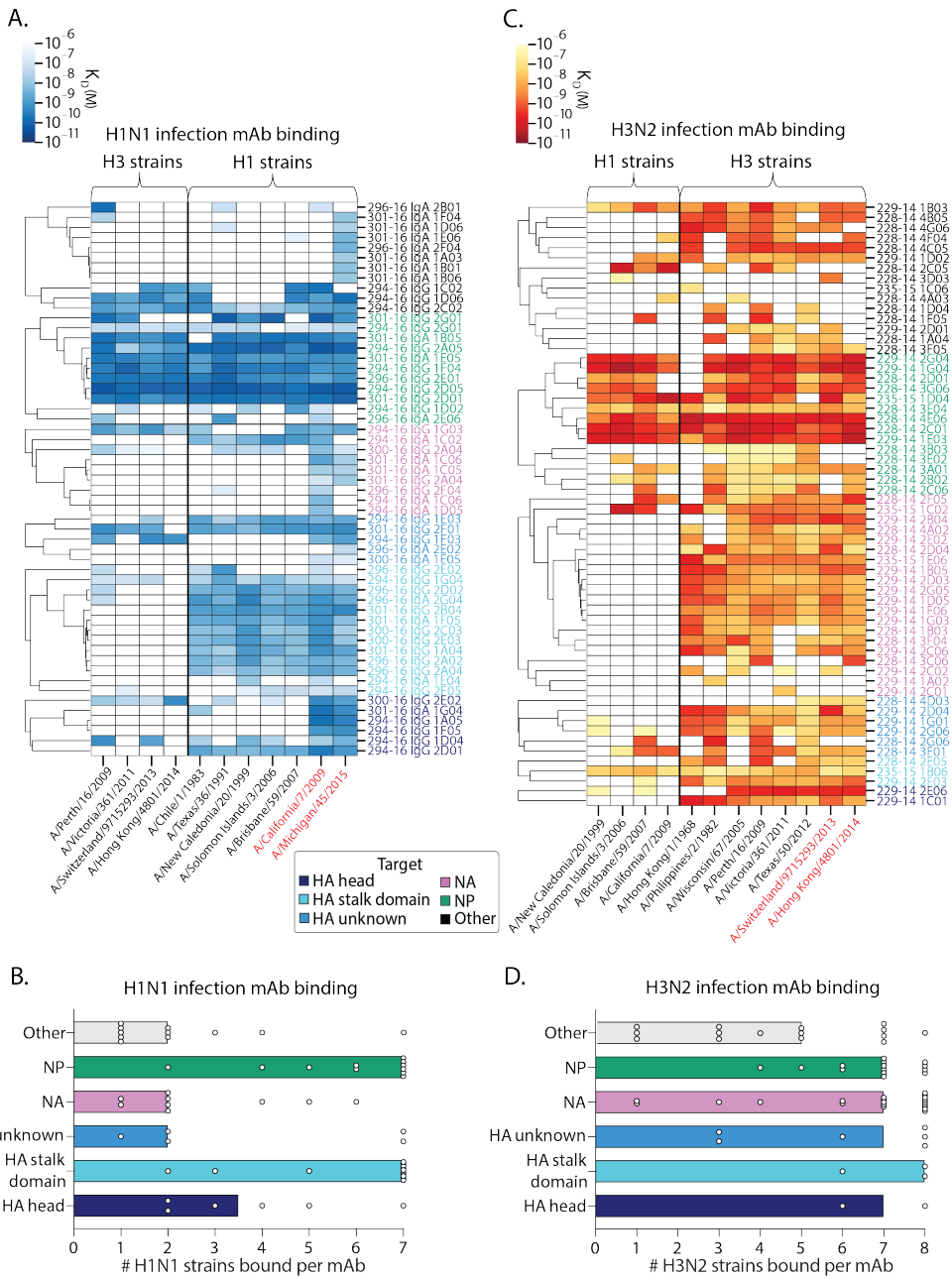

Figure 2.7. The degree of influenza virus infection-induced antibody cross-reactivity is influenced by antigen-reactivity and infecting subtype. (A, B) The viral binding breadth of H1N1 infection-induced mAbs is represented by heatmap analysis displaying affinity (K_D) for contemporary and historical H1N1 and H3N2 whole virus strains **(A)** and bar graphs summarizing the number of homosubtypic H1N1 viral strains bound per H1N1 infection-induced mAb (n= 55), subset by antigen specificity (**B**; bars indicate median). **(C, D)** The viral binding breadth of H3N2 infection-induced mAbs is represented by heatmap analysis displaying affinity (K_D) for contemporary and historical H3N2 and H1N1 whole viral strains **(C)** and bar graphs summarizing the number of homosubtypic H3N2 viral strains bound per H3N2 infection-induced mAb (n= 60), subset by antigen specificity (**D**; bars indicate median). Heatmap data are depicted as ELISA binding affinity (K_D) values for each individual mAb tested against the respective viruses, and antigen reactivity of each mAb is indicated by the color coding in the legend. For both heatmaps, the strains colored in red text represent contemporary circulating strains during the time of mAb isolation. Data are representative of 2–3 independent experiments performed in duplicate.

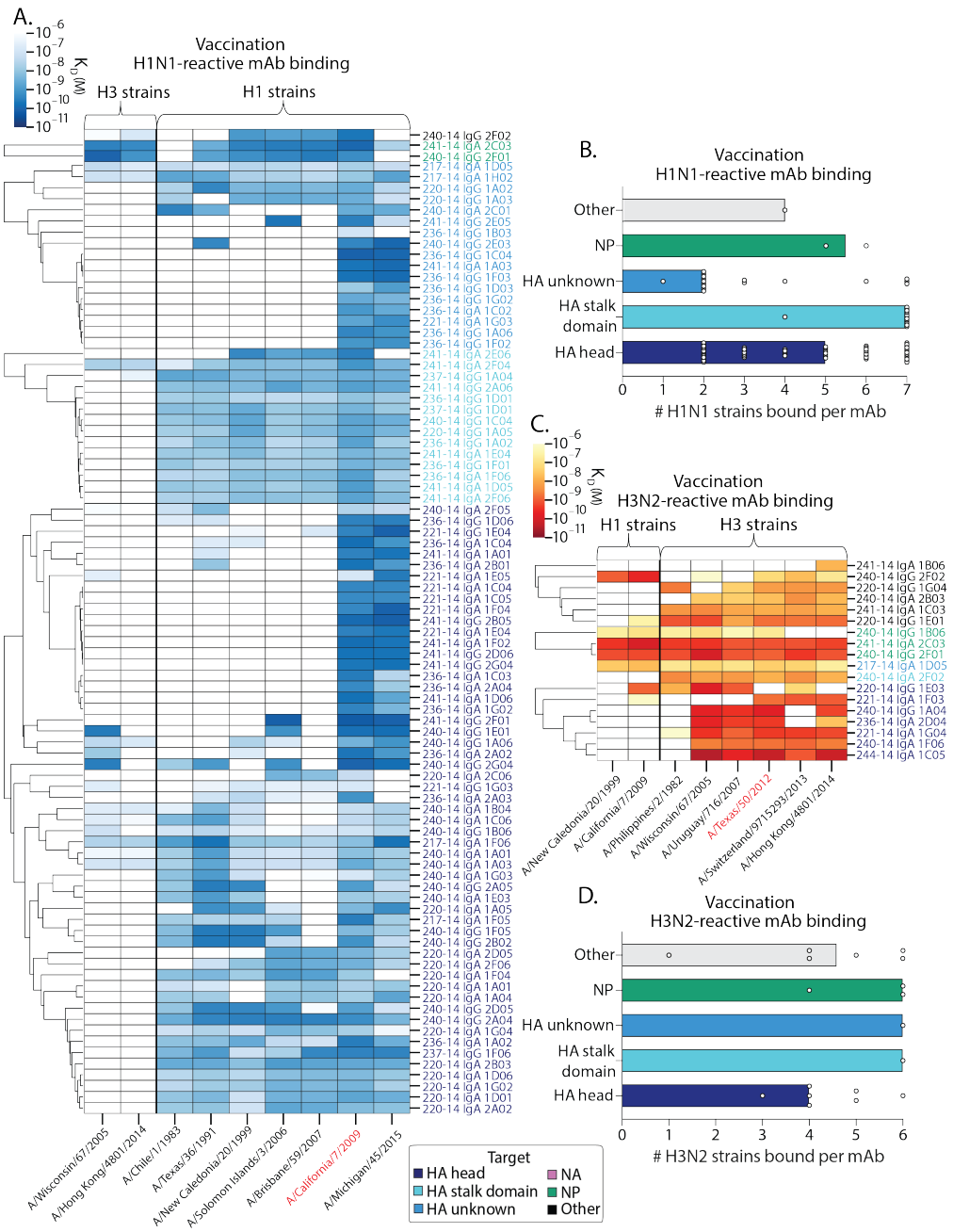

Figure 2.8. The degree of influenza virus vaccination-induced antibody cross-reactivity is influenced by antigen-reactivity and vaccine strain-reactivity. **(A, B)** The viral binding breadth of H1N1-reactive quadrivalent vaccine-induced mAbs is represented by heatmap analysis displaying affinity (K_D) to contemporary and historical H1N1 and H3N2 whole viral strains **(A)** and bar graphs summarizing the number of homosubtypic H1N1 viral strains bound per H1N1-reactive mAb (n= 90), subset by antigen specificity (**B**; bars indicate median). **(C, D)** The viral binding breadth of H3N2-reactive quadrivalent vaccine-induced mAbs is represented by heatmap analysis displaying affinity (K_D) to contemporary and historical H3N2 and H1N1 whole viral strains **(C)** and bar graphs summarizing the number of homosubtypic H3N2 viral strains bound per H3N2-reactive mAb (n= 18), subset by antigen specificity (**D**; bars indicate median). Heatmap data are depicted as ELISA binding affinity (K_D) values for each individual mAb tested against the respective viruses, and antigen reactivity of each mAb is indicated by the color coding in the legend. For both heatmaps, the strains colored in red text represent the vaccinating strains present in the vaccines at the time of mAb isolation. Data are representative of 2–3 independent experiments performed in duplicate.

2.4.5 Early infection-induced antibodies are less protective in mice compared to vaccination-induced antibodies

The majority of early cross-reactive infection-induced mAbs failed to neutralize virus in vitro, suggesting that they may have limited protective ability in vivo in comparison to HA head-reactive mAbs induced by vaccination. To evaluate this possibility, we prophylactically administered representative cocktails of mAbs covering the spectrum of reactivities induced by infection versus vaccination (Figure 2.9A). The mAb cocktails were administered intraperitoneally at a dose titration of 5 mg/kg, 1 mg/kg, and 0.2 mg/kg to BALB/c mice, which were intranasally challenged two hours post mAb transfer with a lethal dose (10 LD_{50}) of mouse-adapted A/Netherlands/602/2009 H1N1 or A/Philippines/2/1982 H3N2 influenza virus. We generated four separate cocktails each comprising 10 mAbs: an H1N1 infection-induced cocktail, an H3N2 infection-induced cocktail, and two cocktails of H1N1- and H3N2-reactive vaccination-induced mAbs (Table 2.4), all of which were representative of typical binding and neutralization characteristics within each cohort.

H1N1-reactive vaccination-induced mAbs were potently protective against 10 LD_{50} of A/Netherlands/602/2009 virus at 1 mg/kg, whereas H1N1 infection-induced mAbs failed to provide protection, with mice displaying increased mortality and weight loss relative to mice receiving the vaccination cocktail ($p = 0.0003$, survival; Figure 2.9B, C). While H3N2-reactive vaccination-induced mAbs could provide protection at 1 mg/kg against A/Philippines/2/1982 virus, H3N2 infection-induced mAbs provided substantially reduced protection when administered at the same dose ($p = 0.0080$, survival; Figure 2.9D, E). For both infection- and vaccination-induced mAb cocktails, 100% protection was provided at the highest dose of 5 mg/kg, and neither infection- nor vaccination-induced mAbs provided full protection at 0.2 mg/kg (Figure 2.10).

The limited protective ability of infection-induced mAbs suggested that the specificities recalled by infection in this cohort were subpar for protection compared to vaccination-induced mAbs, which largely targeted the HA head. We therefore tested the protective ability of mAbs targeting distinct epitopes by prophylactically administering

cocktails of H1N1-reactive mAbs targeting the HA head, HA stalk domain, NA, or NP (Table 2.5) into BALB/c mice intraperitoneally, which were subsequently intranasally challenged with 10 LD_{50} of mouse-adapted A/Netherlands/602/2009 H1N1. Of note, HA stalk domain-, NA-, and NP-reactive mAbs were derived from infected individuals, while HA head-reactive mAbs were induced by both infection and vaccination. At 5 mg/kg, we saw clear resolution of the different potencies of these cocktails. Mice receiving the HA head-reactive mAb cocktail lost the least weight, followed by the HA stalk domain mAb cocktail, the NA mAb cocktail, which provided intermediate protection, and finally, the NP-reactive mAb cocktail, which provided the least protection (Figure 2.9F, G). At 1 mg/kg, the protective ability of the HA stalk domain-reactive mAb cocktail decreased to the same degree as the NA-reactive mAb cocktail, and mice in these groups lost substantially more weight relative to the HA head-reactive mAb cocktail (Figure 2.9H, I). At both 5 mg/kg and 1 mg/kg, the NP-reactive mAbs provided minimal protection in vivo.

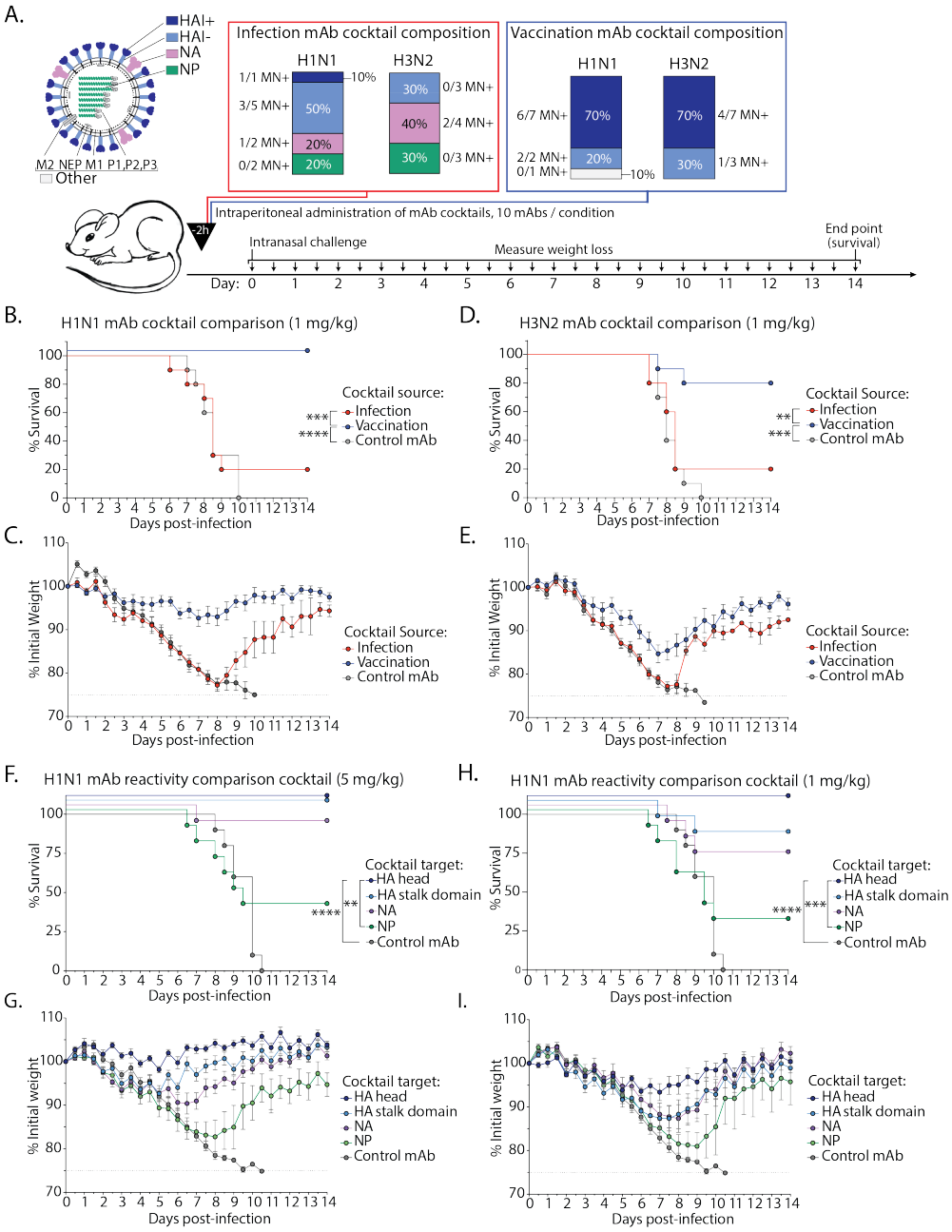

Figure 2.9. Influenza virus infection-induced antibodies are less protective in vivo than vaccination-induced antibodies. (**A**) Bar charts display the composition of H1N1 and H3N2 infection- and vaccination-induced mAb cocktails. For the infection cocktails, all H1N1 mAbs were originally induced by H1N1 infection, and all H3N2 mAbs were originally induced by H3N2 infection. The vaccination cocktails were comprised of either H1N1- or H3N2-reactive vaccination-induced mAbs. Each cocktail reflects the antigen reactivity and neutralization frequencies seen in our analyses. (**B, C**) Survival and weight loss curves display in vivo prophylactic protective ability of H1N1 infection- and vaccination-induced mAb cocktails administered intraperitoneally at 1 mg/kg to 6–8-week-old female BALB/c mice challenged with 10 LD_{50} mouse-adapted A/Netherlands/602/2009 H1N1 virus. (**D, E**) Survival and weight loss curves display in vivo prophylactic protective ability of H3N2 infection and vaccination-induced mAb cocktails administered intraperitoneally at 1 mg/kg to 6–8-week-old female BALB/c mice challenged with 10 LD_{50} mouse-adapted A/Philippines/2/1982 H3N2 virus. (**F, G, H, I**) Survival and weight loss curves display in vivo prophylactic protective ability of HA head-, HA stalk domain-, NA-, and NP-reactive mAb cocktails (5 mAbs/cocktail) administered intraperitoneally at 5 mg/kg (**F, G**) or 1 mg/kg

Figure 2.9, continued
(**H, I**) to 6–8-week-old female BALB/c mice challenged with 10 LD_{50} mouse-adapted A/Netherlands/602/2009 H1N1 virus. Data are representative of two independent experiments and depicted as survival (**B, D, F, H**) and weight loss (**C, E, G, I**) curves. Statistical significance for survival curves was determined using a Mantel-Cox log-rank test (**B**: ****p<0.0001, ***p=0.0003; **D**: ***p=0.0002, **p=0.0080; **F**: ****p<0.0001, **p=0.0047; **H**: ****p<0.0001, ***p=0.0004). Weight loss is presented as mean ± SEM (n=9–10 mice per group).

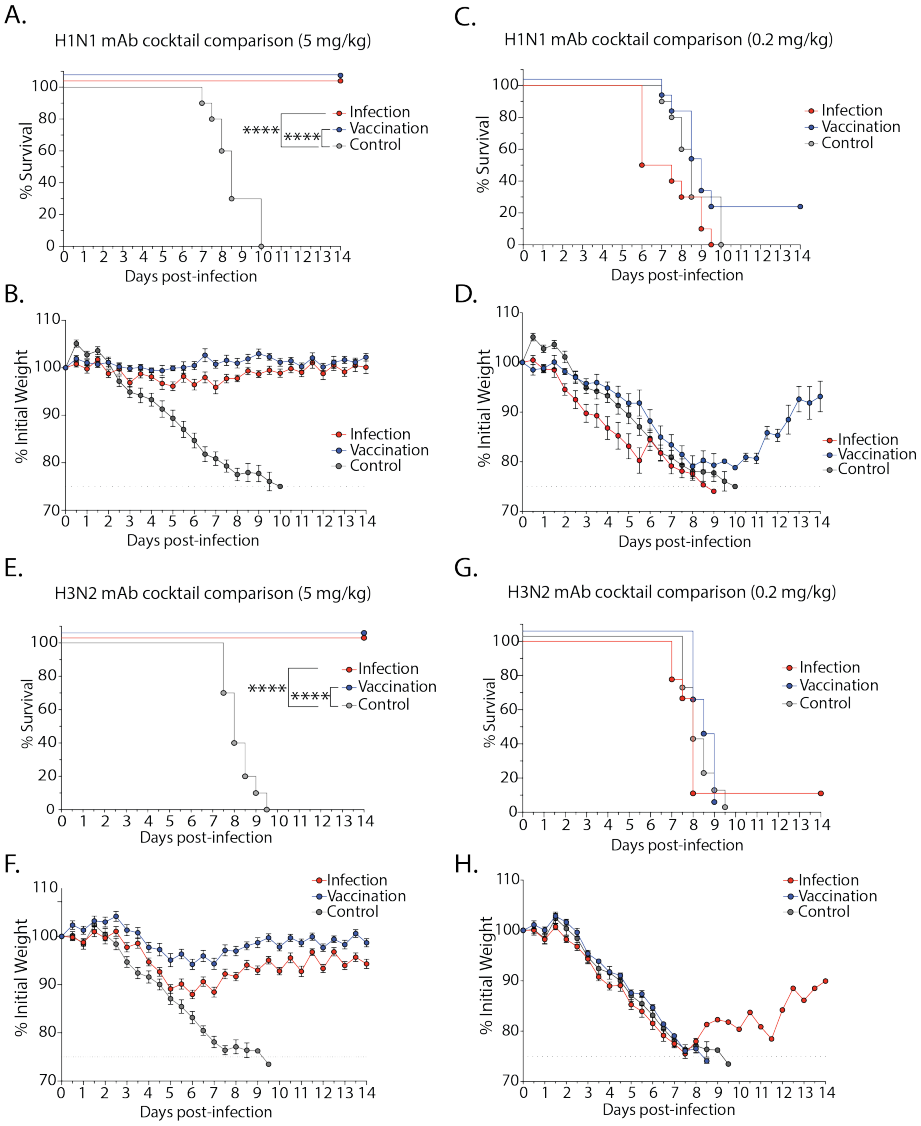

Figure 2.10. Prophylactic protection of influenza virus infection- and vaccination-induced antibodies at 0.2 mg/kg and 5 mg/kg. (**A–D**) Weight loss and survival curves display in vivo prophylactic protective ability of infection- and vaccination-induced mAb cocktails administered intraperitoneally at 5 mg/kg (**A–B**) or 0.2 mg/kg (**C–D**) to 6–8-week-old female BALB/C mice challenged with 10 LD_{50} mouse-adapted A/Netherlands/602/2009 H1N1 virus. (**E–H**) Weight loss and survival curves display in vivo prophylactic protective ability of infection and vaccination-induced mAb cocktails administered intraperitoneally at 5 mg/kg (**E–F**) or 0.2 mg/kg (**G–H**) to 6–8-week-old female BALB/C mice challenged with 10 LD_{50} mouse-adapted A/Philippines/2/1982 H3N2 virus. Data are representative of two independent experiments and depicted as survival (**A, C, E, G**) and weight loss (**B, D, F, H**) curves. Statistical significance for survival curves was determined using a Mantel-Cox log-rank test, ****p<0.0001. Weight loss is presented as mean±SEM (n=9–10 mice per group).

Table 2.4. Monoclonal antibodies used for influenza virus infection- and vaccination-induced antibody cocktails. NL09: A/Netherlands/602/2009 H1N1 virus; Phil82: A/Philippines/2/1982 H3N2 virus.

Infection-induced mAb cocktails			
H1N1 Infection	**Antigen Reactivity**	**Heterosubtypic**	**Neutralizing (NL09)**
294 1A05	HA head	No	Yes
294 1E03	HA unknown	Yes	No
296 2A04	HA stalk/unknown	No	Yes
296 2E02	HA stalk/unknown	Yes	No
296 2G04	HA stalk/CR9114 epitope	Yes	Yes
301 1A04	HA stalk/CR9114 epitope	No	Yes
294 1C02	NA/near active site	No	Yes
294 1G03	NA/unknown	Yes	No
296 2E01	NP	Yes	No
301 1E05	NP	Yes	No
H3N2 Infection	**Antigen Reactivity**	**Heterosubtypic**	**Neutralizing (Phil82)**
229 1G01	HA unknown	Yes	No
229 2G06	HA unknown	Yes	No
228 3F01	HA unknown	Yes	No
229 1F06	NA/active site	No	No
229 1G03	NA/active site	No	Yes
229 1B05	NA/near active site	No	No
229 2C06	NA/near active site	No	Yes
228 2C06	NP	Yes	No
228 3A01	NP	Yes	No
235 1D04	NP	Yes	No
Vaccination-induced mAb cocktails			
H1N1-reactive	**Antigen Reactivity**	**Heterosubtypic**	**Neutralizing (NL09)**
220 2F06	HA head	No	Yes
236 IgA 1A02	HA head	No	No
236 IgG 1A02	HA stalk/unknown	No	Yes
236 1C04	HA head	No	Yes
236 1D01	Other	No	No
236 2A04	HA head	No	Yes
240 1A01	HA head	Yes	Yes
241 2F01	HA head	No	Yes
240 1C04	HA stalk/CR9114 epitope	No	Yes
240 1E01	HA head	Yes	Yes
H3N2-reactive	**Antigen Reactivity**	**Heterosubtypic**	**Neutralizing (Phil82)**
220 1E03	HA head	No	Yes
220 1G04	HA head	No	No
240 1A06	HA head	Yes	Yes
217 1D05	HA/unknown	Yes	No
008-10 5E04	HA head	Yes	No
217 1H02	HA/unknown	Yes	Yes
240 2F02	HA stalk	No	No
034 3E01	HA head	Yes	Yes
DR2A02	HA head	No	Yes
041 1C04	HA head	Not tested	No

Table 2.5. Monoclonal antibodies used in antigen comparison cocktails.

HA Head	Heterosubtypic	Neutralizing (H1)	Source
294 1A05	No	Yes	Infection
236 1C04	No	Yes	Vaccination
014 3A02	Yes	Yes	Vaccination
019 3E05	Yes	Yes	Vaccination
039 5E03	No	Yes	Vaccination
HA Stalk			
296 2A04	No	Yes	Infection
301 1A04	No	Yes	Infection
296 2D02	Yes	Yes	Infection
296 2G04	Yes	Yes	Infection
294 1G04	Yes	No	Infection
NA			
300 2A04	Yes	Yes	Infection
301 1C05	No	No	Infection
296 2F04	No	No	Infection
294 1C02	No	Yes	Infection
294 1G03	Yes	No	Infection
NP			
296 2E01	Yes	No	Infection
294 1F04	Yes	No	Infection
301 1B05	Yes	No	Infection
301 1E05	Yes	No	Infection
294 1D02	Yes	No	Infection

2.5 DISCUSSION

It is well-appreciated that protective antibody responses to influenza in adults are biased by past exposures, explained by the concept of original antigenic sin. However, it remains unclear how preexisting immunity shapes the immunodominance hierarchy among influenza virus proteins targeted early after natural infection and seasonal vaccination in humans and how such hierarchies correlate with protection. In this study, we revealed that preexisting immunity biased the early antibody response to infection toward conserved yet less protective viral epitopes in an original antigenic sin-like fashion. Most of the B cells activated as plasmablasts in our infected cohort targeted the HA stalk domain, NA, NP, and other unknown viral antigens, and the majority exhibited equal or stronger affinity to past strains relative to inducing strains. The minority of mAbs bound potently neutralizing HA stalk and NA epitopes, reflecting the immunosubdominance of these regions. Conversely, we identified that seasonal influenza vaccines induced early antibodies targeting highly cross-reactive and protective HA head epitopes, highlighting the value of influenza vaccination and

the potential of universal vaccine strategies that draw upon preexisting immunity to elicit protective antibody responses to conserved epitopes.

Whereas the landscape of protective specificities was diverse between infection and vaccination, we observed inherent differences in the ability of H1N1 and H3N2 viruses to induce cross-reactive antibody responses, regardless of exposure type. Reactivity to childhood and past viral strains was especially prominent for H3N2-reactive mAbs whether they were induced by vaccination or infection, which may result from the rapid evolutionary rate of the H3N2 HA (*72, 185*). As the HA head of H3N2 viruses rapidly mutates, repeated exposures to antigenically drifted H3N2 viruses could further bias the antibody response toward more conserved epitopes on HA or other viral antigens, as these are the only epitopes that will be recognized by the preexisting MBC repertoire upon exposure. Indeed, we observed increased targeting of NA, NP, and other unknown viral antigens in response to H3N2 infection, whereas H1N1 infection was more biased toward generating HA-reactive responses. Furthermore, we observed that vaccination generally induced a greater magnitude of H1N1-reactive plasmablasts relative to H3N2, consistent with findings from a recent study that suggested these differences may account for differential vaccine effectiveness against H1N1 and H3N2 viruses (*186*). In the future, it will be important to investigate the role of preexisting immunity in shaping antibody responses to H1N1 versus H3N2 viruses, which are largely contrasting in the severity of cases they inflict and in their rates of antigenic evolution.

Through this study, we uncovered a role for preexisting immunity in shaping broadly-reactive and neutralizing anti-HA head responses to vaccination. It is currently appreciated that influenza vaccination provides effective immunity to vaccine strains; however, immune pressure drives antigenic drift of the major head epitopes of circulating strains, limiting the effectiveness of seasonal vaccines (*167-170, 187, 188*). The extent to which seasonal vaccines elicit cross-reactive protective responses to the HA head remains unclear, and we hypothesized that preexisting immunity to HA may bias the induction of highly cross-reactive HA head-specific responses. Indeed, the majority of HA head-reactive mAbs induced by

vaccination exhibited broad binding to current, past, and drifted strains circulating years after mAb isolation, with the minority being strain-specific. As the overwhelming majority of these mAbs were neutralizing and potently protective in vivo, these data suggest that vaccination can harness preexisting immunity to induce more potently protective antibody responses than currently appreciated. Moving forward, it will be important to investigate mechanisms by which cross-reactive responses can be preferentially induced by vaccination in a durable fashion, in order to develop vaccines that effectively elicit long-lived protective responses at the population level.

In contrast to vaccination, infection induced a higher frequency of antibodies targeting conserved influenza virus epitopes on the HA stalk domain, NA, and NP, supported by previous serology studies (*177*). Whereas numerous studies have shown that antibodies reactive to the HA stalk and NA can provide potent viral neutralization and protection (*36, 50, 189-191*), approximately half of all HA stalk domain- and NA-reactive infection-induced mAbs isolated in this study were non-neutralizing, potentially reflecting an unappreciated role for original antigenic sin in inducing antibodies targeting conserved yet less protective epitopes on these antigens. Conversely, over 80% of stalk domain-binding antibodies induced by vaccination targeted neutralizing epitopes, highlighting the ability of influenza virus vaccination to induce protective stalk antibody responses. We identified several HA stalk domain-specific mAbs that did not compete with CR9114, a mAb specific for a well-characterized neutralizing stalk epitope (*184*), but did bind a headless HA stalk construct (*60*), signifying that these antibodies bind stalk epitopes yet to be characterized.

Consistent with the reduced neutralization potential of infection-induced mAbs, we identified that mixed-epitope cocktails of H1N1 and H3N2 infection-induced mAbs were less protective in vivo compared to vaccination-induced mAbs targeting the HA head. To date, few studies have directly compared the protective ability of mAbs targeting distinct conserved influenza virus epitopes on the HA stalk domain, NA, and NP relative to the HA head in vivo (*192*). Previous studies have shown that antibodies against the HA stalk are less potent than antibodies against the HA head in vitro but have the potential to confer robust

protection in vivo, consistent with our findings (*36*). It has also been shown that NA-reactive mAbs are protective in vivo (*50, 193*), though the NA-reactive mAbs from our cohort were less prophylactically protective relative to HA head and stalk domain-reactive mAbs. While NA-inhibiting antibodies reduce influenza illness and transmission, past studies have debated their role as an independent correlate of protection from initial infection, likely due to their inability to directly inhibit viral entry (*194-198*). All of the NP-reactive mAbs isolated in this study were non-neutralizing in vitro and provided limited protection in vivo, though some studies have suggested anti-NP mAbs may play a role in protection through antibody-dependent cellular cytotoxicity or complement-dependent cytotoxicity (*199*). In summary, our in vivo data highlight differences in how preexisting B cells reactive to distinct influenza epitopes provide protection against infection.

Inherent differences in exposure route as well as the nature of inactivated virus vaccines versus live viral infections are likely to create differences in antibody epitope targeting. The greater abundance of non-HA antigens during natural infection compared to vaccination may bias MBC recall to conserved yet less protective non-HA head epitopes, as MBCs targeting these regions are likely at an early competitive advantage. Moreover, memory CD4 T cells recognizing H1N1 and H3N2 viruses largely target NP- and NA-derived peptides, suggesting CD4 T cell help could influence MBC recall towards these epitopes (*200*). The antibody response to vaccination characterized in the elderly is similarly biased toward non-HA head epitopes, which may be due to the lack of new naïve B cells and adaptability of MBCs to new influenza viruses encountered with age, increased reliance on CD4 T cell help for B cell activation, and the competitive advantage of MBCs targeting conserved epitopes (*72*).

Our study was limited in that we were only capable of characterizing the early plasmablast response to infection in symptomatic patients from a single time point. Previous studies have shown that influenza virus infection can induce broad and durable antibody responses, which may be due to sustained antigen availability and priming of B cell and T cell responses (*178, 201*). Additionally, it has been shown that infection induces MBCs with

broad reactivity toward both the HA head and stalk, with evidence of adaptation to the infecting strain (*36, 202*). The induction of long-lived MBCs targeting conserved viral epitopes after natural infection could provide superior protection against future infections relative to the short-lived immunity induced by vaccination. Although we were able to show that our collection of infection-induced mAbs provided suboptimal protection in mice, it is unclear how antibody targeting of these epitopes affords protection in humans. Indeed, past studies have shown that non-HAI antibodies can serve as a correlate of protection against infection in humans, and natural infection is capable of providing long-lived protection from re-infection with the same subtype (*197, 198, 203, 204*). Future studies should assess the kinetics of epitope targeting across multiple time points at both the cellular and serological level to better determine correlates of protection. In addition, household cohort studies, controlled human infections, or vaccine efficacy studies will be required to determine whether preexisting immune biases toward particular viral epitopes directly affect susceptibility or protection in humans.

In order to understand the formation of bias within the adaptive immune repertoire, it is critical that we study the response to natural influenza virus infection versus vaccination in cohorts of different ages, particularly in naïve infants and children. In our study, we were only able to assess the antibody response in a limited number of adults, but future pediatric studies assessing mechanisms of imprinting will be key for evaluating which B cell specificities are recruited by primary infection. A pressing question in the field of influenza vaccine development is whether priming naïve children by initial infection or vaccination leads to better B cell-mediated immunity. It will be important to determine the extent to which children are capable of mounting antibody responses to conserved protective viral epitopes, and how age and degree of viral exposure correlates with antibody adaptability. On the opposite end, it is important to study whether and how high-dose and adjuvanted influenza vaccination of elderly individuals can overcome immunosenescence and promote adaption to new influenza viruses.

The precise epitopes that should be targeted for increased vaccine effectiveness is an area of active investigation. Our data confirm the well-accepted notion that vaccine-induced antibodies against the HA head domain are potently protective, but the age-old problem remains: constant immune pressure drives antigenic drift of the HA head, limiting the effectiveness of seasonal vaccines when circulating strains are not well matched (*167-170, 187, 188*). Moreover, it remains to be determined whether cross-reactive antibody responses to HA elicited by vaccination can provide potent and durable protection against antigenically drifted strains in humans. Although not as potently protective as antibodies against the HA head, antibodies against conserved HA stalk and NA epitopes are associated with protection against influenza virus infection (*198, 205-207*) and several vaccine platforms targeting these epitopes are in pre-clinical and clinical trials (*39, 60, 208, 209*). The best vaccination platform to achieve both viral binding breadth and potent protection may be one that drives naïve and MBC maturation against antigenically drifted HA head epitopes but can also induce potent antibodies against conserved HA and NA epitopes to protect against antigenically drifted and novel influenza viruses. Further studies on B cell immunodominance patterns in response to such vaccine platforms are necessary to understand whether antibodies can be induced against both conserved and non-conserved protective epitopes. Additionally, future research is warranted to address differences in the potency of antibodies targeting distinct epitopes on HA and NA, as not all conserved viral epitopes will be equally protective to target. In summary, our results point to inherent differences in the ability of influenza virus infection and vaccination to induce early protective antibody responses, largely dependent on preexisting immunity to distinct conserved epitopes and the IAV subtype encountered.

2.6 Methods

2.6.1 Study design

We recruited human participants approximately 7–11 days post-onset of influenza virus infection (2015–2016 H1N1 and 2014–2015 H3N2) or seven days post-vaccination (2010–2011 trivalent influenza vaccine, 2014–2015 quadrivalent influenza vaccine) to assess the role of immune history in shaping antibody targeting of conserved viral epitopes. We generated monoclonal antibodies (mAbs) from single cell sorted plasmablasts, which peak in expansion between day 5–14 and largely derive from the preexisting MBC pool. Notably, plasmablasts were not antigen bait-sorted, and there is no obvious bias in our mAb generation protocol toward particular influenza virus antigens. Therefore, the sampling of mAbs per individual is expected to be representative of the overall plasmablast specificities elicited. We generated and characterized mAbs from 7 infected individuals and 18 vaccinated individuals across multiple influenza seasons. Because vaccinated individuals from controlled seasonal vaccine trials were readily accessible to our group, we included more vaccinated individuals than infected individuals in our study. We characterized all influenza-reactive mAbs that could be isolated from individual participants within the limitations of the labor-intensive process of generating mAbs. We comprehensively characterized antigen specificity and viral cross-reactivity of all mAbs by ELISA, neutralization potency by microneutralization or plaque assay, and in vivo protective ability in a mouse model to identify how preexisting immunity shaped early antibody responses to natural influenza virus infection versus vaccination. Because these groups were vaccinated or infected in different years with the vaccinating and infecting strains distinct for each year, this study was unblinded and not randomized.

All studies were performed with the approval of the University of Rochester and the University of Chicago institutional review boards. Informed consent was obtained after the research applications and possible consequences of the studies were disclosed to study participants. Clinical information is detailed in Table 2.1 and Table 2.2. PCR-confirmed

influenza virus-infected individuals were recruited and only included in the study if they did not have co-infections and were not being treated with immunosuppressive therapies.

All experiments were done in accordance with the University of Chicago Institutional Animal Care and Use Committee and in adherence to the NIH Guide for the Care and Use of Laboratory Animals. Six to eight-week old female BALB/c mice were used for these studies as the virus dose was titrated in mice of this same age and sex. Nine to ten mice were used per group, and a power analysis was used to determine the number of mice per experiment. All mice from independent experiments were included in data analysis until the point of euthanasia, which occurred upon 25% weight loss from the initial starting weight or upon completion of the experiment (14 days). Mice were provided standard diet chow and water and were housed in the ABSL-2 facility within the Carlson Animal Research Facility at the University of Chicago.

2.6.2 Cell culture

Human embryo kidney (HEK) 293T cells (ThermoFisher) were maintained at 37°C with 5% CO_2 in Advanced Dulbecco's Modified Eagle Medium (Advanced DMEM, GIBCO) with 2% Ultra-Low IgG fetal bovine serum (FBS, GIBCO), 1% L-Glutamine (GIBCO), and 1% Antibiotic-Antimycotic (GIBCO). Madin-Darby canine kidney (MDCK) cells (ATCC or London) were maintained in culture at 37°C with 5% CO_2 in Dulbecco's Modified Eagle Medium (DMEM, GIBCO) supplemented with 10% FBS (GIBCO), 1% L-Glutamine (GIBCO), and 1% penicillin-streptomycin (GIBCO).

2.6.3 Viruses and recombinant proteins

Influenza viruses used in all assays were grown in-house in specific pathogen-free (SPF) eggs, harvested, purified, and titered. Recombinant HA and NA proteins derived from A/Michigan/45/2015 (H1N1), A/California/7/2009 (H1N1), A/Hong Kong/4801/2014 (H3N2), A/Switzerland/9715293/2013 (H3N2), A/Texas/50/2012 (H3N2), A/Perth/16/2009 (H3N2), and A/Philippines/2/1982 (H3N2) were obtained from

Biodefense and Emerging Infections Research Resources Repository or kindly provided as gifts from the Krammer laboratory at Icahn School of Medicine at Mount Sinai. A/Texas/36/1991 and A/Chile/1/1983 H1N1 viruses were provided by the Hensley laboratory at The University of Pennsylvania. Stabilized trimeric headless hemagglutinin protein was provided by Dr. Lynda Coughlan at Icahn School of Medicine at Mount Sinai. Recombinant NP proteins derived from A/Puerto Rico/8/1934 (H1N1) and A/Aichi/2/1968 (H3N2) were obtained from Sino Biological.

2.6.4 Monoclonal antibodies

Monoclonal antibodies were generated as previously described (*44, 179, 210*). Peripheral blood was obtained from each individual 7 days post-vaccination or approximately 7–11 days post-onset of infection. Lymphocytes were isolated and enriched for B cells using RosetteSep human B cell negative selection enrichment cocktail (STEMCELL). Enriched B cells were stained for 30 min with anti-human CD3 FITC, clone 7D6 (Invitrogen; 1:50 dilution), anti-human CD19 Pacific Blue, clone H1B19 (Biolegend; 1:100 dilution), anti-human CD27 PE, clone O323 (Biolegend; 1:100 dilution), and anti-human CD38 AF647, clone HIT2 (Biolegend; 1:200 dilution) in 500 mL 1X PBS supplemented with 0.2% bovine serum albumin (Sigma). Plasmablasts ($CD3^-$ $CD19^+CD27^{hi}CD38^{hi}$) were single-cell-sorted into 96-well plates and immunoglobulin heavy and light chain genes were amplified by reverse transcription polymerase chain reaction (RT-PCR). Briefly, the first PCR of a two-step nested PCR was performed on amplified cDNA templates from individual plasmablasts. Three separate PCRs were carried out to amplify heavy, kappa, and lambda chain genes using DreamTaq Green PCR 2× MasterMix (ThermoFisher). A second nested PCR was then performed using the first PCR product as a template. Second PCR products were then sequenced, and the first PCR product was used to perform a cloning PCR for cloning heavy and light chain genes into human IgG1 expression vectors. The first PCR, second PCR, and cloning PCR primers for heavy, kappa, and lambda chain genes were obtained from IDT Technologies and detailed in Table 1 of

a previously published protocol from our group (*44*). Expression vectors for heavy and light chain pairs corresponding to individual mAbs were then co-transfected into HEK 293T cells (ThermoFisher). Secreted mAbs were purified from the supernatant using protein A agarose beads (ThermoFisher).

2.6.5 Enzyme-linked immunosorbent assay (ELISA)

High-protein binding microtiter plates (Costar) were coated with 8 hemagglutination units (HAU) of virus in carbonate buffer per well or with recombinant HA, NA, or NP, or headless HA stalk construct at 1 μg/ml in phosphate-buffered saline (PBS) overnight at 4°C. Plates were washed the next morning with PBS + 0.05% Tween 20 and blocked with PBS containing 20% FBS for 1 hr at 37°C. Antibodies were then serially diluted 1:3 starting at 10 μg/ml and incubated for 1 hr at 37°C. Horse radish peroxidase (HRP)-conjugated goat anti-human IgG antibody diluted 1:1000 (Jackson Immuno Research) was used to detect binding of mAbs, and plates were subsequently developed with Super Aquablue ELISA substrate (eBiosciences). Absorbance was measured at 405 nm on a microplate spectrophotometer (BioRad). To standardize the assays, control antibodies with known binding characteristics were included on each plate and the plates were developed when the absorbance of the control reached 3.0 OD_{405} units. To determine mAbs that bound the HA head, HAI assays were performed. To determine which mAbs bound the HA stalk domain, competition ELISAs were carried out using the known stalk-binding mAb CR9114 as a competitor mAb (*184*), or by performing ELISAs using chimeric HA (cH5/1; cH7/3) and a headless HA stalk construct derived from the stalk of A/Brisbane/59/2007 (*60*). Notably, all viruses used in virus-specific ELISAs for the study are shown in Figure 2.7 and Figure 2.8. All experiments were performed in duplicate.

2.6.6 NA enzyme-linked lectin assay (ELLA)

ELLAs were performed as previously described (*211*). Briefly, flat-bottom 96-well plates (Thermo Scientific) were coated with 100 μL of fetuin (Sigma Aldrich) at 25 μg/ml

and incubated at 4°C overnight. MAbs were serially diluted two-fold at a starting concentration of 300 μg/ml in Dulbecco's phosphate-buffered saline (DPBS) containing 0.133 g/L $CaCl_2$ and 0.1 g/L $MgCl_2$ with 0.05% Tween 20 and 1% bovine serum albumin (DPBSTBSA), then incubated in fetuin-coated plates with an equal volume of the desired antigen dilution in DPBSTBSA. Plates were sealed and incubated for 20 hr at 37°C. Plates were then washed six times with PBS 0.05% Tween 20, and 100 ml/well of HRP-conjugated peanut agglutinin lectin (PNA-HRPO, Sigma Aldrich) in DPBSTBSA was added at room temperature (RT) for 2 hr in the dark. Plates were washed six more times and subsequently developed with Super Aquablue ELISA substrate (eBiosciences). Absorbance was read at 405 nm on a microplate spectrophotometer (BioRad). Data was analyzed using Prism software and the 50% inhibitory concentration (IC_{50}) was determined as the concentration at which 50% of NA activity was inhibited compared to negative control (PBS). All experiments were performed in duplicate.

2.6.7 NA-STAR assay

NA-STAR assays were performed according to the Resistance Detection Kit manufacturer's instructions (Applied Biosystems). Briefly, 25 μL test mAbs (starting concentration of 100 μg/mL) were prepared in serial two-fold dilutions in NA-STAR assay buffer, mixed with 25 μL of 4X EC_{50} of virus, and incubated at 37°C for 20 min. After adding 10 μL of 1000X diluted NA-STAR substrate, the plates were incubated at RT for 30 min. The reaction was stopped by adding 60 μL of NA-STAR accelerator. Chemiluminescence was determined by using the DTX 880 plate reader (Beckman Coulter). IC_{50} values were determined using the Prism software. All experiments were performed in duplicate.

2.6.8 Hemagglutination Inhibition Assay

Viruses were diluted to 8 HA units/50 μl in PBS. 25 μl was combined with an equal volume of mAb serially diluted 1:3 in PBS in duplicate, and subsequently incubated at RT

for 45 min. 50 µl of 0.5% Turkey red blood cells (Lampire Biological) was added to each well and incubated for 1 hr at RT. Minimum effective concentrations were then calculated based on the final dilution of mAb for which hemagglutination inhibition was observed. All experiments were performed in duplicate.

2.6.9 Microneutralization assay

Microneutralization assay for mAb characterization was carried out as previously described (*50, 102*). MDCK cells were maintained in DMEM supplemented with 10% FBS, 1% L-Glutamine, and 1% penicillin-streptomycin at 37°C with 5% CO_2. On the day before the experiment, confluent MDCK cells in a 96-well format were washed twice with sterile PBS and incubated in minimal essential medium (MEM) supplemented with 1 µg/ml tosyl phenylalanyl chloromethyl ketone (TPCK)-treated trypsin. Serial two-fold dilutions (starting concentration 128 µg/ml) of mAb were mixed with an equal volume of 100 50% tissue culture infectious doses ($TCID_{50}$) of virus and incubated for 1 hr at 37°C. The mixture was removed, and cells were cultured for 20 hr at 37°C with 1X MEM supplemented with 1 µg/ml TPCK-treated trypsin and appropriate mAb concentration. Cells were washed twice with PBS, fixed with 80% ice cold acetone at -20°C for at least 1 hr, washed 3 times with PBS, blocked for 30 min with 3% bovine serum albumin in PBS (BSA-PBS) and then treated for 30 min with 2% H_2O_2. An anti-NP-biotinylated antibody (1:1000) in 3% BSA-PBS was incubated for 1 hr at RT. The plates were developed with Super Aquablue ELISA substrate at 405 nm. The signal from uninfected wells was averaged to represent 100% inhibition. The signal from infected wells without mAb was averaged to represent 0% inhibition. Duplication wells were used to calculate the mean and standard deviation (SD) of neutralization, and inhibitory concentration 50 (IC_{50}) was determined by a sigmoidal dose response curve. The inhibition ratio (%) was calculated as below: ((OD Pos. Control – OD Sample)/ (OD Pos. Control – OD Neg. Control)) * 100. The IC_{50} was determined using Prism software (GraphPad). All experiments were performed in duplicate.

2.6.10 Plaque reduction assay

Plaque assays were performed using the MDCK London cell line as previously described (*36*) with the exception that cells were incubated with the agar overlay for 48 hr. Plaques were counted, and the final mAb concentration that reduced the number of plaques to 50% was determined using GraphPad Prism software. The assay was performed in duplicate.

2.6.11 *In vivo* challenge experiments

MAbs were passively transferred into 6–8-week-old female BALB/c mice by intraperitoneal injection of 0.2, 1 and 5 mg/kg mAb cocktail. Negative control mice received 5 mg/kg of the anthrax-specific mAb 003-15D03 as an isotype control. Two hr post-mAb injection, mice were anesthetized with isoflurane and intranasally challenged with 10 LD_{50} of mouse-adapted A/Netherlands/602/2009 H1N1 virus diluted in 20 µl sterile 1x PBS to test protective ability of H1N1-binding mAbs, or A/Philippines/2/1982 H3N2 virus to test protective ability of H3N2-binding mAbs. As a read out, survival and weight loss were monitored twice a day for two weeks.

2.6.12 Clustering of monoclonal antibodies

Monoclonal antibodies (mAbs) were clustered based on their affinity for a panel of test viruses using a hierarchical clustering approach. First, each mAb was defined as a vector whose elements were the binding affinity (ELISA K_D) of that mAb against each of the H1N1 and H3N2 viruses in our test panel. Then, the Euclidean distance between each mAb was calculated. The unweighted pair group method with arithmetic mean (UPGMA) was applied to the distance matrix to obtain a hierarchical clustering of all mAbs, which was visualized as a dendrogram (Figure 2.7A, C and Figure 2.8A, C). Clustering was performed separately for groups of mAbs belonging to the depicted epitope-reactivity categories.

2.6.13 Statistical analysis

All statistical analyses were performed using Prism software (Graphpad Version 8.0). Sample sizes (n) for the number of mAbs are indicated directly in the figures or in the corresponding figure legends, and sample sizes (n) for animals, number of biological replicates for experiments, and specific tests for statistical significance used are indicated in the corresponding figure legends. P values less than or equal to 0.05 were considered significant. *p<0.05, **p<0.01, ***p<0.001, ****p<0.0001.

2.7 Acknowledgements: We kindly thank Scott E. Hensley and Seth Zost for providing influenza viruses and recombinant HA proteins. We are thankful to all individuals who participated in this study. We thank Katelyn Gostic and Matthew Knight for providing thoughtful discussion related to the manuscript. Lastly, we thank Sarah F. Andrews for the initial sample collection for the 2010–2011 trivalent influenza vaccine cohort. **Funding:** This project was funded in part by the National Institute of Allergy and Infectious Disease; National Institutes of Health grant numbers U19AI082724 (P.C.W.), U19AI109946 (P.C.W.), U19AI057266 (P.C.W.), the NIAID Centers of Excellence for Influenza Research and Surveillance (CEIRS) grant numbers HHSN272201400005C (P.C.W.) and HHSN272201400008C (F.K.; L.C.), and University of Chicago Committee on Immunology T32-AI007090 (H.L.D.) and T32-HL007605 (J.J.G.). S.C.[3] and P.A. were supported by NIH Young Investigator Award DP2AI117921 (S.C.) and NIH F32AI145177 (P.A.). **Author contributions:** H.L.D. and J.J.G. designed and performed experiments, analyzed the data, and wrote the manuscript. P.A. generated heat maps, imprinting probabilities, and provided feedback. M.H. performed mAb cloning. Y.-Q.C. and K.E.N. sorted plasmablasts and generated mAbs for the infection cohorts. Y.-Q.C. and O.S. performed NA-STAR and ELLA assays. N.-Y.Z. purified influenza viruses and provided materials. L.Y.-L.L., M.E.T., C.T.S., and A.-K.E.P. performed and assisted in mouse infection experiments. C.H. collected and processed samples and provided materials and feedback on the manuscript. D.B., S.C.[2], and H.A.U. performed ELISAs. S.C.[3] provided advice for experimental design

and critical feedback on the manuscript. F.K. and L.C. provided materials and helpful feedback on the manuscript. P.C.W. supervised the work and wrote the manuscript. **Competing interests:** All authors declare no conflicts of interest, and we have no related consulting or patents to disclose. **Data and Materials Availability:** All data associated with this study are in the paper or supplementary materials. All antibody sequences have been deposited to GenBank and are available under the following accession numbers: MW067375–MW067608 and MW079531–MW079816.

CHAPTER 3

ANTIBODY IMMUNODOMINANCE TO SARS-COV-2 INFECTION

Haley L. Dugan[1,14], Christopher T. Stamper[1,14], Lei Li[2,14], Siriruk Changrob[2], Nicholas W. Asby[3], Peter J. Halfmann[4], Nai-Ying Zheng[2], Min Huang[2], Dustin G. Shaw[1], Mari S. Cobb[5], Steven A. Erickson[2], Jenna J. Guthmiller[2], Olivia Stovicek[2], Jiaolong Wang[2], Emma S. Winkler[6x], Maria Lucia Madariaga[7], Kumaran Shanmugarajah[7], Maud O. Jansen[8], Fatima Amanat[9], Isabelle Stewart[2], Henry A. Utset[2], Jun Huang[1,3], Christopher A. Nelson[6], Ya-Nan Dai[6], Paige D. Hall[6], Robert P. Jedrzejczak[10,11], Andrzej Joachimiak[10,11,12], Florian Krammer[9], Michael S. Diamond[6xy], Daved H. Fremont[6], Yoshihiro Kawaoka[4,13], Patrick C. Wilson[1,2,15*]

Affiliations:

[1]Committee on Immunology, University of Chicago, Chicago, IL 60637, USA.

[2]University of Chicago Department of Medicine, Section of Rheumatology, Chicago, IL 60637, USA.

[3]Pritzker School of Molecular Engineering, University of Chicago, Chicago, IL 60637, USA.

[4]Influenza Research Institute, Department of Pathobiological Sciences, School of Veterinary Medicine, University of Wisconsin-Madison, Madison, WI 53711.

[5]Section of Genetic Medicine, University of Chicago, Chicago, IL 60637, USA.

[6]Departments of Medicine, [x]Pathology and Immunology, and [y]Molecular Immunology, Washington University School of Medicine, St Louis, MO 63130, USA.

[7]University of Chicago Department of Surgery, Chicago, IL 60637, USA.

[8]University of Chicago Department of Medicine, Chicago, IL 60637, USA.

[9]Department of Microbiology, Icahn School of Medicine at Mount Sinai, New York, NY 10029, USA.

[10]Center for Structural Genomics of Infectious Diseases, Consortium for Advanced Science and Engineering, University of Chicago, Chicago, IL 60637, USA.

[11]Structural Biology Center, X-ray Science Division, Argonne National Laboratory, Lemont, IL 60439, USA.

[12]Department of Biochemistry and Molecular Biology, University of Chicago, Chicago, IL 60637, USA.

[13]Division of Virology, Department of Microbiology and Immunology, Institute of Medical Science, University of Tokyo, 108-8639 Tokyo, Japan.

[14]These authors contributed equally.

[15]Lead Contact.

*Correspondence: wilsonp@uchicago.edu (P.C.W.)

3.1 ABSTRACT

Dissecting the evolution of memory B cells (MBCs) against SARS-CoV-2 is critical for understanding antibody recall upon secondary exposure. Here, we utilized single-cell sequencing to profile SARS-CoV-2-reactive B cells in 38 COVID-19 patients. Using oligo-tagged antigen baits, we isolated B cells specific to the SARS-CoV-2 spike, nucleoprotein (NP), open reading frame 8 (ORF8), and endemic coronavirus (HCoV) spike proteins. SARS-CoV-2 spike-specific cells were enriched in the memory compartment of acutely infected and convalescent patients several months post-symptom onset. With severe acute infection, substantial populations of endemic HCoV-reactive antibody-secreting cells were identified and possessed highly mutated variable genes, signifying preexisting immunity. Finally, MBCs exhibited pronounced maturation to NP and ORF8 over time, especially in older patients. Monoclonal antibodies against these targets were non-neutralizing and non-protective in vivo. These findings reveal antibody adaptation to non-neutralizing intracellular antigens during infection, emphasizing the importance of vaccination for inducing neutralizing spike-specific MBCs.

3.2 One sentence summary: Longitudinal analysis of memory B cells in SARS-CoV-2 infection reveals evolution toward non-protective viral targets, pronounced in older patients.

Published in Immunity 06 May 2021: Vol. 54 [entire article presented herein] (212)

3.3 Introduction

Since the emergence of SARS-CoV-2 in December 2019, the World Health Organization has reported over 125 million infections and 2.8 million deaths worldwide, with these statistics continuing to rise. Faced with such persistence, the prospect of re-infection or infection with newly emerging variants warrants studies evaluating the generation of durable B cell memory upon infection.

Early in the pandemic, several independent groups identified potently neutralizing antibodies against the SARS-CoV-2 spike protein, the major antigenic glycoprotein of the virus (*54, 124, 125, 129, 213, 214*). Since then, there has been a dedicated interest in the identification of durable memory B cells (MBCs) that can provide protection from re-infection. Our group and others have identified MBCs against the spike, nucleoprotein (NP) and open reading frame 8 (ORF8) proteins in convalescence, and some studies show these populations persist up to 6 months post-infection (*135, 136, 215, 216*). Beyond the identification of durable MBCs, spike-specific MBCs continue to adapt to SARS-CoV-2 up to 6 months post-infection, in a manner consistent with antigen persistence and ongoing germinal center reactions (*133, 134, 151*). Finally, recent data suggest that particular B cell subsets may be associated with disease severity, including the expansion of antibody-secreting cells (ASCs) and double negative B cells lacking surface expression of CD27 and IgD (*143, 217*).

Despite these advances, we lack a clear understanding of MBC immunodominance and adaptation to distinct SARS-CoV-2 antigens over time, and how this correlates with factors such as patient age or disease severity. Moreover, it remains to be determined whether MBCs to targets such as NP and ORF8 can provide protection from infection. Finally, the role of preexisting immunity to endemic human coronaviruses (HCoV) in shaping MBC responses to SARS-CoV-2 is poorly understood.

To address these knowledge gaps, we characterized the SARS-CoV-2-specific B cell repertoire in 38 COVID-19 patients, both severe acute and convalescent, approximately 1.5–5 months post-infection using single-cell RNA sequencing. Through this approach, we

provide a tool for evaluating human B cell subsets, immunodominance, and antibody adaptation to SARS-CoV-2, and have made a repository of over 13,000 antigen-specific antibody sequences available to the SARS-CoV-2 research community.

Our studies reveal that MBCs display substantial reactivity toward NP and ORF8, and continue to expand and adapt over time, particularly in older patients. While SARS-CoV-2 RBD-specific monoclonal antibodies (mAbs) were potently neutralizing and protective, we showed that anti-NP and anti-ORF8 mAbs failed to neutralize and provide protection *in vivo*. Analogous to findings in the influenza virus field, B cells to non-neutralizing viral targets may be preferentially induced in natural infection, and shaped by factors such as preexisting immunity and age (*72, 163*). Therefore, preexisting MBC bias to non-neutralizing targets in SARS-CoV-2 could impact susceptibility to or severity of re-infection. Together, these findings highlight the importance of SARS-CoV-2 vaccines, which are optimally formulated to develop protective MBC responses against the spike.

3.4 Results

3.4.1 Single cell RNA-seq reveals substantial complexity among endemic HCoV- and SARS-CoV-2-specific B cells

MBCs have potential to act as an early line of defense against viral infection, as they rapidly expand into antibody-secreting cells (ASCs) upon antigen re-encounter. To determine the landscape of MBC reactivity toward distinct SARS-CoV-2 and endemic HCoV spike viral targets, we collected peripheral blood mononuclear cells (PBMCs) and serum between April and May of 2020 from 10 severely infected acute subjects and 28 subjects upon recovery from SARS-CoV-2 viral infection (Table 3.1–3.4). In addition, 4 convalescent subjects returned approximately 4.5 months post-infection for a second blood draw, with similar volumes of whole blood processed across timepoints. Severe acute infected samples were collected days 0, 1, 3, 5, and 14 before (day 0) and after receiving convalescent plasma therapy (Table 3.3 and Table 3.4). All sampling timepoints were pooled from the same subjects for analysis due to low cell numbers.

Table 3.1. Convalescent COVID-19 patient information. *SOB = shortness of breath; SC = sinus congestion; ST = sore throat; BAP = body aches and pain; AP = abdominal pain; LOS = loss of smell; LOT = loss of taste. Starred symptom start to donation values indicate the value for follow-up visit donation (V2). Severity scoring method has been described previously (*136*).

Subject ID	Age	Sex	Reported symptoms*	Severity Score	Severity Category	Duration of symptoms (days)	Symptom start to donation (days)
24	34	M	Fatigue, cough, SOB, SC, fever, headache, BAP, diarrhea, LOS, LOT	19	Severe	12	41
20	31	M	Fatigue, cough, SOB, SC, fever, headache, BAP, LOS, LOT	29	Critical	19	48
564	24	F	Fatigue, cough, SOB, SC, ST, fever, headache, BAP, diarrhea, LOS, LOT	24	Severe	32	60
144	56	M	Fatigue, cough, SC, ST, headache, BAP, LOS	17	Moderate	23	54
214	47	M	Fatigue, cough, SOB, SC, ST, headache, BAP, LOS, LOT	20	Severe	24	59
171	37	F	Fatigue, cough, SOB, SC, fever, headache, BAP, diarrhea, LOS, LOT	21	Severe	16	44
92	35	M	Fatigue, cough, SC, ST, fever, headache, BAP	16	Moderate	16	47
48	45	F	Fatigue, cough, SOB, SC, ST, fever, headache, AP, diarrhea, LOS, LOT	19	Severe	8	40
537	36	M	Fatigue, cough, fever, BAP	13	Moderate	14	59
586	32	F	Fatigue, cough, SOB, SC, headache, BAP, AP, diarrhea	18	Moderate	17	61
376	36	F	Diarrhea, LOS, LOT	8	Mild	7	48
305	43	F	Fatigue, cough, SC, ST, fever, headache, BAP, LOS, LOT	14	Moderate	4	47
116	65	F	Cough, SOB, fever, LOS, LOT	13	Moderate	18	49
166	42	F	Fatigue, cough, SOB, SC, fever, headache, BAP, diarrhea, LOS, LOT	18	Moderate	17	55
155	47	F	Fatigue, cough, SOB, ST, fever, BAP, LOS, LOT	20	Severe	29	64

Table 3.1. Convalescent COVID-19 patient information, continued

609	26	F	Fatigue, SOB, ST, fever, headache, BAP, LOS, LOT	16	Moderate	7	57
130	52	M	Fatigue, SC, headache, LOS, LOT	10	Mild	7	35
281	70	M	Cough, fever, BAP	9	Mild	7	48
272	42	M	Fatigue, cough, SOB, fever, headache, BAP, LOS, LOT	18	Moderate	14	43
50	35	M	Fatigue, SC, fever, BAP, LOS, LOT	13	Moderate	10	40
65	40	F	Fatigue, SC, fever, headache, BAP, diarrhea, LOS, LOT	16	Moderate	13	47
33	36	M	Fatigue, cough, SOB, SC, fever, headache, BAP, AP, diarrhea, LOS, LOT	22	Severe	14	48
201	56	M	Fatigue, cough, SOB, SC, ST, fever, headache, BAP, LOS, LOT	20	Severe	18	58
218	51	F	Fatigue, cough, SOB, fever, headache, BAP, AP, diarrhea	19	Severe	19	48
266	19	F	Fatigue, cough, SC, headache, BAP	9	Mild	4	32, 137 V2*
356	51	F	Fatigue, cough, ST, fever, headache, BAP, AP, diarrhea, LOS, LOT	20	Severe	14	43, 137 V2*
407	34	M	Fatigue, cough, SC, fever, BAP, AP, diarrhea, LOS, LOT	16	Moderate	11	43, 131 V2*
210	47	M	Fatigue, cough, SOB, fever, headache, BAP, LOS, LOT	16	Moderate	7	41, 125 V2*

Table 3.2. Distribution of clinical parameters for convalescent COVID-19 patients included in the study.

Median Age	41
Mean Age	42
Mode Age	47
Range Age	19–70
Number of Males	14
Number of Females	14
Median Duration of Symptoms (days)	14
Mean Duration of Symptoms (days)	14
Mode Duration of Symptoms (days)	7
Range Duration of Symptoms (days)	4–32
Median symptom start to donation (days)	48
Mean symptom start to donation (days)	49
Mode symptom start to donation (days)	48
Range symptom start to donation (days)	32–64

Table 3.3. Severe acute COVID-19 patient information. *LOT: Loss of taste; ECMO: Extracorporeal membrane oxygenation. *AKA, above the knee amputation; CHF, congestive heart failure; DM, diabetes mellitus; DVT, deep venous thrombosis; ESRD, end-stage renal disease; HTN, hypertension; NAFLD, non-alcoholic fatty liver disease; PE, pulmonary embolism; PVD, peripheral vascular disease.

Subject ID	Age	Sex	Reported symptoms*	Symptom start to donation (days)	Co-morbidities*	COVID treatment
R1	57	M	Fever, cough, nausea	3	HTN, DM, NAFLD	Tocilizumab, mechanical ventilation
R2	61	M	Cough, weakness, hiccups, altered mental status	16	None	Hydroxychloroquine, nasal cannula
R3	51	F	Fever, cough, dyspnea	21	HTN, DM, PE, asthma	Remdesivir, tocilizumab, venovenous ECMO*
R4	70	F	Fever, altered mental status	2	HTN, Alzheimer's disease	Nasal cannula
R5	66	F	Altered mental status, dyspnea	9	HTN, PE/DVT, recent hospitalization for orthopedic procedure	Nasal cannula
R6	59	M	Fever, chills, decreased appetite, dizziness	20	HTN, DM	Remdesivir, tocilizumab, Venovenous ECMO
R7	57	M	Dyspnea	9	HTN, Myelodysplastic syndrome s/p stem cell transplant	Tocilizumab, anakinra, nasal cannula
R8	30	M	Fever, chills, fatigue, LOT*	13	Cystic fibrosis s/p bilateral lung transplant, DM	Room air
R9	78	M	Fever, cough	14	HTN, prostate cancer	High-flow nasal cannula
R10	86	F	Dyspnea, abdominal pain	6	ESRD on HD, stroke, PVD s/p AKA, DM, PE/DVT, CHF	Nasal cannula

Table 3.4. Distribution of clinical parameters for severe acute COVID-19 patients included in the study. *Samples were collected day 0 (pre-plasma transfusion), 1, 3, 5, and 14 post-plasma transfusion and all time points per subject were pooled for analysis due to low cell numbers. See methods for additional details.

Median Age	60
Mean Age	61.5
Mode Age	57
Range Age	30–86
Number of Males	6
Number of Females	4
Median symptom start to first donation* (days)	11
Mean symptom start to first donation* (days)	11
Mode symptom start to first donation* (days)	9
Median symptom start to last donation* (days)	25
Mean symptom start to last donation* (days)	25
Mode symptom start to last donation* (days)	23

To identify SARS-CoV-2-specific B cells, we used the SARS-CoV-2 (SARS2) spike protein, spike RBD, NP, and ORF8 to generate probes for bait-sorting enriched B cells for subsequent single-cell RNA sequencing analysis. This was done by conjugating distinct PE-streptavidin (SAV)-oligos to individual biotinylated antigens (Figure 3.1A). To control for non-specific B cell reactivity and B cells reactive to PE, we included an empty PE-SA-oligo, along with an irrelevant viral antigen control on APC, Hantavirus PUUV, to improve the specificity of sorting and downstream analysis. Finally, to understand the impacts of preexisting immunity to endemic HCoVs, which share up to 30% amino acid identity with the SARS2 spike, we included a cocktail of spike proteins from four HCoV strains that cause mild upper respiratory infections in the vast majority of individuals: HCoV-229E, HCoV-NL63, HCoV-HKU1, and HCoV-OC43, on an additional APC-SAV-oligo.

From a total of 38 subjects analyzed (including four matched follow-up visits ~5 months post-infection), we detected small percentages (0.02–1.25%) of SARS-CoV-2-reactive total $CD19^+$ B cells, which were subsequently used to prepare 5' transcriptome, immunoglobulin (Ig) VDJ, and antigen-specific probe feature libraries for sequencing (Figure

3.1A). We sorted on total CD19+ B cells with elevated mean fluorescence intensity in order to capture highly specific cells regardless of naïve-like or MBC origin, though a caveat of this approach may be the exclusion of lower affinity B cells. We integrated sequencing results from all 38 subjects using Seurat to remove batch effects and identified 16 transcriptionally distinct B cell clusters based on expression profiles (Figure 3.1B). Adopting the ROGUE scoring method, which compares how similar all transcriptomes within a cluster are to one another, we determined most clusters were highly pure, with the majority having a score over 0.9 (1.0 being 100% pure) (Figure 3.1C) (*218*). We next ensured our feature libraries correlated with single probe antigen-specific reactivity via a series of filtering steps to remove cells that were probe-negative, multi-reactive and non-specific, empty SAV-PE$^+$, or Hanta-PUUV$^+$. Due to the nature of this approach and the inability to clone antibodies from every B cell, it remains likely that a fraction of cells included in the analysis are non-specific and that a fraction of cells excluded either by gating or pre-filtering were actually specific. Therefore, our dataset represents only a subset of the total antigen-specific B cells induced by SARS-CoV-2. After all pre-filtering steps were complete, mapping only the cells that bound a single probe revealed that antigen-specific cells were enriched in distinct transcriptional clusters (Figure 3.1D, E), with considerable variation observed amongst individual subjects (Figure 3.2A, B). Notably, we did not identify obvious differences in B cell subset distribution or antigen reactivity in B cells from severe acute subjects analyzed early (days 0, 1, 3) or late (days 7, 14) post-convalescent plasma therapy (Figure 3.2C, D). In summary, this method revealed substantial complexity in the B cell response to distinct CoV antigens, which we then further dissected by subset.

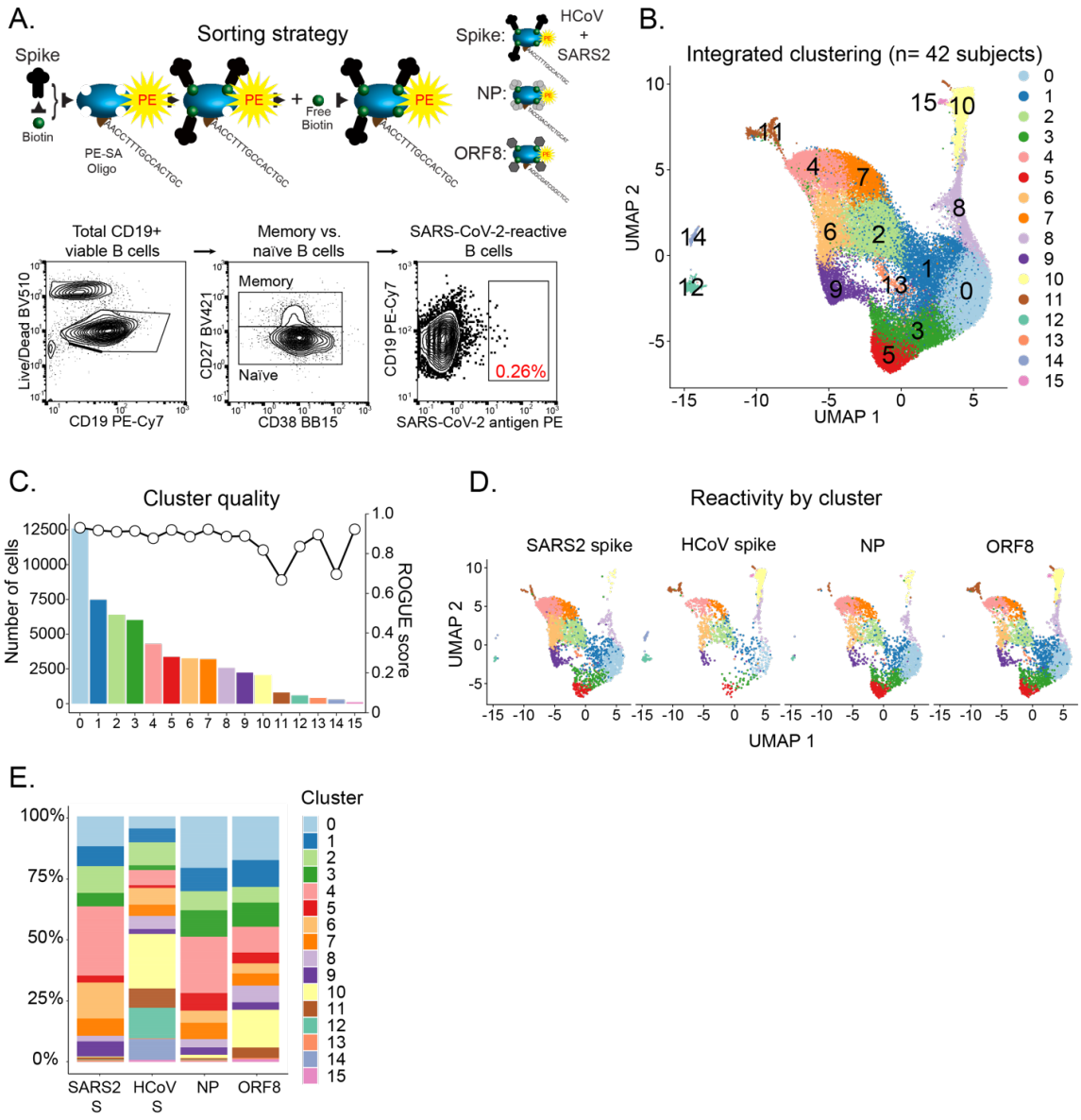

Figure 3.1. SARS-CoV-2-specific B cells comprise multiple distinct clusters. (**A**) Model demonstrating antigen probe preparation and representative gating strategy for sorting antigen-positive B cells. (**B**) Integrated transcriptional UMAP analysis of distinct B cell clusters (n=38 subjects; 55,656 cells). (**C**) Cluster quality score determined by ROGUE analysis. (**D**) UMAP projections showing CoV-specific cells used in all downstream analyses and the clusters they derive from. (**E**) Quantitative visualization of CoV-specific cells and their distributions across distinct clusters.

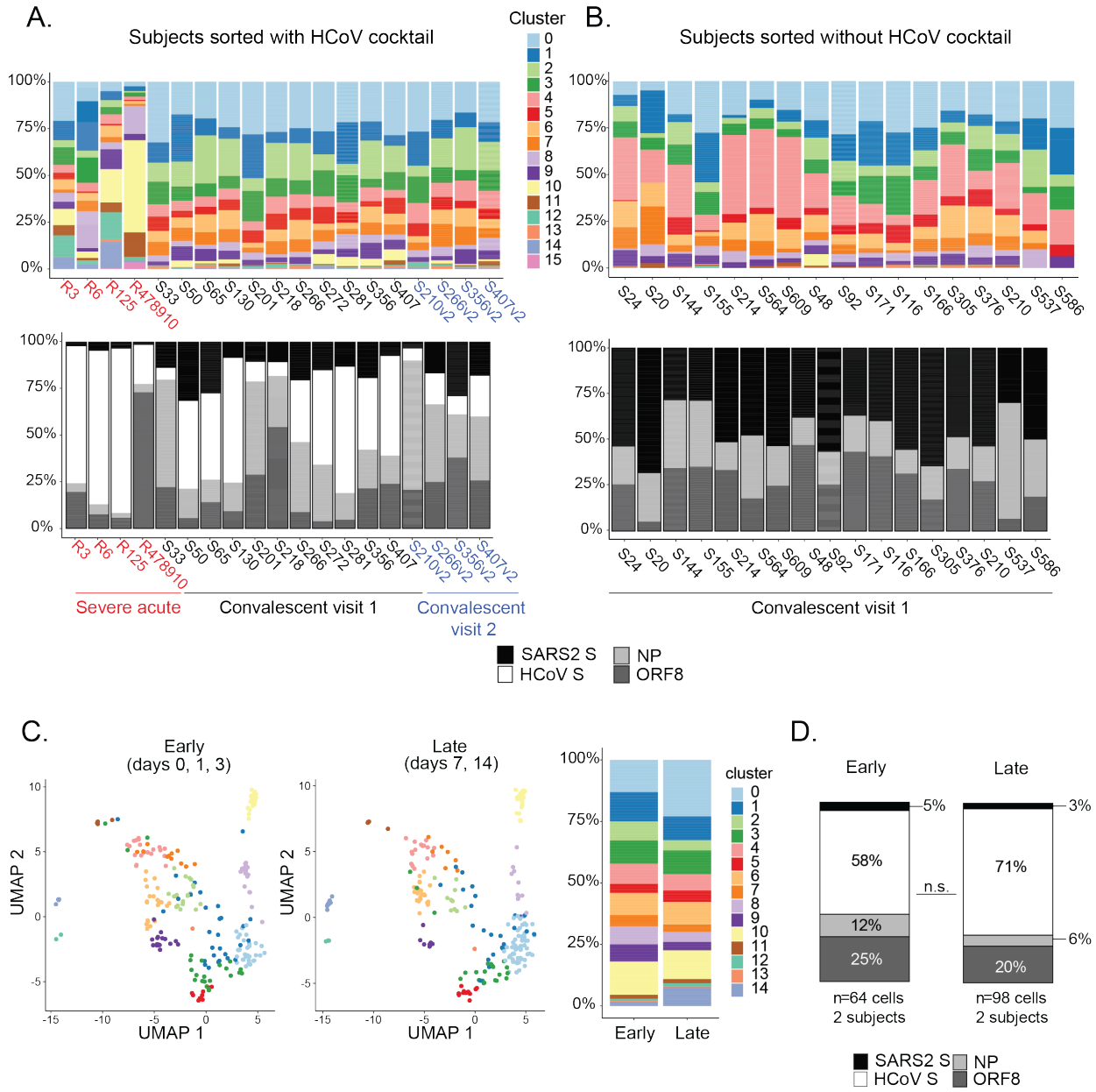

Figure 3.2. B cell cluster distribution and SARS-CoV-2 antigen specificity by subject. (**A**) Overall B cell subset distribution (top) and percentage of antigen-specific B cells targeting each antigen (bottom) for subjects sorted with SARS2 and endemic HCoV spike (S) proteins, as well as SARS2 RBD, NP, and ORF8. (**B**) Overall B cell subset distribution (top) and percentage of antigen-specific B cells targeting each antigen (bottom) for subjects sorted only with SARS2 spike, RBD, NP, and ORF8. Study cohort is indicated below each graph. (**C**) Integrated UMAP analysis showing cluster distribution for two severe acute subjects (R3 and R6) at pooled early (days 0, 1, 3) and late (days 7, 14) sampling time points post-convalescent plasma therapy (left) and summary of cluster distribution per timepoint (right). (**D**) Distribution in antigen-reactivity for pooled early and late timepoints post-convalescent plasma therapy for severe acute subjects R3 and R6. Statistics are Chi square test, n.s.

3.4.2 The SARS-CoV-2-specific B cell landscape is defined by naïve-like and memory B cell subsets

To discern the identity and specificity of each B cell cluster, we analyzed Ig repertoire, variable heavy (VH) chain somatic hypermutation (SHM) rates, and differentially expressed genes. Different B cell clusters varied widely in their degree of class-switch recombination (CSR) and SHM, consistent with the presence of both naïve-like and memory-like B cell clusters. Moreover, we quantitatively identified that targeting of viral antigens was variable across clusters (Figure 3.3A). To confirm B cell subset identities, we curated lists of differentially expressed genes across clusters associated with naïve B cells, MBCs, recent GC emigrant cells, ASCs, and innate-like B cells (including B1 B cells and marginal zone B cells) (Table 3.5 and Table 3.6; Figure 3.3B). Clusters 0, 1, 3, and 5 expressed Ig genes with little to no SHM or CSR and gene signatures associated with naïve B cells, suggesting these subsets are comprised of naïve-like B cells or very recently activated B cells (Figure 3.3A, B). Clusters with patterns of higher CSR and SHM were then further investigated for memory gene signatures. Based on expression of key genes, we identified clusters 4, 6, 7, and 8 as MBCs; clusters 2, 9, and 13 as recent memory or GC emigrants; and clusters 10, 11, and 15 as ASCs. Finally, we identified clusters 12 and 14 as innate-like in nature, though genes for these subsets are not well-defined in humans (Figure 3.3A, B). We next visualized how cells clustered based on identity by overlaying gene signatures for MBCs, recent GC emigrants, and ASCs (Table 3.6; Figure 3.4A–C). Using these gene signatures, we generated identity scores for each cluster and projected them onto UMAP, allowing us to visualize how closely associated clusters related to one another based on their B cell subset score (Figure 3.3C).

Of note, we identified that ASC clusters 10, 11, and 15 displayed a high degree of SHM, suggesting they may derive from preexisting memory that was driven against endemic HCoV spike proteins. These clusters also were predominantly class-switched to IgA, an isotype most associated with mucosal immunity (Figure 3.3A). To explore this possibility, we mapped the expression of genes related to mucosal surface homing and found them be

highly upregulated in ASC clusters, implying memory to past HCoV infection generates a large plasmablast response during SARS-CoV-2 infection that re-circulates in the blood and should localize to mucosal surfaces (Figure 3.4D). In conclusion, we confirm that the landscape of B cell reactivity to SARS-CoV-2 and HCoV antigens is defined by distinct naïve-like and MBC subsets.

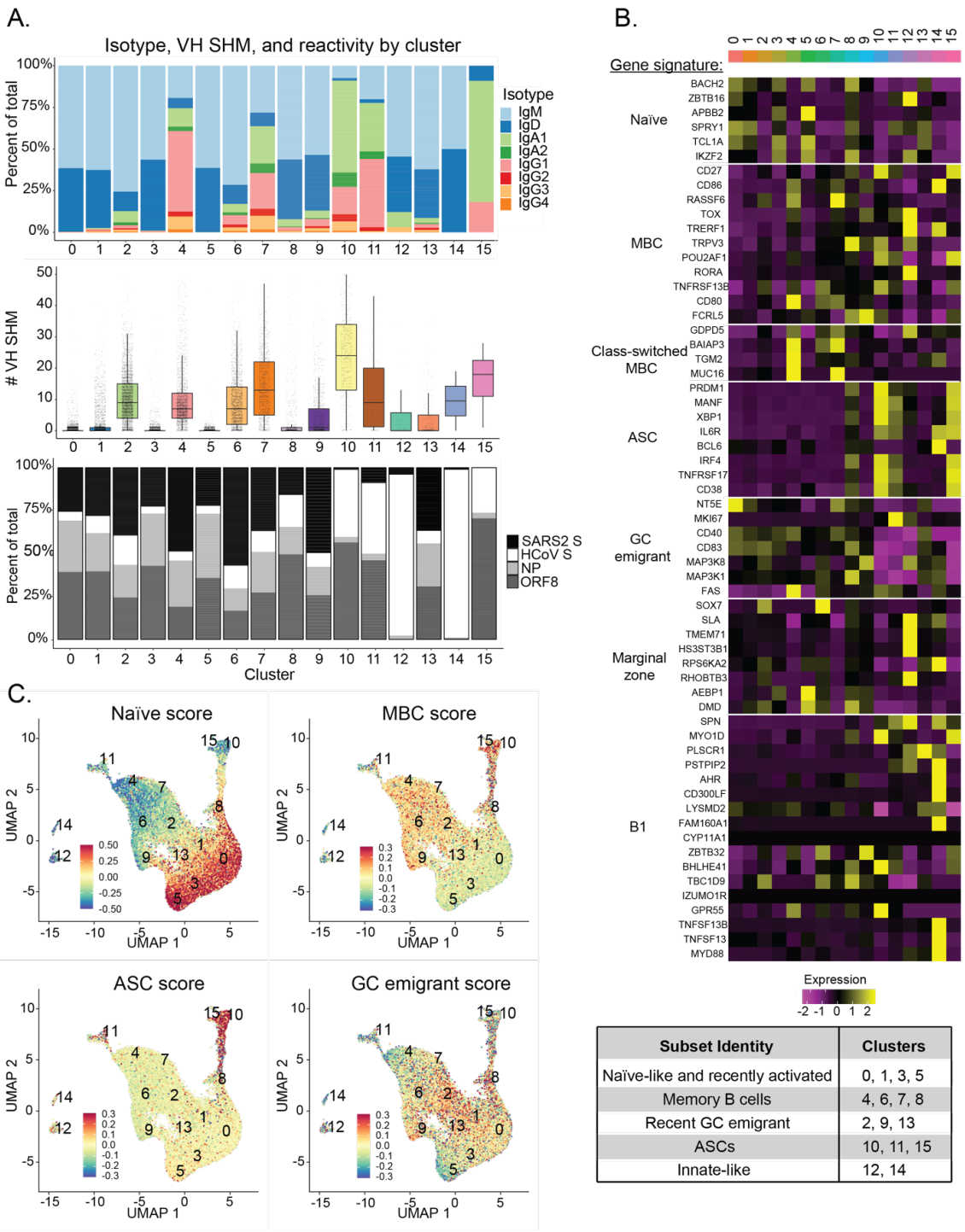

Subset Identity	Clusters
Naïve-like and recently activated	0, 1, 3, 5
Memory B cells	4, 6, 7, 8
Recent GC emigrant	2, 9, 13
ASCs	10, 11, 15
Innate-like	12, 14

Figure 3.3. B cell receptor and transcriptional analysis reveals cluster identities.
(**A**) BCR isotype usage, VH SHM, and antigen reactivity by cluster for all integrated samples from each cohort. SHM data are plotted with the overlay indicating the median with interquartile range. (**B**) Heatmap displaying differentially expressed genes across clusters. A summary of cluster identities is provided below. (**C**) UMAP projections with cell color indicating gene module scoring for the indicated B cell subsets. Also see Table 3.5 and Table 3.6.

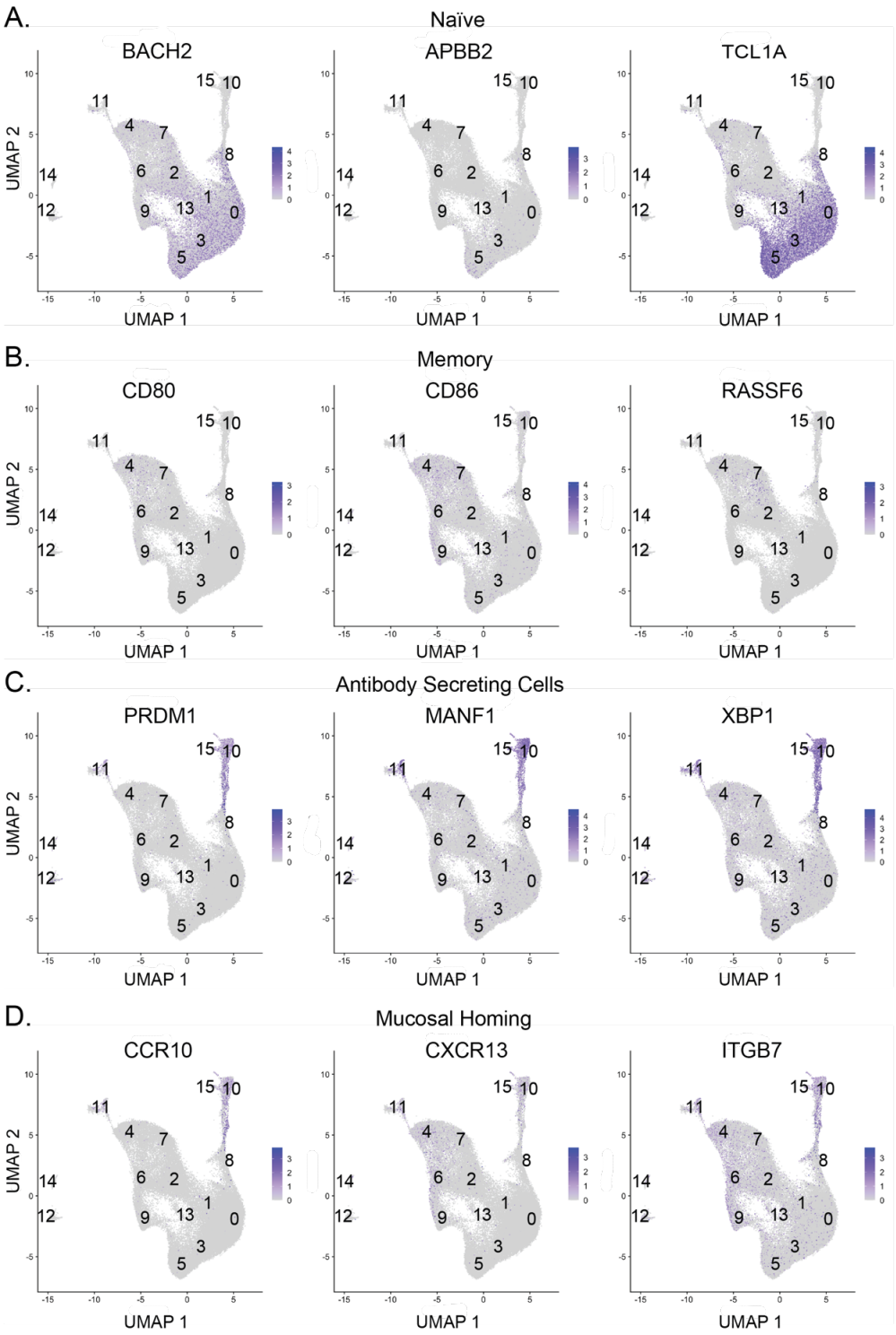

Figure 3.4. Expression maps of select genes induced upon SARS-CoV-2 infection. (**A–D**) UMAP projections with cells colored by expression level of the indicated genes, associated with naïve (**A**), MBCs (**B**), ASCs (**C**), or mucosal homing (**D**). Also see Table 3.5 and Table 3.6.

Table 3.5. Top 10 most differentially expressed genes per transcriptional cluster. Significance is indicated by adjusted p value.*Cluster 1 only expressed 8 genes above the significance threshold.

Gene	q-val (adj p val)	Cluster
SELL	2.27E-284	0
HLA-DRA	5.20E-275	0
CCR7	6.42E-261	0
PFDN5	3.78E-217	0
HLA-DQB1	2.49E-208	0
MEF2C	4.29E-208	0
HVCN1	2.99E-199	0
HLA-DRB5	3.33E-192	0
FAM26F	2.90E-175	0
SARAF	1.64E-171	0
BTG1	2.00E-104	1
TSC22D3	2.14E-67	1
DUSP1	2.70E-64	1
JUN	1.71E-37	1
ZFP36L2	1.02E-17	1
RPS26	1.07E-14	1
RPS4Y1	9.15E-08	1
MT-ND6	0.02353042	1
SMARCB1	2.80E-286	2
TNFRSF13B	1.36E-285	2
SAT1	8.77E-261	2
EEF1B2	2.92E-259	2
RPL9	1.16E-257	2
UBC	9.26E-256	2
CD82	3.50E-254	2
H3F3B	3.51E-244	2
DUSP2	1.32E-239	2
CTSH	7.68E-239	2
RPS24	2.13E-280	3
FOS	2.22E-224	3
YBX3	6.57E-210	3
BTG1	8.51E-189	3
FAM129C	7.36E-183	3
CD79B	6.60E-170	3
H3F3A	3.45E-165	3
CD79A	1.33E-162	3
DUSP1	3.20E-159	3
CXCR4	2.99E-149	3
C4orf48	3.48E-303	4
MTMR14	1.41E-300	4
ARL6IP5	3.78E-300	4
PDLIM1	6.07E-300	4
ATP5B	1.01E-299	4
POU2AF1	1.25E-299	4
TMEM156	2.81E-299	4
PPP1CA	1.13E-294	4
RPLP1	3.43E-287	4
PKM	5.02E-287	4
FCRLA1	2.29E-293	5

Table 3.5. Top 10 most differentially expressed genes per transcriptional cluster, continued

HCK	1.59E-279	5
GADD45B1	5.30E-258	5
VPREB31	6.56E-242	5
ACTG1	2.26E-228	5
BCL7A1	2.37E-217	5
UCP22	5.88E-212	5
ACTB	9.61E-211	5
CD79A1	1.40E-196	5
RPS11	1.65E-187	5
GAPDH	5.19E-290	6
ITGB1	5.43E-272	6
SYK1	1.26E-271	6
FCRL2	3.00E-262	6
CD27	5.44E-261	6
PLAC8	7.41E-240	6
ANXA4	1.65E-239	6
AC079767.4	1.66E-239	6
AP2S11	2.27E-237	6
CD241	4.50E-236	6
RPL14	3.83E-301	7
PDE4D	8.43E-301	7
RPS25	4.39E-284	7
RPS15A	1.62E-221	7
RPS3	3.64E-214	7
TPT1	3.28E-212	7
RPL32	8.50E-211	7
RPLP2	1.88E-210	7
RPS6	7.54E-196	7
RPS181	4.77E-191	7
MT-CO1	3.28E-256	8
MT-CO2	2.24E-177	8
MT-CYB	3.85E-147	8
MT-ND4L	6.61E-120	8
MT-CO3	4.50E-108	8
MT-ND3	2.45E-87	8
MT-ND5	1.62E-76	8
MT-ATP8	1.02E-62	8
MT-ND1	9.47E-57	8
MZB1	5.49E-45	8
FCRL5	1.93E-301	9
HLA-DRB1	1.33E-294	9
HLA-DPA1	7.60E-247	9
RGS2	2.48E-245	9
HLA-DPB1	1.47E-237	9
B2M	4.95E-231	9
HCK	2.78E-222	9
HLA-DQA1	4.05E-222	9
LITAF	3.32E-217	9
RHOB	7.50E-217	9
MRPL27	7.31E-303	10
FAM173A	4.65E-300	10

Table 3.5. Top 10 most differentially expressed genes per transcriptional cluster, continued

OAS1	1.41E-299	10
COA3	9.63E-296	10
TUFM	3.86E-294	10
GOLGB1	1.66E-293	10
MFF	1.89E-293	10
UQCRH	8.40E-293	10
NDUFA4	1.38E-291	10
MRPL24	1.87E-291	10
SRPRB	3.60E-302	11
CALU	2.84E-301	11
TMEM106C	8.66E-300	11
SLC35B1	2.73E-298	11
PRDX4	4.73E-291	11
MT2A	1.77E-290	11
YWHAE	4.34E-290	11
OSTC	1.63E-287	11
CD38	1.34E-286	11
DNAJB11	2.82E-286	11
LCP2	2.59E-299	12
RHOC	8.46E-296	12
RARRES3	1.81E-289	12
CTSD	1.62E-286	12
AAK1	4.65E-276	12
IFITM2	3.02E-248	12
B2M	1.97E-233	12
DDIT4	3.48E-233	12
S100A11	4.36E-230	12
TPST2	7.72E-228	12
TPST2	1.01E-275	13
XAF1	3.67E-223	13
MX1	4.71E-206	13
IFITM1	5.27E-163	13
EPSTI1	1.44E-160	13
EIF2AK2	7.68E-157	13
IFI6	1.65E-149	13
PLSCR1	1.33E-147	13
ISG15	1.32E-146	13
STAT1	1.83E-140	13
MX2	2.00E-121	13
MT2A	6.19E-302	14
MS4A7	4.81E-301	14
CCDC88A	9.92E-300	14
MYD88	1.02E-284	14
NAGA	1.47E-279	14
FAM45A	8.59E-262	14
RNF144B	7.72E-257	14
ALDH2	5.68E-254	14
SLC7A7	5.93E-250	14
GBP2	6.72E-242	14
AQP3	4.41E-291	15
TXNDC5	1.42E-256	15

Table 3.5. Top 10 most differentially expressed genes per transcriptional cluster, continued

LGALS3	2.35E-233	15
FKBP11	3.31E-229	15
PRDM1	4.18E-225	15
FNDC3B	5.54E-204	15
IFI27L1	4.57E-196	15
SDF2L1	9.78E-193	15
DERL3	2.11E-188	15
IFI27	1.05E-187	15

Table 3.6. Key genes used in the identification of SARS-CoV-2 specific B cell subsets.

Gene	B Cell Subset	Rationale	Citation
BACH2	Naïve	Promotes B cell development, maintains mature B cells	(*219*)
ZBTB16	Naïve	Downregulated in memory compared to naïve	(*220*)
APBB2	Naïve	Foxp1 target important for mature FO B cell survival	(*221*); The Human Protein Atlas (*222*)
SPRY1	Naïve	Proliferation inhibitor, differentially expressed (DE) between naïve and memory	(*223*) The Human Protein Atlas (*222*)
TCL1A	Naïve	DE between B cell pop. High in Naïve, low in GC, absent in memory and ASC	(*224*)
IKZF2	Naïve	DE between memory and naïve, higher in naïve	(*220*)
CD27	Memory	Classic memory marker	(*3*)
CD86	Memory	DE between memory and naïve, higher in memory	(*225*)
RASSF6	Memory	Increased in memory	(*220*)
TOX	Memory	Increased in memory	(*220*)
TRERF1	Memory	Increased in memory	(*220*)
TRPV3	Memory	Increased in memory	(*220*)
POU2AF1	Memory	B cell-specific TF	(*13*)
RORA	Memory	Increased in memory	(*220*)
TNFRSF13B	Memory	BAFF-binding receptor expressed in memory and ASC	(*226*)
CD80	Memory	High affinity memory marker	(*3*)
FCLR5	Memory	Atypical memory marker	(*227*)
GDPD5	Class-switched Memory	Highest in class-switched memory B cells	The Human Protein Atlas (*222*)
BAIAP3	Class-switched Memory	DE in switched memory, ion channel Ca^{2+} flux	(*220*)
TGM2	Class-switched Memory	DE in switched memory, Ca^{2+} signal transduction	(*220*)
MUC16	Class-switched Memory	DE in class-switched memory, membrane adhesion	(*220*)
PRDM1	ASC	Lineage-defining TF	(*17*)
MANF	ASC	ER stress	(*17*)
XBP1	ASC	Unfolded protein response	(*17*)
IL6R	ASC	Receptor for IL6, promotes PC fate and mAb production	(*228*)
BCL6	ASC	Drops in GCs to promote PC fate	(*3*)
IRF4	ASC	Rises as BCL6 drops to promote PC fate	(*3*)
TNFSR17	ASC	Genetic KOs experience sig PC reduction	(*17*)
CD38	ASC	Classic PC marker	(*17*)
NT5E	GC emigrant / recent MBC	Important for class-switch	(*229*)
MKI67	GC emigrant / recent MBC	Proliferation marker	(*230*)

Table 3.6. Key genes used in the identification of SARS-CoV-2 specific B cell subsets, continued

CD40	GC emigrant / recent MBC	Required for memory formation	(*231*)
CD83	GC emigrant / recent MBC	GC composition	(*232*)
MAP3K8	GC emigrant / recent MBC	DE during GC reaction	(*233*)
MAP3K1	GC emigrant / recent MBC	Required for CD40 signaling	(*234*)
FAS	GC emigrant / recent MBC	DE during GC reaction	(*235*)
Marginal Zone genes	Marginal Zone B cells	DE in MZBs	(*236*)
SPN	B1 B Cells	Classic B1 marker	(*237*)
MYO1D	B1 B Cells	DE in B1s	(*238*)
PSTPIP2	B1 B Cell	DE during activation	(*239*)
AHR	B1 B Cell	Highest expression in B1	(*240*)
CD300LF	B1 B Cell	DE in B1s	(*238*)
LYSMD2-GPR55	B1 B Cell	DE in mouse B1s	(*241*)
IZUMO1R	B1 B Cell	DE in B1s	(*238*)
TNFSF13B-MYD88	Innate-like B cells	Highly expressed in MZB and B1	(*242*)

3.4.3 B cell immunodominance and adaptability to SARS-CoV-2 and HCoVs changes with time after infection

The kinetics and evolution of B cells against the spike and non-spike antigens are poorly understood. We investigated whether there were notable changes in B cell subsets and their antigenic targets over time in severe acute and convalescent subjects. By color-coding cells belonging to the severe acute cohort (red), convalescent visit 1 (~1.5 months post-infection; blue), and convalescent visit 2 (~5 months post-infection; yellow) in the integrated UMAP, it became evident that distinct B cell subsets were enriched in different timepoints/cohorts. As expected, ASC clusters 10, 11, and 15 were derived almost entirely from severe acute subjects (Figure 3.5A). The two convalescent timepoints were largely comprised of naïve-like and MBC clusters, with convalescent visit 2 being the most enriched for canonical class-switched MBCs (clusters 4 and 7) (Figure 3.5A). The severe acute cohort exhibited minimal targeting of the SARS2 spike protein, and instead targeted HCoV spike and ORF8 (Figure 3.5B, C). As these ASCs were activated by SARS-CoV-2, they are likely boosted MBCs with higher affinity for the HCoV spikes, and therefore displayed BCRs predominately loaded with HCoV spike probe when stained. By contrast, convalescent visit

1 was most enriched for SARS2 spike binding, which subsequently declined in convalescent visit 2, in which the frequency of B cells to NP and ORF8 was increased (Figure 3.5B, C).

The dynamic change observed in antigen targeting over time led us to examine antigen reactivity within distinct B cell subsets for each cohort. For the severe acute cohort, B cells binding intracellular proteins were dominated by ASC clusters, whereas SARS2 spike-specific B cells were enriched in early memory and GC emigrant B cell clusters (Figure 3.5D). As previously noted, HCoV spike-specific B cells were enriched in ASCs of the severe acute cohort, indicative of re-activation of preexisting immune memory. Consistent with this, HCoV spike-specific B cells were highly mutated compared to SARS2 spike-, NP-, and ORF8-specific B cells (Figure 3.6A).

Across the two convalescent visits, the percentage of MBCs to ORF8 and NP was increased in proportion relative to spike MBCs (Figure 3.5E–G; total cell numbers indicated), and the degree of SHM for all antigen-specific B cells was increased across study visits (Figure 3.5H, Figure 3.6B, C). Notably, while spike- and ORF8-specific B cells showed signs of adaptation across visits, the majority of cells displaying the highest degree of SHM in convalescent visit 2 were NP-specific (Figure 3.5I, J). At the individual level, all four subjects displayed an increase in the percentage of MBCs to NP across time points, and half of the subjects displayed modest increases to ORF8. The change in percentage for spike-specific B cells across visits was negligible for three out of four subjects, with one subject displaying a substantial decrease (Figure 3.6D; S210). Previous groups have identified that spike-specific MBCs increase over time (*132, 135, 151*), and our study is limited in that this analysis was performed on only four subjects. However, our data support the claim that there is MBC maturation to NP, and to a lesser extent, ORF8 over time.

Analyzing isotype frequencies by antigen specificity for each cohort revealed additional differences across timepoints. The majority of class-switched B cells were IgA in the severe acute cohort, regardless of antigen-reactivity (Figure 3.6E). By contrast, class-switching to IgG1 was prominent for SARS2 spike, NP, and ORF8-reactive B cells in convalescent visit 1, while HCoV spike-reactive B cells remained largely IgA (Figure 3.6F).

Class-switched B cells specific to the SARS2 spike declined in convalescent visit 2, and IgG1 class-switched B cells to ORF8 and NP increased in proportion (Figure 3.6G).

Finally, we did not identify substantial differences in serum titer to distinct antigens across convalescent visit time points (Figure 3.6H–3.6J). Similarly, reactivity patterns in serological titer and probe hit to distinct antigens in individual subjects did not appear to be correlated (Figure 3.7A–E). This may be related to differences in B cell affinity to 3-dimensional probes in the bait sorting assay versus ELISA, or the fact that the cellular response is sampled at one snapshot in time (over 1-month post-infection), with serology reflective of antibody that has accumulated since initial infection.

Together, our results point to differences in B cell immunodominance and adaptability landscapes across severe acute and convalescent cohorts, independent of serum titer. For both the severe acute cohort and convalescent visit 1 time point, SARS2 spike-specific B cells were initially most enriched in memory. However, NP- and ORF8-reactive MBCs increased in proportion and showed signs of adaptation over time.

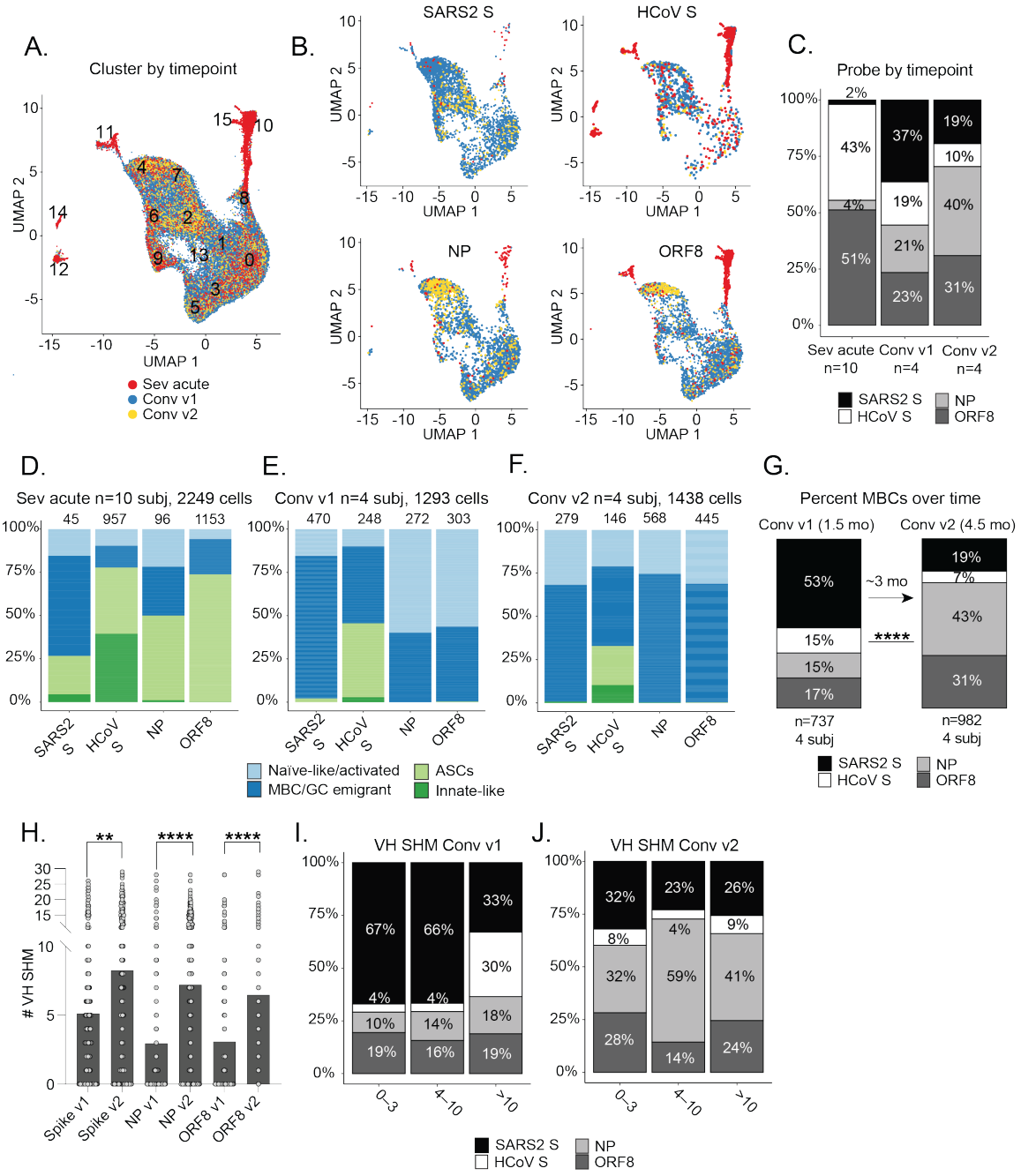

Figure 3.5. B cell immunodominance and adaptability landscapes vary in acute SARS-CoV-2 infection in convalescence. **(A)** UMAP projection showing cells colored by cohort/timepoint of blood draw. Conv v1= convalescent visit 1; Conv v2= convalescent visit 2. **(B)** UMAP projections showing only cells binding the specified antigens, colored by cohort/timepoint of blood draw. **(C)** Percentage of B cells targeting distinct antigens by cohort. Four Conv v1 and Conv v2 subjects represent matched visits. **(D–F)** Quantification of B cell subsets targeting distinct antigens across cohorts. Numbers above bars indicate the number of specific cells isolated. **(G)** Percentage of total antigen-specific memory B cells over time from ~1.5–3 months post-infection in matched-convalescent subjects. Statistics are Chi-square test, ****p<0.0001. **(H)** VH SHM of antigen-specific B cells across both convalescent timepoints for four matched subjects. Statistics used are unpaired non-parametric Mann-Whitney tests, ****p<0.0001; **p=0.0021. **(I and J)** Antigen-specific MBCs divided by SHM tertiles at Conv v1 **(I)** and Conv v2 **(J)** for four matched subjects.

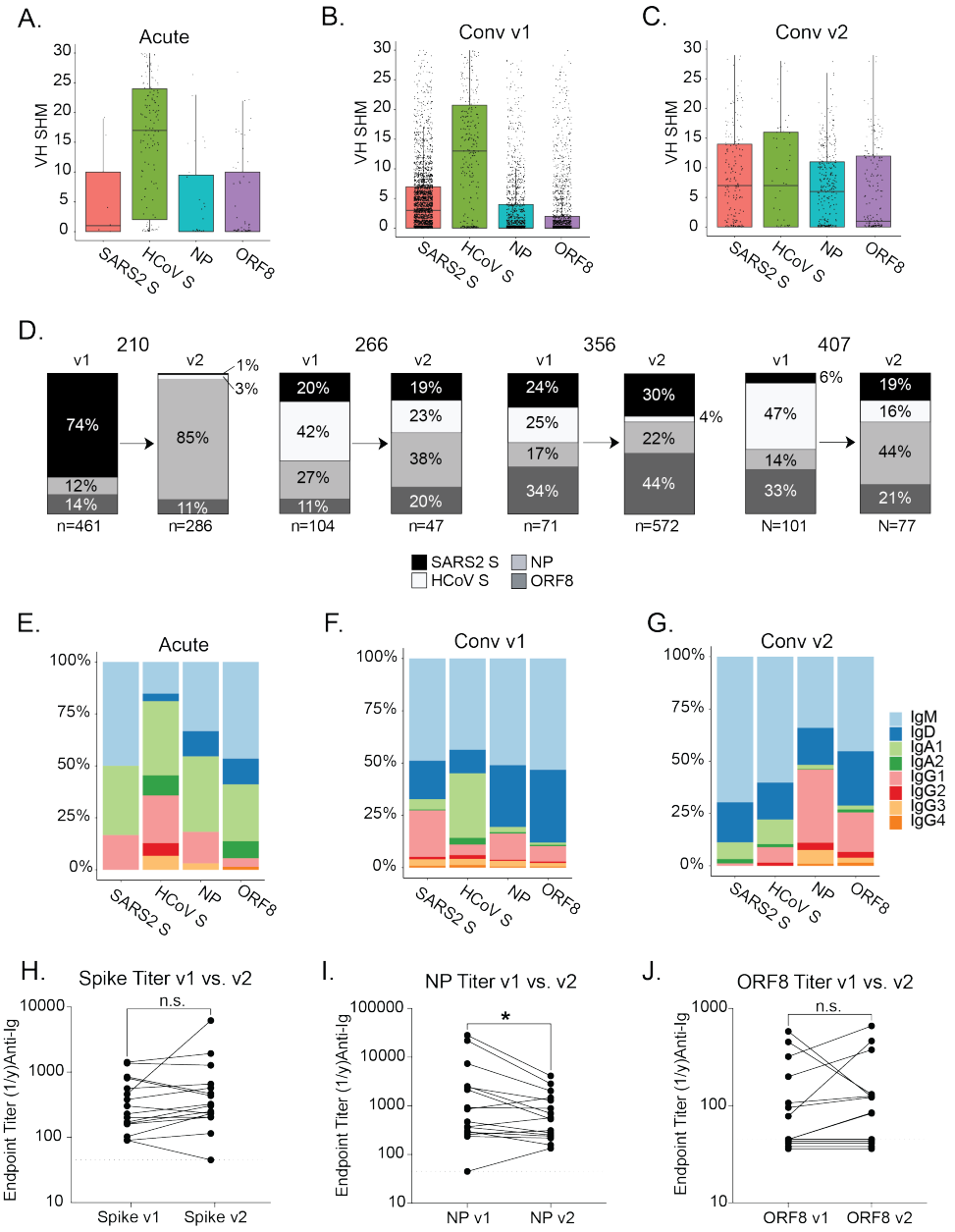

Figure 3.6. Analysis of SARS-CoV-2 antigen-specific B cell properties across distinct cohorts and timepoints. (**A–C**) VH SHM by antigen-specific B cells shown for severe acute (**A**), Conv v1 (**B**), or Conv v2 (**C**). Overlay shows median with interquartile range. (**D**) Distribution of MBC specificity across timepoints for Conv v1 and Conv v2 subjects, sampled at approximately 1.5- and 4.5-months post-infection. Also see Table S1. (**E–G**) BCR isotype usage by antigen-specific B cells shown for severe acute (**E**), Conv v1 (**F**), or Conv v2 subjects (**G**). (**H–J**) Total anti-Ig serum titers across timepoints for 16 matched convalescent subjects, shown for SARS2 spike (**H**), NP (**I**), and ORF8 (**J**). Dashed line at y= 45 indicates cutoff for positivity; values are staggered to avoid overlap. Statistics are paired non-parametric Wilcoxon test, *p=0.0386.

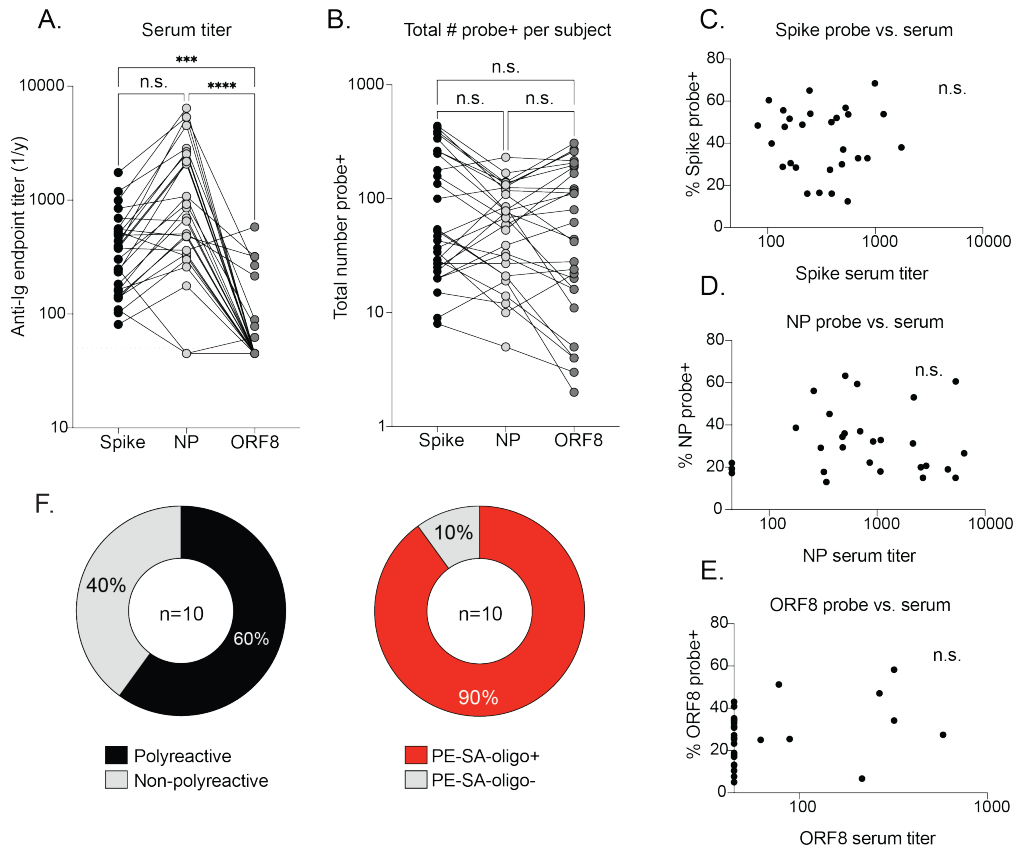

Figure 3.7. Correlation between SARS-CoV-2 antigen-probe positive B cells and serum titers. (**A**) Matched serum titers for spike, NP, and ORF8 for convalescent subjects. Statistics are paired non-parametric Friedman test with Dunn's post-test for multiple comparisons, ****p<0.0001; ***p=0.0002; n.s.= not significant. (**B**) Matched antigen-specific probe hit per convalescent subject. Statistics are paired non-parametric Friedman test with Dunn's post-test for multiple comparisons, no differences were significant (n.s.). (**C–E**) Percentage of B cells specific for spike (**C**), NP (**D**), or ORF8 (**E**) compared to serum titer levels for the same antigen. Statistics are nonparametric Spearman correlation, two-tailed, CI = 95%. No correlations were significant (n.s.). (**F**) MAbs cloned from non-specific multi-reactive B cells tested for polyreactivity (left) and PE-SA binding (right) by ELISA.

3.4.4 SARS-CoV-2-specific B cells display unique repertoire features and protective ability

The identification of B cells against distinct antigens is typically associated with stereotypical VH and variable light chain (VK or VL) gene usages. Immunodominant and neutralizing spike and RBD epitopes are of particular interest, as they represent key targets for vaccine-induced responses. We investigated whether antigen-specific B cells displayed enriched variable gene usages. We identified unique VH and VK/VL pairs for B cells targeting HCoV spike, non-RBD spike epitopes, and RBD-specific epitopes. A B cell was considered non-RBD spike-specific if it bound full-length spike probe and not RBD, and a

cell that bound both RBD and full-length spike was considered to be RBD-specific. Using this approach, we found that B cells against HCoV spike, non-RBD SARS2 spike epitopes, and the SARS2 RBD were enriched for VH1-69 gene usage (Figure 3.8A–3.8C). VH1-69 is commonly utilized by bnAbs against the hemagglutinin stalk-domain of influenza viruses, as well as the gp120 co-receptor binding site of HIV-1 due to its ability to bind conserved hydrophobic regions of viral envelope glycoproteins (*243*). VH1-69 usage by B cells that cross-react to SARS-CoV-2 and HCoV has also been indicated (*33*). However, VH1-69 usage for B cells targeting HCoV and non-RBD SARS2 spike epitopes was predominantly enriched in convalescent visit 1 subjects and not convalescent visit 2, suggesting that the repertoire may continue to evolve months after infection (Figure 3.8A, B; right). However, several VH gene usages were enriched in both convalescent visits, regardless of antigen specificity. For non-RBD SARS2 spike-specific B cells, VH3-7 and VH1-24 were also commonly used, which we confirmed by characterizing cloned mAbs from our cohort (Figure 3.8B, D, Table 3.7). While NP-specific antibodies utilized similar variable gene usages as SARS2 RBD-specific antibodies (Figure 3.8C, D), ORF8-specific antibodies were enriched for VH1-2 and VH1-3 paired with VK3-20, and enrichment for these VH genes persisted across both convalescent timepoints (Figure 3.8E). Finally, by analyzing the frequency of heavy and light chain gene pairings per subject across both convalescent timepoints, we observed variability amongst individual subjects and timepoints as expected (Figure 3.8F).

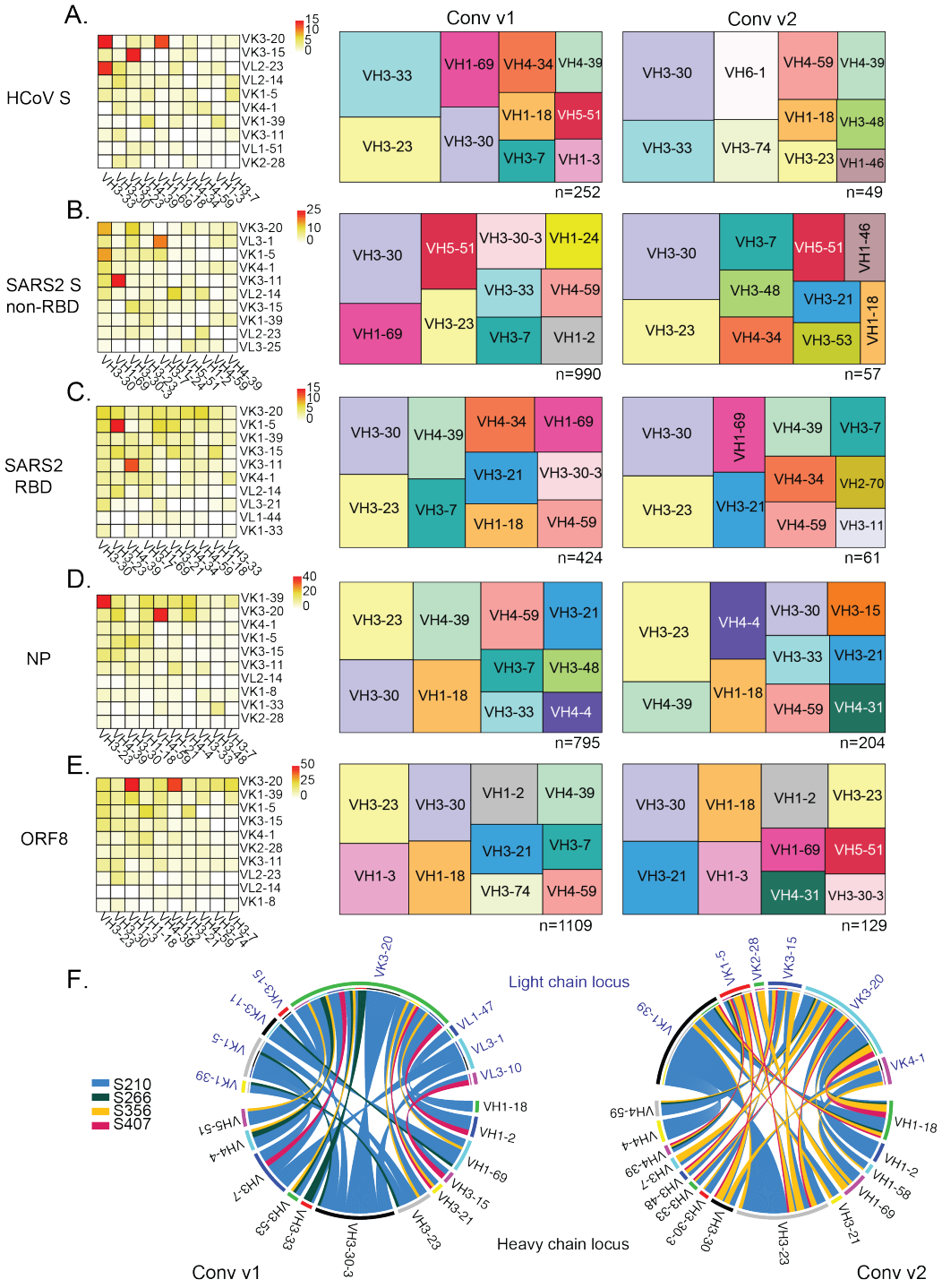

Figure 3.8. B cells targeting distinct CoV antigens display unique variable gene usages. (**A–E**) Heatmaps showing the frequency of heavy and light chain pairings binding the indicated antigens using integrated data from all cohorts (left; legend indicates number of cells per pairing), and dendrograms showing the top ten variable heavy chain (VH) gene usages for Conv v1 (n=28) and Conv v2 (n=4) cohorts. The number of cells encompassing the top 10 VH genes per antigen is indicated below each dendrogram. (**F**) Circos plots showing the top 10 heavy and light chain gene pairings shared across 4 matched Conv v1 (left; n=1293 cells) and Conv v2 (right; n=1438 cells) subjects. Total antigen-specific cells are shown.

To better understand antigen-specific BCRs and how antigenic reactivity related to immune effectiveness, we next investigated the binding, neutralization potency, and *in vivo* protective ability of mAbs cloned from select BCRs. To do so, we expressed nearly 100 mAbs against the spike, NP, and ORF8 from convalescent subjects, representing a multitude of clusters (Table 3.7). Cells from which to clone antibodies were chosen at random, and were not chosen based on specific sequence features. However, we note that the results described herein may be affected by sampling bias, as only a small subset of antigen-specific mAbs were cloned. We confirmed that cells designated as specific bound with moderate to high affinity to their corresponding antigens (Figure 3.9A), and cells identified as multi-reactive exhibited features of polyreactivity or bound to PE (Figure 3.7F). We next tested the antibodies for viral neutralization by SARS-CoV-2/UW-001/Human/2020/Wisconsin virus plaque assays. Whereas 77% percent of mAbs to the RBD were neutralizing including 40% exhibiting complete inhibition, only 23% of mAbs to spike regions outside of the RBD were neutralizing, and these showed relatively low potency (Figure 3.9B). Notably, NP- and ORF8-specific mAbs were entirely non-neutralizing (Figure 3.9B). Using animal models of SARS-CoV-2 infection, we confirmed that anti-RBD antibodies were therapeutically protective *in vivo*, preventing weight loss and reducing lung viral titers relative to PBS control and an irrelevant Ebola anti-GP133 mAb (Figure 3.9C, D).

Table 3.7. SARS-CoV-2-specific mAbs generated from heavy and light chain gene sequences. U.k.: unknown.

mAb ID	Specificity	Isotype	Cluster	# HC SHM	VH Gene	# LC SHM	VK/L gene
S20-15	Spike/RBD	IgG1	4	8	VH 4-59	1	VL 3-21
S20-31	NP	IgG4	4	30	VH 1-24	22	VK 3-20
S20-40	NP	IgM	5	0	VH 4-4	1	VL 2-14
S20-58	Spike/RBD	IgG1	7	5	VH 4-30	2	VK 2-24
S20-74	Spike/RBD	IgG1	6	6	VH 4-59	3	VL 2-8
S20-86	Spike	IgG1	3	9	VH 3-9	2	VL 2-14
S24-68	ORF8	IgG1	4	4	VH 4-59	3	VL 1-44
S24-105	ORF8	IgG1	4	6	VH 3-48	4	VK 3-20
S24-178	NP	IgG1	4	2	VH 3-33	7	VL 2-14
S24-188	NP	IgG3	4	2	VH 1-69	3	VL 2-14
S24-202	NP	IgG1	6	3	VH 5-10	6	VK 3-11
S24-278	ORF8	IgG1	4	3	VH 1-2	1	VK 3-20
S24-339	Spike/RBD	U.k.	4	5	VH 3-49	1	VK 3-15
S24-472	ORF8	IgG1	4	5	VH 4-4	4	VL 4-16
S24-490	ORF8	IgM	7	2	VH 1-46	4	VK 3-20
S24-494	Spike/RBD	IgG3	2	0	VH 4-39	0	VK 1-39
S24-566	ORF8	IgG1	4	3	VH 3-49	1	VK 2-28
S24-636	ORF8	IgD	7	1	VH 3-7	4	VL 8-61
S24-740	ORF8	IgG1	4	5	VH 1-3	1	VK 4-1
S24-791	NP	IgG1	4	4	VH 4-59	6	VK 3-20
S24-902	Spike/RBD	IgG1	6	0	VH 1-69	0	VL 7-46
S24-921	NP	IgG1	4	8	VH 4-59	7	VK 1-39
S24-1063	NP	IgG1	4	3	VH 4-59	1	VK 3-20
S24-1224	Spike/RBD	IgG1	4	7	VH 1-46	7	VL 1-40
S24-1271	Spike/RBD	IgM	4	6	VH 3-66	6	VL 3-1
S24-1339	Spike/RBD	IgG1	7	1	VH 3-53	1	VK 3-20
S24-1345	ORF8	IgD	3	0	VH 4-39	0	VK 1-13
S24-1378	ORF8	IgM	3	0	VH 3-53	0	VL 8-61
S24-1379	NP	IgG1	0	0	VH 4-59	0	VL 1-47
S24-1384	Spike/RBD	IgG1	4	2	VH 3-48	4	VL 3-21
S24-1476	Spike/RBD	IgG	1	2	VH 3-49	0	VK 3-15
S24-1564	NP	IgG1	4	10	VH 4-59	4	VK 1-39

Table 3.7. SARS-CoV-2-specific mAbs generated from heavy and light chain gene sequences, continued

S24-1636	NP	IgG1	2	3	VH 3-33	0	VK 3-11
S24-1002	Spike/RBD	IgM	3	3	VH 3-30	5	VK 1-13
S24-1301	Spike	IgG1	3	4	VH 1-24	4	VL 10-54
S24-223	Spike/RBD	IgM	2	1	VH 2-5	3	VL 2-14
S24-461	Spike/RBD	IgG1	4	7	VH 4-59	3	VL 3-16
S24-511	NP	IgD	2	0	VH 3-30	0	VL 3-1
S24-788	Spike/RBD	IgM	6	0	VH 3-33	1	VL 3-1
S24-821	Spike/RBD	IgM	4	4	VH2-70	0	VK 1-5
S144-67	Spike/RBD	IgG1	4	7	VH 5-51	5	VL 1-40
S144-69	Spike/RBD	IgG1	4	2	VH 5-51	3	VK 1-5
S144-94	ORF8	IgG3	4	11	VH 3-30	0	VK 2-28
S144-113	ORF8	IgG1	4	9	VH 3-23	6	VK 1-39
S144-175	ORF8	IgG1	4	9	VH 1-2	1	VL 1-47
S144-208	ORF8	IgG1	4	6	VH 1-2	7	VL 2-11
S144-339	NP	IgG1	4	11	VH 3-21	7	VK 3-20
S144-359	ORF8	IgG3	4	5	VH 3-23	5	VK 1-39
S144-460	Spike/RBD	IgA1	4	34	VH 3-15	24	VK1D-17
S144-466	Spike/RBD	IgG3	4	6	VH 5-51	6	VK 1-5
S144-469	ORF8	IgG1	4	3	VH 4-59	2	VK 2-28
S144-509	Spike/RBD	IgG1	4	3	VH 5-51	1	VK 1-5
S144-516	ORF8	IgG1	4	5	VH 1-2	7	VL 1-40
S144-568	Spike/RBD	IgA2	7	11	VH 4-59	11	VK 3-20
S144-576	Spike/RBD	IgG1	4	3	VH 1-69	2	VK 1-5
S144-588	ORF8	IgG1	4	1	VH 4-39	3	VL 3-1
S144-628	Spike/RBD	IgA1	6	9	VH 5-51	10	VL 1-40
S144-740	ORF8	IgG1	4	1	VH 1-2	5	VK 3-20
S144-741	ORF8	IgG1	4	5	VH 1-2	1	VL 1-44
S144-803	Spike/RBD	IgG1	4	5	VH 5-51	3	VK 1-5
S144-843	ORF8	U.k.	6	20	VH 3-30	8	VK 3-20
S144-877	Spike/RBD	IgG1	4	2	VH 3-30	6	VK 1-33
S144-952	NP	IgM	4	4	VH 1-18	2	VK 4-1
S144-971	ORF8	IgG1	4	6	VH 3-64	3	VK 4-1
S144-1036	NP	IgG1	4	2	VH 4-34	5	VK 4-1
S144-1079	Spike/RBD	IgG1	4	7	VH 1-69	3	VK 3-20

Table 3.7. SARS-CoV-2-specific mAbs generated from heavy and light chain gene sequences, continued

S144-1299	ORF8	IgG1	4	5	VH 4-59	0	VL 1-47
S144-1339	Spike/RBD	IgG1	4	12	VH 1-2	5	VL 2-14
S144-1406	Spike/RBD	IgG2	4	3	VH 1-3	0	VK 1-5
S144-1407	Spike/RBD	IgG1	4	6	VH 1-69	2	VK 1-5
S144-1569	ORF8	IgG1	4	7	VH 1-18	1	VL 9-49
S144-1827	Spike/RBD	IgM	2	20	VH 3-7	5	VK 3-20
S144-1848	NP	IgG1	4	4	VH 3-21	8	VL 1-47
S144-1850	Spike/RBD	IgG1	4	2	VH 3-23	3	VK 1-5
S144-2234	ORF8	IgG1	4	4	VH 1-69	3	VK 4-1
S564-105	NP	IgG1	4	5	VH 4-61	2	VL 2-14
S564-14	Spike/RBD	IgD	6	3	VH 3-7	0	VK 3-21
S564-68	Spike/RBD	IgG1	4	6	VH 1-2	2	VL 2-8
S564-98	NP	IgG3	4	0	VH 4-59	3	VK 1-39
S564-105	NP	IgG1	4	5	VH 4-61	2	VL 2-14
S564-134	Spike/RBD	IgG1	4	2	VH 1-2	6	VL 2-8
S564-138	Spike/RBD	IgG1	4	8	VH 1-2	1	VL 2-14
S564-152	Spike/RBD	IgG1	11	4	VH 3-33	4	VK 1-33
S564-249	NP	IgA1	7	19	VH 3-64	19	VL 2-14
S564-265	Spike/RBD	IgG1	4	4	VH 1-2	3	VL 2-8
S564-275	NP	IgM	4	3	VH 4-59	6	VK 1-39
S116-2822	Spike	IgM	0	0	VH 3-30	0	VK 1-5
S166-32	Spike	IgG1	6	9	VH 3-11	2	VK 1-5
S166-2395	Spike	IgD	4	2	VH 4-4	5	VL 3-21
S166-2620	Spike	IgM	6	1	VH 3-7	1	VL 3-1
S210-852	Spike	IgM	6	8	VH 3-7	2	VL 3-1
S210-896	Spike	IgM	9	1	VH 3-30	2	VK 3-21
S210-1626	Spike	IgD	1	0	VH 4-4	0	VK 3-20
S305-399	Spike	IgM	7	1	VH 1-24	4	VK 3-15
S305-1456	Spike	IgG2	7	2	VH 1-24	3	VK 3-15
S376-780	Spike	IgM	3	0	VH 3-30	0	VK 1-27

While mAbs to NP and ORF8 were non-neutralizing *in vitro*, they might still provide protection *in vivo*, potentially through Fc-mediated pathways if the proteins were exposed on the virus or cell surface at appreciable levels. However, neither ORF8-reactive mAbs nor

NP-reactive mAbs conferred protection from weight loss or viral infection in the lung *in vivo* (Figure 3.9E–H). Altogether, our data suggest that while B cells may continue to expand and evolve to intracellular antigens upon SARS-CoV-2 infection, B cell responses against these targets may not provide substantial protection from re-infection.

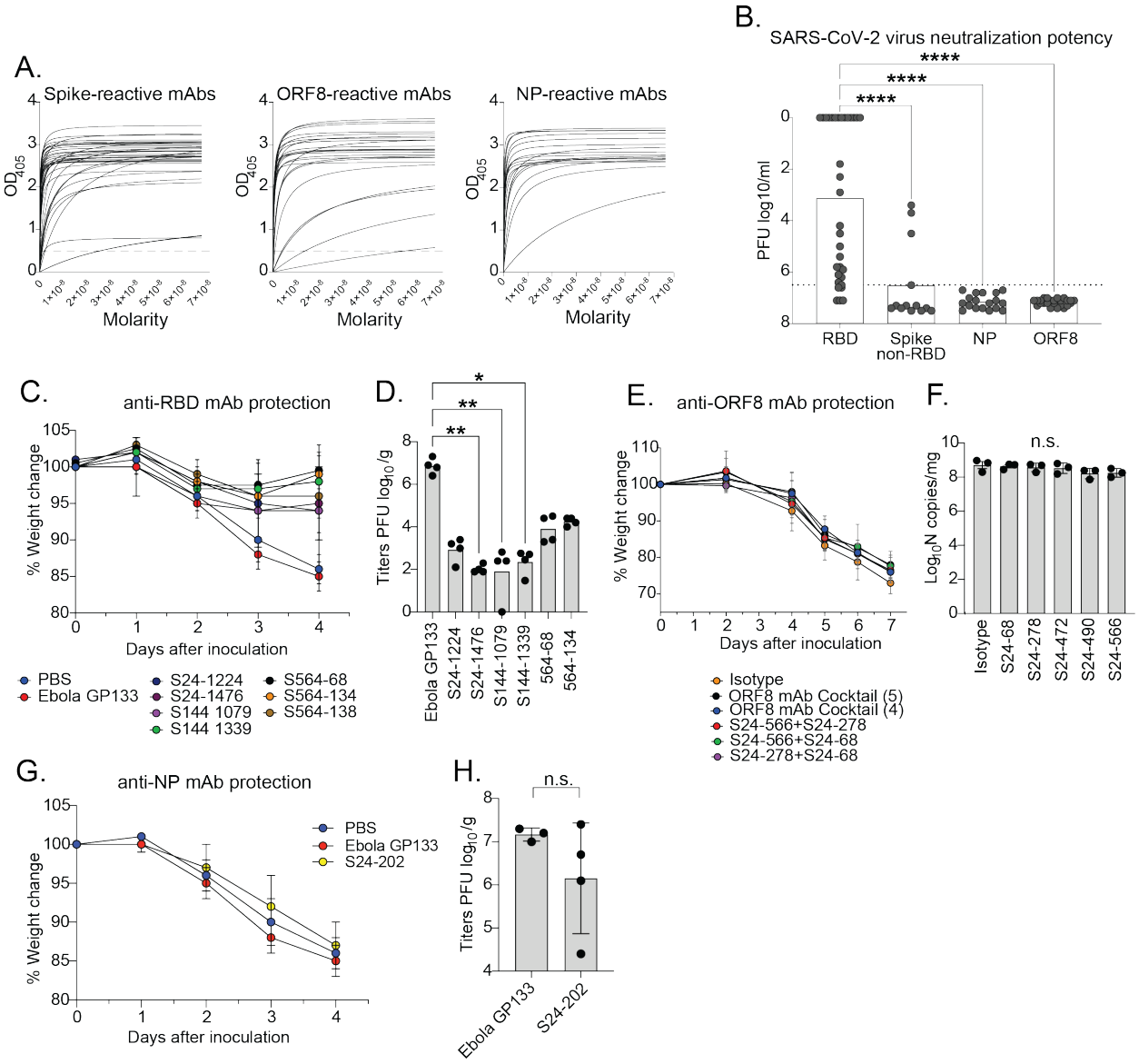

Figure 3.9. Neutralization capacity and in vivo protective ability of mAbs to the SARS-CoV-2 spike and intracellular proteins. (**A**) Antigen binding curves by ELISA of antigen-specific mAbs. Dashed line at y= 0.5 on ELISA curves represents the OD405 cutoff of 0.5 for positivity. (spike, n= 48; RBD, n=36; NP, n=19; ORF8, n=24). Also see Table S6. (**B**) Neutralization potency (log10 PFU/ml) of mAbs tested by SARS-CoV-2 virus plaque assay. Dashed line at x= 6.5 indicates the cutoff for neutralization. Statistics are non-parametric Kruskal-Wallis with Dunn's post-test for multiple comparisons, ****p<0.0001. (**C**) Weight change in hamsters intranasally challenged with SARS-CoV-2, followed by therapeutic intraperitoneal (I.P.) administration of anti-RBD antibodies (mean ± SD, n= four biological replicates for each mAb). Control conditions are PBS injection, or injection of an irrelevant Ebola virus anti-GP133 mAb. (**D**) Viral

Figure 3.9, continued
titers of SARS-CoV-2 in lungs harvested from hamsters post-challenge in (**C**). Statistics are unpaired non-parametric Kruskal-Wallis with Dunn's post-test for multiple comparisons, **p=0.0011; **p=0075; *p=0.0135. (**E**) Weight change of mice intranasally challenged with SARS-CoV-2, followed by therapeutic I.P. administration of anti-ORF8 antibody cocktails (mean ± SD, n= three biological replicates for each mAb). (**F**) Viral titers of SARS-CoV-2 in lungs harvested from mice post challenge in (**E**). Titers are presented as N gene copy number compared to a standard curve. Statistics performed are non-parametric Kruskal-Wallis with Dunn's post-test for multiple comparisons, no differences were significant. (**G**) Weight change in hamsters intranasally challenged with SARS-CoV-2, followed by therapeutic intraperitoneal (I.P.) administration of an anti-NP antibody (mean ± SD, n= four biological replicates for each mAb). (**H**) Viral titers of SARS-CoV-2 in lungs harvested from hamsters post challenge shown in (**G**). Statistics performed are non-parametric Mann-Whitney test, no differences were significant.

3.4.5 B cell immunodominance is shaped by age, sex, and disease severity

Previous studies from our group and others have suggested that serum antibody titers to the spike and intracellular proteins correlate with age, sex, and SARS-CoV-2 severity (*129, 136, 244*). We therefore analyzed the distribution of B cell subsets and frequencies of B cells specific to the spike, NP, and ORF8 in convalescent subjects stratified by age, sex, and severity of disease. Disease severity was stratified into three categories: mild, moderate, and severe, based on symptom duration and symptoms experienced (Table 3.1). Our disease severity scoring method has been defined previously (*136*).

We found that the reactivity of total B cells toward different antigens varied widely by subject, likely reflecting host-intrinsic differences (Figure 3.10A). With age, we identified a decrease in the generation of spike-specific B cells, and an increase in ORF8 and NP-specific B cells (Figure 3.10B). Similarly, the percentage of total spike-specific B cells was reduced in subjects with more severe disease, whereas ORF8-specific B cells were increased (Figure 3.10C). Lastly, we identified females had increased percentages of ORF8-reactive cells, whereas males showed slightly greater percentages of NP-reactive cells (Figure 3.10D). To address whether differences in B cell reactivity with age and severity were associated with naïve-like or MBC subsets, we analyzed reactivity by subset. We observed a substantial decrease in spike-specific MBCs and an increase in NP- and ORF8-reactive MBCs with age, while naïve-like B cell subsets were more evenly distributed in reactivity across age groups (Figure 3.10E, Figure 3.11A). Notably, we identified a significant correlation with age and the percentage of ORF8-reactive MBCs in females, but not in males (Figure 3.11B, C). By

contrast, the generation of specific MBCs was not different between mild and severe cases, though naïve-like subsets targeting ORF8 were increased across mild, moderate, and severe disease (Figure 3.10F, Figure 3.11D).

While B cell memory to the spike was decreased in older patients, the overall median number of VH SHMs for antigen-specific MBCs was increased relative to younger patients (Figure 3.10G). However, while the majority of MBCs harboring the most mutations targeted the SARS2 spike in younger age groups (Figure 3.10H, I), mutated MBCs against NP and ORF8 were proportionately increased relative to the spike in older patients (Figure 3.10J). Finally, we observed variability in the percentages of MBCs and naïve-like B cells across subjects (Figure 3.10K), with older patients, patients with severe disease, and female patients generating reduced percentages of MBCs (Figure 3.10L–N). These findings strongly point to older patients exhibiting poorly adapted MBC responses to the spike, instead exhibiting increased targeting and adaptation to intracellular antigens. These data are analogous to B cell responses to influenza virus vaccination in the elderly, and may be attributed to the effects of immunosenescence impairing the ability to form new memory over time (*72, 158*). Alternatively, these findings may reflect potential effects of preexisting immunity on the boosting of NP-specific cross-reactive MBCs.

In summary, our study highlights the diversity of B cell subsets expanded upon novel infection with SARS-CoV-2. Using this approach, we identified that B cells against the spike, ORF8, and NP differ in their ability to neutralize and derive from functionally distinct and differentially adapted B cell subsets; that memory B cell output overtime shifts from the spike to intracellular antigens; and that targeting of these antigens is impacted by age, sex, and disease severity.

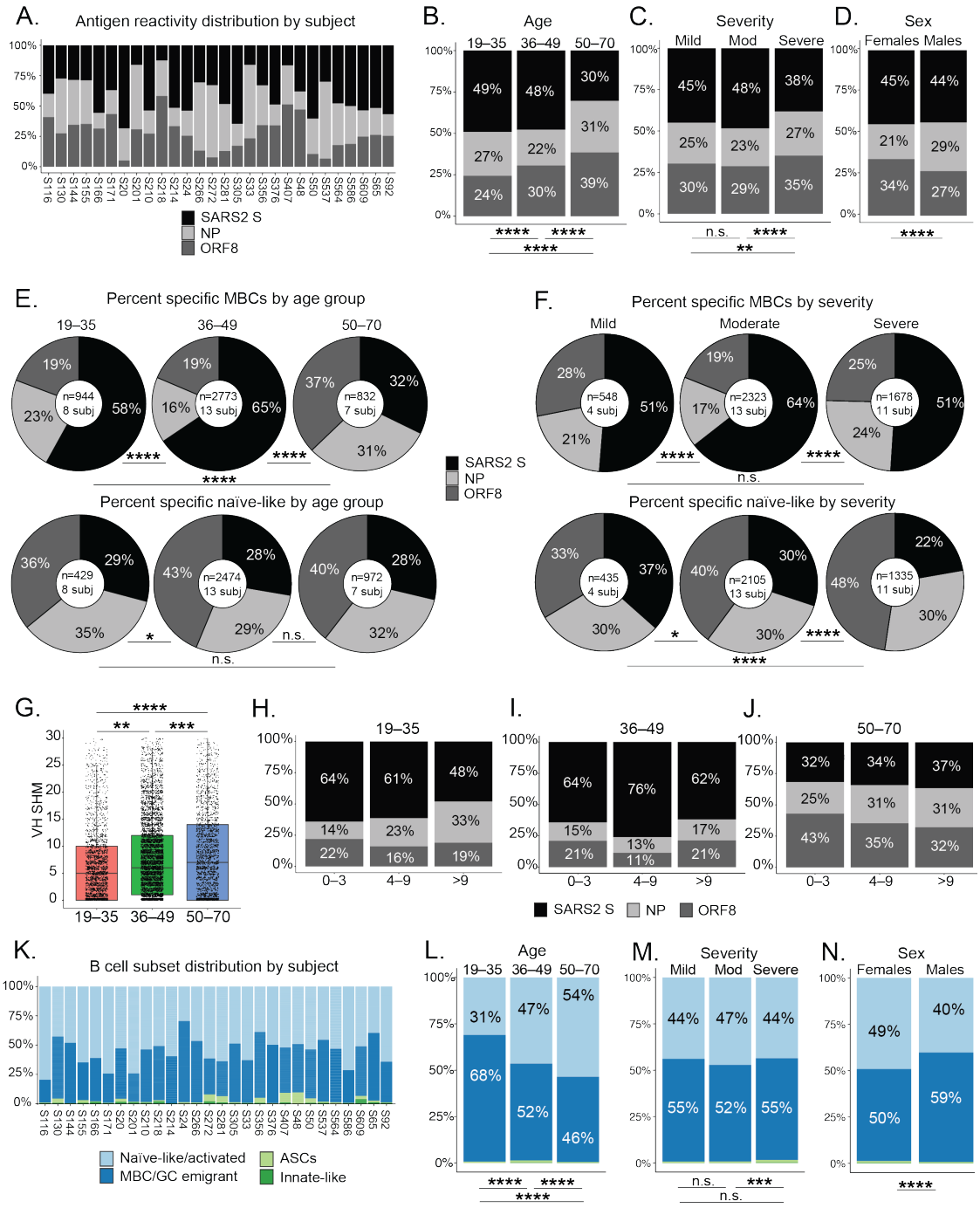

Figure 3.10. SARS-CoV-2 antigen-specificity and B cell subset distribution is linked to clinical features. (**A**) Reactivity distribution of total antigen-specific B cells by subject for the convalescent cohort (n= 28). (**B–D**) Reactivity distribution of total antigen-specific B cells by age (**B**), disease severity (**C**), and sex (**D**). Statistics are Chi-squared post-hoc tests with Holm-Bonferroni adjustment, ****p<0.0001; **p=0.0012; n.s.= not significant. For age groups, 19–35: n= 1382 cells, 8 subjects; 36–49: n= 5319 cells, 13 subjects; 50–70: n= 1813 cells, 7 subjects. For severity groups, mild: n= 990 cells, 4 subjects; moderate: n= 4462 cells, 13 subjects; severe: n= 3062 cells, 11 subjects. For sex, females: n= 5005 cells, 14 subjects; males: n= 3509 cells, 14 subjects. (**E**) Reactivity of antigen-specific memory B cells (top) or naïve B cells (bottom) by age group. Statistics are Chi-squared post-hoc tests with Holm-Bonferroni adjustment, ****p<0.0001; *p=0.0145;

Figure 3.10, continued
n.s.= not significant. **(F)** Reactivity of antigen-specific memory B cells (top) or naïve B cells (bottom) by disease severity. Statistics are Chi-squared post-hoc tests with Holm-Bonferroni adjustment, ****p<0.0001; *p=0.0143; n.s.= not significant. **(G)** VH SHM for MBCs by age group (overlay shows median with interquartile range). Statistics are unpaired non-parametric ANOVA with Tukey's test for multiple comparisons, ****p<0.0001, ***p=0.0008, **p=0.002. **(H–J)** Antigen-specific MBCs by age, divided by SHM tertiles. **(K)** B cell subset distribution by subject. **(L–N)** B cell subset distribution by age **(L)**, disease severity **(M)**, and sex **(N)**. Statistics are Chi-squared post-hoc tests with Holm-Bonferroni adjustment, ****p<0.0001; ***p=0.0007; n.s.= not significant. For each group, n is the same as in **(B–D)**.

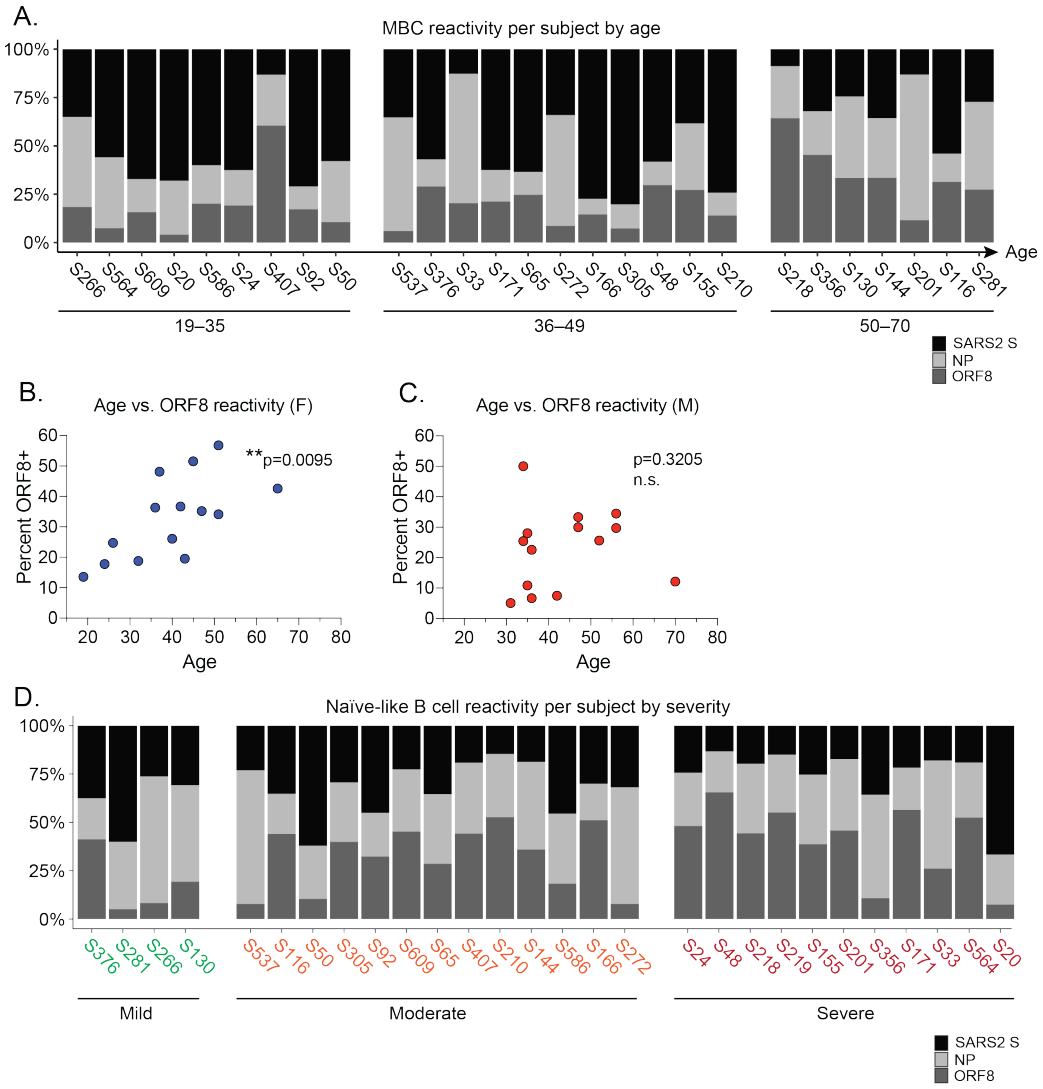

Figure 3.11. Additional analyses of SARS-CoV-2 antigen reactivity by clinical parameter. **(A)** Percentages of antigen-specific MBCs shown per subject by age. Age increases left to right along the graph. **(B)** Percentage of MBCs specific for ORF8 versus age for female (F) subjects. Statistics are nonparametric Spearman correlation, two-tailed, CI = 95%. **(C)** Percentage of MBCs specific for ORF8 versus age for male (M) subjects. Statistics are nonparametric Spearman correlation, two-tailed, CI = 95%. P values are indicated. **(D)** Percentages of antigen specific naïve-like B cells shown for each subject by severity. Severity score increases left to right along the graph, also see Table 3.1 for severity score per subject.

3.5 Discussion

The COVID-19 pandemic continues to pose one of the greatest public health and policy challenges in modern history, and robust data on long-term immunity is needed to evaluate future decisions regarding COVID-19 responses. Our approach combines three powerful aspects of B cell biology to address human immunity to SARS-CoV-2: B cell transcriptome, Ig sequencing, and recombinant mAb characterization. Our approach enables the identification of potently neutralizing antibodies and the characteristics of the B cells that generate them. Importantly, we show that antibodies targeting key protective spike epitopes are enriched within MBC populations, but over time the MBC pool shifts towards non-protective intracellular antigens which could be a molecular hallmark of waning spike-mediated protection. This is further evidence that widespread vaccination, which only elicits a response to the spike, may be critical to end the pandemic.

Identification of multiple distinct subsets of naïve, innate-like B cells, recent and older MBCs, and ASCs illustrates the complexity of the B cell response to SARS-CoV-2, revealing an important feature of the immune response against any novel pathogen. The approximately 55,000 B cell transcriptomes with corresponding B cell receptor sequences herein may provide biomarkers or new gene signatures to help identify distinct B cell populations. Such populations can be used to evaluate future responses to infections of various kinds, vaccine formulations, and aid in a better understanding of human B cell biology and how it shifts over the course of the immune response. Thus, future studies further elucidating distinct identities and functions of these subsets are necessary and will provide key insights into various aspects B cell immunology.

Through this data, we revealed that the landscape of antigen targeting and B cell subsets varied widely across severe acute subjects and convalescent subjects between 1.5–5-months post-infection. Severe acute patients mounted a large ASC response toward HCoV spike and ORF8, largely derived from IgA ASC populations. Plasmablasts are reflective of ongoing germinal center or extrafollicular responses to infection, and are often re-activated from preexisting immune memory (*163*). The expansion of highly mutated plasmablasts to

HCoV spike in severe acute patients suggests that the early response to SARS-CoV-2 in some patients may be dominated by an original antigen sin response. It remains unclear whether such responses worsen the severity of disease, or reflect an inability to adapt to novel SARS2 spike epitopes. Alternatively, whether HCoV spike binding B cells adapt to the SARS2 spike and can provide protection is of interest for the potential generation of a universal coronavirus vaccine. Further investigation into the protection afforded by cross-reactive antibodies are warranted, as previous studies have identified cross-reactive HCoV and SARS1 binding antibodies can neutralize SARS-CoV-2 (*33, 152*). Importantly, vaccine-induced responses to the spike are likely similarly shaped by preexisting immunity, and should be investigated.

While SARS2 spike-specific B cells were enriched in memory in our convalescent cohort, we also identified MBCs and ASCs to HCoV spike, which appeared to wane 5 months after infection in the same subjects. This later timepoint coincided instead with an increase in the overall numbers and percentage of ORF8- and NP-specific MBCs, which displayed a marked increase in SHM. This phenotype was particularly evident in older patients, which exhibited reduced MBC targeting of the spike. Notably, older, female, and more severe patients had increased percentages of total ORF8-specific B cells; and older patients tended to create more memory to intracellular proteins over time. We identified B cells targeting these intracellular proteins as exclusively non-neutralizing and non-protective. Mechanistically, these observations may be explained by reduced adaptability of B cells or increased reliance on CD4 T cell help for B cell activation, which have been observed in aged individuals upon viral infections and are dysregulated in aged patients (*72, 158*). Furthermore, T cell responses to SARS-CoV-2 intracellular proteins are prevalent in convalescent COVID-19 patients (*153, 245, 246*). The shift in memory output during convalescence may also reflect the massive difference in protein availability, with each virion producing only dozens of spikes but thousands of intracellular proteins (*153, 247, 248*).

More research is warranted to determine whether B cell targeting of distinct SARS-CoV-2 antigens directly impacts susceptibility and disease severity, and conversely, whether

age or disease severity shape memory formation. Addressing these questions will be paramount for understanding the disease course, determining correlates of protection, and developing vaccines capable of protecting the most vulnerable individuals against SARS-CoV-2 and emerging variants.

3.6 Limitations of the study

A primary limitation to this study is the assumption that the total number and overall distribution of antigen-specific B cells is accurately captured by the bait-sorting method described herein. These parameters could be altered by a number of factors, including probe preparation, staining dilution, flow cytometry gating, and bioinformatics analysis. However, this approach is inherently more sensitive and high-throughput compared to serology and lower-throughput methods for single B cell cloning. The frequencies of memory B cells examined will also be dependent on the numbers that could be isolated by bait-sorting starting from purified B cells, rather than examining reactivity within a controlled number of memory B cells per subject. An additional limitation is that the acute cohort was hospitalized and presented with severe infection, and we were unable to analyze acute subjects presenting a range of disease severity. Finally, we were unable to obtain longitudinal samples from the same individuals across acute, early and late convalescent time points, and future longitudinal studies assessing the evolution of memory B cells to SARS-CoV-2 will be important.

3.7 Methods

3.7.1 Study cohort and sample collection

All studies were performed with the approval of the University of Chicago institutional review board IRB20-0523 and University of Chicago, University of Wisconsin-Madison, and Washington University in St. Louis institutional biosafety committees. Informed consent was obtained after the research applications and possible consequences of the studies were disclosed to study subjects. This clinical trial was registered at ClinicalTrials.gov with identifier NCT04340050, and clinical information for patients included in the study is

detailed in Table S1–S3. Convalescent leukoreduction filter donors were 18 years of age or older, eligible to donate blood as per standard University of Chicago Medicine Blood Donation Center guidelines, had a documented COVID-19 polymerase chain reaction (PCR) positive test, and complete resolution of symptoms at least 28 days prior to donation. Severe acute infected blood donors were 18 years of age or older and blood was collected per standard University of Chicago Medical Center guidelines. Subjects had a documented COVID-19 polymerase chain reaction (PCR) positive test, were hospitalized, and had been scheduled to receive an infusion of convalescent donor plasma. Four blood draws were collected both before and after plasma infusion, at days 0, 1, 3, and 14. PBMCs were collected from leukoreduction filters or blood draws within 2 hours post-collection and, if applicable, flushed from the filters using sterile 1X Phosphate-Buffered Saline (PBS, Gibco) supplemented with 0.2% Bovine Serum Albumin (BSA, Sigma). Lymphocytes were purified by Lymphoprep Ficoll gradient (Thermo Fisher) and contaminating red blood cells were lysed by ACK buffer (Thermo Fisher). Cells were frozen in Fetal Bovine Serum (FBS, Gibco) with 10% Dimethyl sulfoxide (DMSO, Sigma) prior to downstream analysis. On the day of sorting, B cells were enriched using the human pan B cell EasySep™ enrichment kit (STEMCELL).

3.7.2 Recombinant proteins and probe generation

SARS-CoV-2 and Hanta PUUV proteins were obtained from the Krammer laboratory at Mt. Sinai, the Joachimiak laboratory at Argonne, and the Fremont laboratory at Washington University. pCAGGS expression constructs for the spike protein, spike RBD, and hanta PUUV were obtained from the Krammer lab at Mt. Sinai and produced in house in Expi293F suspension cells (Thermo Fisher). Sequences for the spike and RBD proteins as well as details regarding their expression and purification have been previously described (*249, 250*). Proteins were biotinylated for 2 hours on ice using EZ-Link™ Sulfo-NHS-Biotin, No-Weigh™ Format (Thermo Fisher) according to the manufacturer's instructions, unless previously Avi-tagged and biotinylated (ORF8 protein, Fremont laboratory). Truncated

cDNAs encoding the Ig-like domains of ORF8 were inserted into the bacterial expression vector pET-21(a) in frame with a biotin ligase recognition sequence at the c-terminus (GLNDIFEAQKIEWHE). Soluble recombinant proteins were produced as described previously (*251*). In brief, inclusion body proteins were washed, denatured, reduced, and then renatured by rapid dilution following standard methods (*252*). The refolding buffer consisted of 400 mM arginine, 100 mM Tris-HCl, 2 mM EDTA, 200 μM ABESF, 5 mM reduced glutathione, and 500 μM oxidized glutathione at a final pH of 8.3. After 24 hr, the soluble-refolded protein was collected over a 10 kDa ultrafiltration disc (EMD Millipore, PLGC07610) in a stirred cell concentrator and subjected to chromatography on a HiLoad 26/60 Superdex S75 column (GE Healthcare). Site specific biotinylation with BirA enzyme was done following the manufacture's protocol (Avidity) except that the reaction buffer consisted of 100mM Tris-HCl (pH7.5) 150 mM NaCl, with 5mM MgCl2 in place of 0.5 M Bicine at pH 8.3. Unreacted biotin was removed by passage through a 7K MWCO desalting column (Zeba spin, Thermo Fisher). Full-length SARS-CoV-2 NP was cloned into pET21a with a hexahistidine tag and expressed using BL21(DE3)-RIL *E. coli* in Terrific Broth (bioWORLD). Following overnight induction at 25°C, cells were lysed in 20 mM Tris-HCl pH 8.5, 1 M NaCl, 5 mM β-mercaptopethanol, and 5 mM imidazole for nickel-affinity purification and size exclusion chromatography. Endemic HCoV spike proteins (HCoV-229E, HCoV-NL63, HCoV-HKU1, and HCoV-OC43) were purchased from Sino Biological. Biotinylated proteins were then conjugated to Biolegend TotalSeq™ PE streptavidin (PE-SA), APC streptavidin (APC-SA), or non-fluorescent streptavidin (NF-SA) oligos at a 0.72:1 molar ratio of antigen to PE-SA, APC-SA, or NF-SA. The amount of antigen was chosen based on a fixed amount of 0.5 μg PE-SA, APC-SA, or NF-SA and diluted in a final volume of 10 μL. PE-SA, APC-SA, or NF-SA was then added gradually to 10 μl biotinylated proteins 5 times on ice, 1 μl PE-SA, APC-SA, or NF-SA (0.1 mg/ml stock) every 20 minutes for a total of 5 μl (0.5 μg) PE-SA, APC-SA, or NF-SA. The reaction was then quenched with 5 μl 4mM Pierce™ biotin (Thermo Fisher) for 30 minutes for a total probe volume of 20 μL. Probes were then used immediately for staining.

3.7.3 Antigen-specific B cell sorting

PBMCs were thawed and B cells were enriched using EasySep™ pan B cell magnetic enrichment kit (STEMCELL). B cells were stained with a panel containing CD19 PE-Cy7 (Biolegend), IgM APC (Southern Biotech), CD27 BV605 (Biolegend), CD38 BB515 (BD Biosciences), and CD3 BV510 (BD Biosciences). B cells were stained with surface stain master mix and each COVID-19 antigen probe for 30 minutes on ice in 1X PBS supplemented with 0.2% BSA and 2 mM Pierce Biotin. Cells were stained with probe at a 1:100 dilution (NP, ORF8, RBD, PUUV, empty PE-SA) or 1:200 dilution (spike, endemic HCoV spikes). Cells were subsequently washed with 1X PBS 0.2% BSA and stained with Live/Dead BV510 (Thermo Fisher) in 1X PBS for 15 minutes. Cells were washed again and re-suspended at a maximum of 4 million cells/mL in 1X PBS supplemented with 0.2% BSA and 2 mM Pierce Biotin for downstream cell sorting using the MACSQuantTyto cartridge sorting platform (Miltenyi). Cells that were viable/$CD19^+$/antigen-PE^+ or viable/$CD19^+$/antigen-APC^+ were sorted as probe positive. The PE^+ and APC^+ gates were drawn by use of FMO controls. Cells were then collected from the cartridge sorting chamber and used for downstream 10X Genomics analysis.

3.7.4 10X Genomics library construction

VDJ, 5', and probe feature libraries were prepared using the 10X Chromium System (10X Genomics). The Chromium Single Cell 5' Library and Gel Bead v2 Kit, Human B Cell V(D)J Enrichment Kit, and Feature Barcode Library Kit were used. All steps were followed as listed in the manufacturer's instructions. Specifically, user guide CG000186 Rev D was used. Severe acute infected samples were pooled post-sort and hashtagged (Biolegend), and run as a single sample, to account for low cell numbers. Final libraries were pooled and sequenced using the NextSeq550 (Illumina) with 26 cycles apportioned for read 1, 8 cycles for the i7 index, and 134 cycles for read 2.

3.7.5 Computational analyses for single cell sequencing data

We adopted Cell Ranger (version 3.0.2) for raw sequencing processing, including 5' gene expression analysis, antigen probe analysis, and immunoprofiling analysis of B cells. Based on Cell Ranger output, we performed downstream analysis using Seurat (version 3.9.9, an R package, for transcriptome, cell surface protein and antigen probe analysis) and IgBlast (version 1.15, for immunoglobulin gene analysis). For transcriptome analysis, Seurat was used for cell quality control, data normalization, data scaling, dimension reduction (both linear and non-linear), clustering, differential expression analysis, batch effects correction, and data visualization. Unwanted cells were removed according to the number of detectable genes (number of genes <200 or >2500 were removed) and percentage of mitochondrial genes for each cell. A soft threshold of percentage of mitochondrial genes was set to the 95th percentile of the current dataset distribution, and the soft threshold was subject to a sealing point of 10% as the maximum threshold in the case of particularly poor cell quality. Transcriptome data were normalized by a log-transform function with a scaling factor of 10,000 whereas cell surface protein and antigen probe were normalized by a centered log-ratio (CLR) normalization. We used variable genes in principal component analysis (PCA) and used the top 15 principal components (PCs) in non-linear dimension reduction and clustering. High-quality cells were then clustered by Louvain algorithm implemented in Seurat under the resolution of 0.6. Differentially expressed genes for each cell cluster were identified using a Wilcoxon rank-sum test implemented in Seurat. Batch effects correction analysis was performed using an Anchor method implemented in Seurat to remove batch effects across different datasets. All computational analyses were performed in R (version 3.6.3).

3.7.6 ROGUE scoring

To assess the quality of B cell subsets identified in this study we used ROGUE scoring, an entropy-based metric for assessing the purity of single cell populations, adapted from a previous study (*218*). The expression entropy for each gene was calculated using

"SE_fun" from the "ROGUE" package (version 1.0). Based on the expression entropy, the ROGUE score for each cluster was calculated using the "rogue" function from the same package with parameters "platform" set to "UMI" and "span" set to 0.6.

3.7.7 Antigen probe reactivity assignment

Antigen probe signals were normalized by a centered log-ratio transformation individually for each subject. All B cells were subsequently clustered into multiple probe-specific groups according to their normalized probe signals. By investigating all normalized antigen-probe binding signals, we arbitrarily set a threshold equal to 1 for all normalized probe signals to distinguish probe binding cells as "positive" or "negative". Cells that were negative to all probes were clustered into the "negative" group; those positive to only one probe were clustered into corresponding probe-specific groups; and those that were positive to multiple probes were further investigated. Only cells whose top hit probe value was at least two-fold greater than their second hit probe value were clustered into the top hit probe-specific group; others were clustered into the "multi-reactive" group that indicates non-specific cells. To account for the inclusion of endemic HCoV spike protein reactivity in some samples, cells positive to both SARS2 spike and endemic spike were further clustered into a group we assigned as "spike cross-reactive" in the code. For samples in which we included separate SARS2 spike and RBD oligo tags, we placed cells positive to both SARS2 spike and SARS2 RBD into the "spike" group.

3.7.8 Gene module scoring

Scores for B-cell-genotype-related gene modules (e.g. MBC score, naïve score, ASC score, and GC emigrant score) were calculated using the "AddModuleScore" function from the Seurat package (*253*). The naïve score was calculated based on the genes *BACH2*, *ZBTB16*, *APBB2*, *SPRY1*, *TCL1A*, and *IKZF2*; the MBC score was calculated based on the genes *CD27*, *CD86*, *RASSF6*, *TOX*, *TRERF1*, *TRPV3*, *POU2AF1*, *RORA*, *TNFRSF13B*, *CD80*, and *FCRL5*; the ASC score was calculated based on genes *PRDM1*,

MANF, *XBP1*, *IL6R*, *BCL6*, *IRF4*, *TNFRSF17*, and *CD38*; and the GC emigrant score was calculated based on genes *NT5E*, *MKI67*, *CD40*, *CD83*, *TNFRSF13B*, *MAP3K8*, *MAP3K1*, and *FAS*.

3.7.9 Selection of antibodies for monoclonal antibody (mAb) synthesis

Representative antibodies from each subject were chosen for synthesis by choosing random samplings of B cells that bound to a given antigen probe with higher intensity relative to all other probes. B cells with varying ranges of probe-binding intensities were chosen for confirmation by ELISAs. In addition, B cells representing select public clonal expansions were also chosen for cloning. B cells binding to all probes in a polyreactive manner were also chosen and validated for polyreactivity by polyreactivity ELISA (see methods below).

3.7.10 Monoclonal antibody generation

Immunoglobulin heavy and light chain genes were obtained by 10X Genomics VDJ sequencing analysis and monoclonal antibodies (mAbs) were synthesized by Integrated DNA Technologies. Cloning, transfection, and mAb purification have been previously described(*44*). Briefly, sequences were cloned into human IgG1 expression vectors using Gibson assembly, and heavy and light genes were co-transfected into 293T cells (Thermo Fisher). Secreted mAbs were then purified from the supernatant using protein A agarose beads (Thermo Fisher).

3.7.11 Enzyme-linked immunosorbent assay (ELISA)

High-protein binding microtiter plates (Costar) were coated with recombinant SARS-CoV-2 proteins at 2 μg/ml in 1X PBS overnight at 4°C. Plates were washed the next morning with 1X PBS 0.05% Tween and blocked with 1X PBS containing 20% fetal bovine serum (FBS) for 1 hour at 37°C. Antibodies were then serially diluted 1:3 starting at 10 μg/ml and incubated for 1 hour at 37°C. Horseradish peroxidase (HRP)-conjugated goat anti-human IgG antibody diluted 1:1000 (Jackson Immuno Research) was used to detect binding of mAbs, and plates were subsequently developed with Super Aquablue ELISA substrate

(eBiosciences). Absorbance was measured at 405 nm on a microplate spectrophotometer (BioRad). To standardize the assays, control antibodies with known binding characteristics were included on each plate and the plates were developed when the absorbance of the control reached 3.0 OD_{405} units. All experiments were performed in duplicate 2–3 times.

3.7.12 Polyreactivity ELISA

Polyreactivity ELISAs were performed as previously described(*38, 254, 255*). High-protein binding microtiter plates (Costar) were coated with 10 μg/ml calf thymus dsDNA (Thermo Fisher), 2 μg/ml Salmonella enterica serovar Typhimurium flagellin (Invitrogen), 5 μg/ml human insulin (Sigma-Aldrich), 10 μg/ml KLH (Invitrogen), and 10 μg/ml Escherichia coli LPS (Sigma-Aldrich) in 1X PBS. Plates were coated with 10 μg/ml cardiolipin in 100% ethanol and allowed to dry overnight. Plates were washed with water and blocked with 1X PBS/0.05%Tween/1mM EDTA. MAbs were diluted 1 μg/ml in PBS and serially diluted 4-fold, and added to plates for 1.5 hours. Goat anti-human IgG-HRP (Jackson Immunoresearch) was diluted 1:2000 in PBS/0.05%Tween/1mM EDTA and added to plates for 1 hour. Plates were developed with Super Aquablue ELISA substrate (eBioscience) until the positive control mAb, 3H9 (*256*), reached an OD_{405} of 3. All experiments were performed in duplicate.

3.7.13 Neutralization assay

The SARS-CoV-2/UW-001/Human/2020/Wisconsin (UW-001) virus was isolated from a mild case in February 2020 and used to assess neutralization ability of monoclonal antibodies (mAbs). Virus (~500 plaque-forming units) was incubated with each mAb at a final concentration of 10 μg/ml. After a 30-minute incubation at 37°C, the virus/antibody mixture was used to inoculate Vero E6/TMPRSS2 cells seeded a day prior at 200,000 cells per well of a TC12 plate. After 30 minutes at 37°C, cells were washed three times to remove any unbound virus, and media containing antibody (10 μg/ml) was added back to each well.

Two days after inoculation, cell culture supernatant was harvested and stored at -80°C until needed. A non-relevant Ebola virus GP mAb and PBS were used as controls.

To determine the amount of virus in the cell culture supernatant of each well, a standard plaque-forming assay was performed. Confluent Vero E6/TMPRSS2 cells in a TC12 plate were infected with supernatant (undiluted, 10-fold dilutions from 10^{-1} to 10^{-5}) for 30 minutes at 37°C. After the incubation, cells were washed three times to remove unbound virus and 1.0% methylcellulose media was added over the cells. After an incubation of three days at 37°C, the cells were fixed and stained with crystal violet solution in order to count the number plaques at each dilution and determine virus concentration given as plaque-forming units (PFU)/ml.

3.7.14 *In vivo* protection assays

To evaluate the efficacy of RBD and NP monoclonal antibodies (mAbs) *in vivo*, groups of 4–5-week-old female Syrian golden hamsters (four animals in each group) were infected with SARS-CoV-2 at a dose of 10^3 PFU by intranasal inoculation. One day later, the hamsters were treated by intraperitoneal injection with one of the mAbs at 5 mg/kg. Control groups of hamsters were injected with either sterile PBS or a non-relevant mAb (Ebola glycoprotein 133/3.16). Weights were recorded daily. Four days after the infection, nasal turbinate and lung samples were collected to determine viral loads in these tissues by standard plaque assay on Vero E6/TMPRRSS2 cells. All animal studies were conducted under BSL-3 containment with an approved protocol reviewed by the Institutional Animal Care and Use Committee at the University of Wisconsin.

Studies with mice were carried out in accordance with the recommendations in the Guide for the Care and Use of Laboratory Animals of the National Institutes of Health. The protocols were approved by the Institutional Animal Care and Use Committee at the Washington University School of Medicine (assurance number A3381–01). Virus inoculations were performed under anesthesia that was induced and maintained with ketamine hydrochloride and xylazine, and all efforts were made to minimize animal

suffering. To evaluate the efficacy of ORF8 mAbs *in vivo*, eight-week-old heterozygous female K18-hACE c57BL/6J mice (strain: 2B6.Cg-Tg(K18-ACE2)2Prlmn/J) received 200 μg of each indicated mAb by intraperitoneal injection one day prior to intranasal inoculation with 10^3 PFU of SARS-CoV-2 (n-CoV/USA_WA1/2020 strain). Weight change was monitored daily and lungs were harvested at 7 days post-infection. Viral RNA levels in lung homogenates were determined by qRT-PCR quantifying N gene copy number and compared to a standard curve as described previously (*257*).

3.7.15 Statistical analysis

All statistical analysis was performed using Prism software (Graphpad Version 9.0) or R. Chi-square tests were corrected for multiple comparisons using post-hoc Chi-square test. Sample sizes (n) are indicated in corresponding figures or figure legends. The number of biological repeats for experiments and specific tests for statistical significance used are indicated in the figure legends. P values less than or equal to 0.05 were considered significant. *p<0.05, **p<0.01, ***p<0.001, ****p<0.0001.

3.8 Acknowledgements

We kindly thank the University of Chicago CAT Facility (RRID: SCR_017760) for their assistance and allowing us to use their facilities. We thank Dr. Nicholas Chevrier for allowing us to use the Pritzker School of Molecular Engineering's sequencing facility. We are thankful to the University of Chicago Genomics Facility (RRID: SCR_019196) for their assistance with sequencing several samples. We thank John Bivona and the staff of the Howard Taylor Ricketts Laboratory for prompt training in BSL-3 practices and procedures and for use of their facilities for severe acute infected sample collection. We are grateful for the training and support provided by Megan Ciarlo and Allison Guiang of Miltenyi Biotech for use of the MACSQuant Tyto. Lastly, we are most appreciative of the patients who donated samples for our research purposes.

CHAPTER 4

DISCUSSION AND FUTURE DIRECTIONS

4.1 Lessons from flu and SARS2: the pitfalls of natural immunity

For the first time, our studies suggest that the overwhelming majority of antibody specificities elicited by natural infection are non-neutralizing and non-protective *in vivo.* We demonstrate this finding in two distinct contexts: influenza virus infection, which is extremely familiar to the human immune system, and SARS-CoV-2 infection, a novel pandemic virus.

In the case of influenza virus infection, the majority of antibodies displayed higher affinity to childhood strains than to currently circulating strains and were highly mutated, indicative of an original antigen sin-like response. Similarly, we observed a substantial effect of preexisting immunity in biasing expansion of plasmablasts cross-reactive to endemic HCoV strains upon infection with SARS-CoV-2. As we analyzed antibody responses in young to middle-aged adults, it was not possible to tease apart isolated effects of preexisting immunity and age, and the two likely both impact antibody responses. To this effect, SARS-CoV-2 infection induced considerable expansion of MBCs to conserved yet non-neutralizing targets including NP and ORF8, and this response was exaggerated in adults aged 50–70 years old. Finally, we observed that in young to middle-aged adults, influenza virus vaccination predominantly recalled neutralizing MBCs specific to HA head epitopes, and many of these antibodies exhibited cross-reactivity to past strains as well.

Together, these data suggest a model whereby natural infection induces antibody responses to viral targets beyond major surface glycoproteins, as several structural and accessory proteins are widely abundant in natural infection (Figure 4.1, top). While natural immunity is accepted to last longer, the pitfall is that it induces several more non-neutralizing antibody specificities. Non-neutralizing antigens such as internal proteins are also more conserved, resulting in continual boosting of preexisting MBCs to undesirable antigens over a lifetime of repeated exposures. As a result, preexisting immunity and age can further exacerbate antibody responses to conserved non-neutralizing antigens. By contrast, vaccines

are enriched for major surface glycoproteins, favoring an antibody response that directly blocks mechanisms of viral entry into host cells (Figure 4.1, bottom). Despite this, our group and others have observed that preexisting immunity and age can also impact the quality of vaccine-induced responses, highlighting the need for next-generation vaccines enriched for conserved neutralizing epitopes(*72, 186*).

Though these observations are likely context-dependent, it is inarguable that complex host factors complicate current vaccination strategies for ever-changing viruses such as influenza and more recently SARS-CoV-2. With the foundation laid by these studies, it is clear that universal vaccination strategies are needed and likely the most promising avenue toward eradicating pandemic-threat viruses.

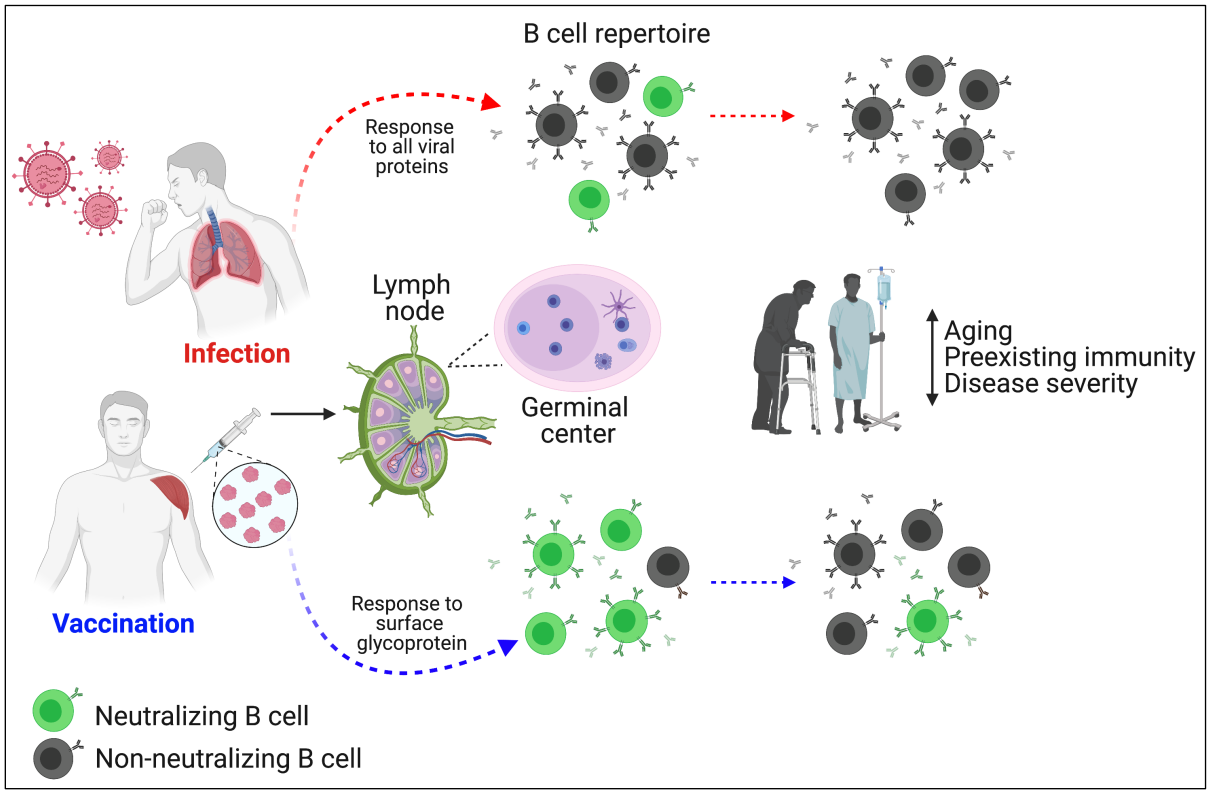

Figure 4.1. Model depicting how preexisting immunity, age, and disease severity shape antibody responses to viruses. In response to natural infection (top), the presentation of multiple viral proteins to the immune system results in a biased antibody response to conserved yet non-neutralizing antigens such as internal virus proteins. Factors such as age, preexisting immunity, and disease severity further amplify infection-induced antibody responses to conserved, non-neutralizing targets. The antibody response to vaccination (bottom) by contrast is biased toward major viral surface glycoproteins, as vaccines are enriched for these components. As a result, the antibody response to vaccination is predominantly neutralizing. However, age, preexisting immunity, and disease severity can still bias vaccine-induced responses to conserved yet non-neutralizing antigens.

4.2 Toward a universal influenza virus vaccine

4.2.1 Surmounting preexisting immunity to combat influenza viruses

Humoral immunity against influenza viruses relies on biased immune memory, referred to as imprinting or original antigenic sin. Imprinting results in MBC biases toward viral epitopes found in childhood viral strains and other past encountered viral strains, hindering adaptation to antigenically drifted viruses seen later in life. Imprinting has both beneficial and detrimental effects on anti-influenza immunity, largely dependent on whether an individual is exposed to a challenging influenza virus antigenically similar to or distinct from viruses previously encountered.; i.e. a virus belonging to the same (homosubtypic) or a different subtype (heterosubtypic). Exposure to a virus homosubtypic to the imprinting virus may result in boosting of cross-reactive antibody responses to homosubtypically conserved viral epitopes, which may have potential to be neutralizing. For example, when individuals are exposed to a similar strain, they are more likely to recall MBCs against neutralizing viral epitopes of the HA head due to smaller antigenic distance between viruses(*255*). By contrast, exposure to a viral subtype opposite of the imprinting virus may result in boosting of antibodies to heterosubtypically conserved viral epitopes, or poorly adapted responses as fewer epitopes are shared across subtypes(*258*).

Despite antibody boosting to conserved viral epitopes in either scenario, several conserved viral epitopes are non-neutralizing or low-potency to target, including NP, NA, and some HA stalk epitopes. In addition, neutralizing MBCs generated from childhood exposures that are recalled against drifted variants of the same subtype could be low affinity and lack the ability to neutralize current strains (*259, 260*). Finally, different subtypes of influenza including H1N1 and H3N2 are in circulation each season and individuals are continually exposed to variants of both throughout their lifetime. Therefore, it is not possible to control which influenza variants an individual is exposed to, and more often than not imprinting could result in poorly adapted immune responses. For these reasons, it is essential that we develop universal influenza virus vaccines that boost durable immunity to conserved, high potency viral epitopes and that can be administered to both children and adults.

In addition to preexisting immunity, we report for the first time that exposure route via natural infection versus vaccination impacts the MBCs that are recalled by influenza virus exposures in adulthood (Chapter 2). We identified that natural infection recalls preexisting immune memory to conserved yet poorly protective viral epitopes, likely due to the abundance of these antigens presented to the immune system during natural infection. By contrast, we observed that vaccination could harness preexisting immunity to draw out cross-reactive antibody responses to the HA head. These data suggest that vaccination has the potential to induce cross-reactive and neutralizing responses, but whether these responses are high enough in magnitude, potency, and durability to provide protection is unclear.

Alternative universal vaccine platforms will be required to overcome antigenic variation and any detrimental effects of imprinting. Several next-generation vaccine platforms that aim to induce antibodies against conserved sites have been approved or are in clinical trials, including high dose vaccines(*261, 262*), chimeric HA vaccines(*40*), headless HA vaccines (*60, 263*), computationally optimized broadly reactive antigen (COBRA)-generated HA protein vaccines(*264-266*), and nanoparticle vaccines(*263, 267, 268*). However, inducing antibody responses to conserved viral epitopes is not enough: next generation vaccination platforms must also focus on increasing the magnitude and durability of antibody responses. In 2018, the National Institute of Allergy and Infectious Disease reported key requirements of a successful universal influenza virus vaccine, including the stipulation that such a vaccine provide durable protection that lasts up to one-year post-vaccination, preferably through multiple seasons(*269*). To this end, different combinations of adjuvants, prime/boost regimens, and delivery routes are being investigated. Nanoparticle display vaccines offer promising results, as they increase the magnitude of immune responses by increasing BCR crosslinking and antigen deposition onto follicular dendritic cells, and increase the recruitment of B cell clones to GCs(*270, 271*). Moreover, due to their potential enhancement of immunogenicity, nanoparticle vaccines may have the ability to recruit lower-affinity B cells and germline B cells into the immune response, allowing for *de novo* responses that are not biased by preexisting immunity(*272*).

Finally, perhaps the most obvious path to overcoming imprinting is to better understand pediatric influenza immunity and develop universal vaccines that can be administered to children(*273*). If vaccines could be administered in early life prior to first infection, one could essentially 'artificially imprint' the immune system to multiple influenza virus antigens through vaccination. This would allow for the development of cross-reactive B cell memory to several influenza viruses before any natural MBC biases are formed. Our understanding of anti-influenza immunity in infants and children is limited, but it is currently appreciated that children mount narrow, strain-specific responses relative to adults(*274*). Logically, children have not been exposed to multiple variants of influenza virus and can therefore more easily mount *de novo* antibody responses, likely regardless of whether they are experiencing a primary infection or not. Administering universal influenza vaccines to children would theoretically allow for the development of *de novo* antibody responses to multiple influenza virus strains simultaneously. However, it remains unknown how natural infection versus vaccination differentially imprint the immune system of children. Some have proposed that the strongest way to imprint the infant immune system via vaccination may be through live attenuated influenza vaccines (LAIV), which can stimulate robust memory T and B cell responses, as well as mucosal immunity(*273*). Unfortunately, LAIV are currently not recommended for children under two years old, due to reports of increased wheezing reactions in that age group(*275*). In addition, LAIV have been shown to be less effective in children than in adults (*276, 277*).

Whether and how universal influenza virus vaccines can be administered to infants and children will depend on increasing our understanding of anti-influenza immunity in pediatric populations. Below, current strides in our understanding of influenza imprinting in children are outlined, including future experiments to dissect mechanisms of imprinting.

4.2.2 Investigating mechanisms of antigenic imprinting in children

Immunity to influenza differs vastly between children and adults, though our understanding of T and B cell responses to influenza virus infection and vaccination in

children is scarce. Moreover, understanding pediatric immunity is further complicated by the presence of circulating maternal antibody in infants. Perhaps the most obvious difference in pediatric immune systems is the substantially larger naïve B and T cell compartments. Due to delayed kinetics of *de novo* antibody responses derived from naïve B cells, the response to influenza viruses in children is likely delayed relative to adults. This could attribute to the increased susceptibility to influenza viruses seen within the pediatric population (5 years and younger). Memory B and T cell responses are nevertheless established in children, with evidence for higher magnitude T cell responses following natural infection versus vaccination (*278, 279*). To date, little is known regarding the B cell repertoire elicited by natural influenza virus infection and vaccination in children, the memory B cell subsets that contribute to early priming and re-call responses, and the B cell immunodominance hierarchies that follow initial exposure. To address these questions, our group has collected longitudinal pediatric influenza virus infection and vaccination PBMC samples and single cell sorted plasmablasts in the 2018–2019 and 2019–2020 influenza seasons. Using single B cell cloning from plasmablasts as in Chapter 2, and oligo-tagged antigen bait sorting and sequencing as in Chapter 3 of this work, we are investigating B cell subsets and immunodominance elicited by early exposures to influenza viruses in children. Through this work, we hope to identify potential mechanisms and immune signatures responsible for B cell focusing to distinct viral epitopes.

4.3 Toward a pan-coronavirus vaccine

4.3.1 Emergence of SARS-CoV-2 viral variants

Relative to influenza viruses, SARS-CoV-2 evolves about half as fast, with its 30,000 base pair genome acquiring about two amino acid mutations per month(*111, 280*). This is largely due to the unique RNA proofreading mechanism endowed by the RNA polymerase of coronaviruses(*281*). However, due to the persistence of the COVID-19 pandemic and the widespread transmission of the virus over the past year and a half, SARS-CoV-2 has inevitably acquired mutations in the spike domain since its emergence. Among the key variants of

concern are the UK (B.1.1.7), South Africa (B.1.351), Brazil and Japan (P.1 and P.2), California (B.1.427 and B.1.429), and Denmark (B.1.1.298) variants (*282-285*). The California variants, harboring a D614G mutation in the spike domain, were originally reported as more infectious and transmissible, though some studies showed effective cross-neutralization using sera from convalescent subjects(*140, 286-288*). Even more infectious is the UK B.1.1.7 variant, which harbors three amino acid deletions and seven missense mutations in spike, including D614G and N501Y in the RBD, with some strains possessing an E484K mutation (*289, 290*). The E484K mutation is also shared across the Brazil and South African variants. These strains are spreading rapidly, and are associated with the first cases of re-infection(*291*). Finally, several strains within the B.1.251 lineage have emerged with multiple mutations in the RBD, including K417N, E484K, and N501Y. Dauntingly, recent data report that these variants can escape vaccine-induced immunity with a reduction in neutralization up to 10-fold (*292-294*).

With the emergence of these variants, more research is warranted to understand features of antibodies capable of cross-neutralization. Of promise, prior infection followed by subsequent SARS-CoV-2 mRNA vaccination has been shown to boost cross-neutralizing antibodies (*293*). Furthermore, the identification of antibodies targeting conserved regions across multiple coronaviruses suggests that a better characterization of conserved viral epitopes may inform novel vaccination and therapeutic strategies(*33*).

4.3.2 The quest for broadly neutralizing anti-SARS-CoV-2 antibodies

Upon viral infection, humans can generate rare antibodies with the ability to neutralize several antigenic variants within the same viral family, dubbed broadly neutralizing antibodies (bnAbs). BnAbs exhibit restricted repertoire features and have been characterized for HIV-1, influenza, and Ebola virus infection, and inducing them is a key goal of vaccination efforts (*295-297*). Currently, mAb therapeutics against COVID-19 have focused on potently neutralizing epitopes of the RBD, though these epitopes are not necessarily evolutionarily conserved. In fact, a recent study using yeast display technology to generate RBD mutants

revealed a single amino acid mutation that could escape the Regeneron Pharmaceuticals antibody cocktail, which consists of two antibodies targeting non-overlapping viral epitopes(*127, 298*). Several other groups have similarly reported viral escape from key bnAbs originally isolated against the Wuhan variant(*299, 300*).

To circumvent viral escape, several groups are investigating bnAb responses to SARS-CoV-2. Harnessing the ability of preexisting immunity to induce antibodies to conserved epitopes, small biotech company Adimab has isolated mAbs originally induced by SARS1 infection that neutralize SARS-CoV-2(*33*). To increase neutralization potency, they generated affinity-matured versions using yeast-display technology, and one lead mAb is currently in phase I clinical trials(*41*). Further studies are warranted to dissect the features of SARS-CoV-2 bnAbs, though key characteristics in VH gene usage, complementarity determining regions, and conformation-dependent binding have been identified through the studies of other viruses(*301*). Progress has already been made in defining how distinct spike mutations alter the activity of neutralizing antibodies – for example, structural and functional characterization of neutralizing antibodies has resulted in identification of three distinct neutralizing SARS-CoV-2 antibody classes(*302*).

Despite the astounding toll that the COVID-19 pandemic has taken over the past year and a half, SARS-CoV-2 research continues to flourish and several advances have been made. Fortunately, the knowledge of antibody responses to other viruses such as influenza has been used as a stepping stone toward generating novel vaccines and antibody therapeutics. In response to a global pandemic, our group was able to rapidly profile the human B cell response to infection, assessing antibody responses to multiple viral targets. Our dataset is the first of its kind to provide B cell specificity, transcriptome, and BCR sequence from single B cells in the context of SARS-CoV-2 infection. As a result, we were able to characterize the protective potential of antibodies not only to the spike protein, but to NP and ORF8 as well. In addition, our transcriptional dataset provides one of the first high-throughput analyses of the B cell response to a completely novel infection. The methodologies, results, and antibody sequences reported herein serve as a framework for

investigating antibody evolution to new variants, and importantly, to vaccination. In the face of persistent viral evolution, studies such as this bring us one step closer to combating one of the deadliest viruses in modern history.

BIBLIOGRAPHY

1. S. H. Kaufmann, Remembering Emil von Behring: from Tetanus Treatment to Antibody Cooperation with Phagocytes. *mBio* **8**, (2017).

2. G. D. Victora, M. C. Nussenzweig, Germinal centers. *Annu Rev Immunol* **30**, 429-457 (2012).

3. A. E. Palm, C. Henry, Remembrance of Things Past: Long-Term B Cell Memory After Infection and Vaccination. *Front Immunol* **10**, 1787 (2019).

4. D. Paus *et al.*, Antigen recognition strength regulates the choice between extrafollicular plasma cell and germinal center B cell differentiation. *J Exp Med* **203**, 1081-1091 (2006).

5. C. Viant *et al.*, Antibody Affinity Shapes the Choice between Memory and Germinal Center B Cell Fates. *Cell* **183**, 1298-1311 e1211 (2020).

6. T. G. Phan *et al.*, High affinity germinal center B cells are actively selected into the plasma cell compartment. *J Exp Med* **203**, 2419-2424 (2006).

7. S. Song, P. D. Matthias, The Transcriptional Regulation of Germinal Center Formation. *Front Immunol* **9**, 2026 (2018).

8. U. Klein *et al.*, Transcriptional analysis of the B cell germinal center reaction. *Proc Natl Acad Sci U S A* **100**, 2639-2644 (2003).

9. U. Klein *et al.*, Gene expression dynamics during germinal center transit in B cells. *Ann N Y Acad Sci* **987**, 166-172 (2003).

10. D. Bhattacharya *et al.*, Transcriptional profiling of antigen-dependent murine B cell differentiation and memory formation. *J Immunol* **179**, 6808-6819 (2007).

11. M. M. Tomayko *et al.*, Systematic comparison of gene expression between murine memory and naive B cells demonstrates that memory B cells have unique signaling capabilities. *J Immunol* **181**, 27-38 (2008).

12. R. Shinnakasu *et al.*, Regulated selection of germinal-center cells into the memory B cell compartment. *Nat Immunol* **17**, 861-869 (2016).

13. C. Zhao *et al.*, POU2AF1, an amplification target at 11q23, promotes growth of multiple myeloma cells by directly regulating expression of a B-cell maturation factor, TNFRSF17. *Oncogene* **27**, 63-75 (2008).

14. S. G. Tangye, Y. J. Liu, G. Aversa, J. H. Phillips, J. E. de Vries, Identification of functional human splenic memory B cells by expression of CD148 and CD27. *J Exp Med* **188**, 1691-1703 (1998).

15. R. Kuppers, Human memory B cells: memory B cells of a special kind. *Immunol Cell Biol* **86**, 635-636 (2008).

16. S. L. Nutt, N. Taubenheim, J. Hasbold, L. M. Corcoran, P. D. Hodgkin, The genetic network controlling plasma cell differentiation. *Semin Immunol* **23**, 341-349 (2011).

17. S. M. Lightman, A. Utley, K. P. Lee, Survival of Long-Lived Plasma Cells (LLPC): Piecing Together the Puzzle. *Front Immunol* **10**, 965 (2019).

18. S. Weller *et al.*, Human blood IgM "memory" B cells are circulating splenic marginal zone B cells harboring a prediversified immunoglobulin repertoire. *Blood* **104**, 3647-3654 (2004).

19. D. Bagnara *et al.*, A Reassessment of IgM Memory Subsets in Humans. *J Immunol* **195**, 3716-3724 (2015).

20. A. Erazo *et al.*, Unique maturation program of the IgE response in vivo. *Immunity* **26**, 191-203 (2007).

21. S. Duchez *et al.*, Premature replacement of mu with alpha immunoglobulin chains impairs lymphopoiesis and mucosal homing but promotes plasma cell maturation. *Proc Natl Acad Sci U S A* **107**, 3064-3069 (2010).

22. Z. Yang, B. M. Sullivan, C. D. Allen, Fluorescent in vivo detection reveals that IgE(+) B cells are restrained by an intrinsic cell fate predisposition. *Immunity* **36**, 857-872 (2012).

23. Y. Xu *et al.*, No receptor stands alone: IgG B-cell receptor intrinsic and extrinsic mechanisms contribute to antibody memory. *Cell Res* **24**, 651-664 (2014).

24. A. D. Gitlin *et al.*, Independent Roles of Switching and Hypermutation in the Development and Persistence of B Lymphocyte Memory. *Immunity* **44**, 769-781 (2016).

25. W. Ise *et al.*, T Follicular Helper Cell-Germinal Center B Cell Interaction Strength Regulates Entry into Plasma Cell or Recycling Germinal Center Cell Fate. *Immunity* **48**, 702-715 e704 (2018).

26. D. Angeletti, J. W. Yewdell, Understanding and Manipulating Viral Immunity: Antibody Immunodominance Enters Center Stage. *Trends Immunol* **39**, 549-561 (2018).

27. H. X. Tan *et al.*, Subdominance and poor intrinsic immunogenicity limit humoral immunity targeting influenza HA stem. *J Clin Invest* **129**, 850-862 (2019).

28. C. Graham *et al.*, Impact of the B.1.1.7 variant on neutralizing monoclonal antibodies recognizing diverse epitopes on SARS-CoV-2 Spike. *bioRxiv*, (2021).

29. S. Sasaki *et al.*, Influence of prior influenza vaccination on antibody and B-cell responses. *PLoS One* **3**, e2975 (2008).

30. S. F. Andrews *et al.*, High preexisting serological antibody levels correlate with diversification of the influenza vaccine response. *J Virol* **89**, 3308-3317 (2015).

31. V. I. Zarnitsyna *et al.*, Masking of antigenic epitopes by antibodies shapes the humoral immune response to influenza. *Philos Trans R Soc Lond B Biol Sci* **370**, (2015).

32. H. Lv *et al.*, Cross-reactive Antibody Response between SARS-CoV-2 and SARS-CoV Infections. *Cell Rep* **31**, 107725 (2020).

33. A. Z. Wec *et al.*, Broad neutralization of SARS-related viruses by human monoclonal antibodies. *Science* **369**, 731-736 (2020).

34. J. T. Ladner *et al.*, Epitope-resolved profiling of the SARS-CoV-2 antibody response identifies cross-reactivity with endemic human coronaviruses. *Cell Rep Med* **2**, 100189 (2021).

35. K. Hancock *et al.*, Cross-reactive antibody responses to the 2009 pandemic H1N1 influenza virus. *N Engl J Med* **361**, 1945-1952 (2009).

36. J. Wrammert *et al.*, Broadly cross-reactive antibodies dominate the human B cell response against 2009 pandemic H1N1 influenza virus infection. *J Exp Med* **208**, 181-193 (2011).

37. Y. Li *et al.*, Immune history shapes specificity of pandemic H1N1 influenza antibody responses. *J Exp Med* **210**, 1493-1500 (2013).

38. S. F. Andrews *et al.*, Immune history profoundly affects broadly protective B cell responses to influenza. *Sci Transl Med* **7**, 316ra192 (2015).

39. D. I. Bernstein *et al.*, Immunogenicity of chimeric haemagglutinin-based, universal influenza virus vaccine candidates: interim results of a randomised, placebo-controlled, phase 1 clinical trial. *Lancet Infect Dis* **20**, 80-91 (2020).

40. R. Nachbagauer *et al.*, A chimeric hemagglutinin-based universal influenza virus vaccine approach induces broad and long-lasting immunity in a randomized, placebo-controlled phase I trial. *Nat Med* **27**, 106-114 (2021).

41. C. G. Rappazzo *et al.*, Broad and potent activity against SARS-like viruses by an engineered human monoclonal antibody. *Science* **371**, 823-829 (2021).

42. D. R. Burton, E. J. Topol, Variant-proof vaccines - invest now for the next pandemic. *Nature* **590**, 386-388 (2021).

43. S. D. Jazayeri, C. L. Poh, Development of Universal Influenza Vaccines Targeting Conserved Viral Proteins. *Vaccines (Basel)* **7**, (2019).

44. J. J. Guthmiller, H. L. Dugan, K. E. Neu, L. Y. Lan, P. C. Wilson, An Efficient Method to Generate Monoclonal Antibodies from Human B Cells. *Methods Mol Biol* **1904**, 109-145 (2019).

45. S. L. Topalian *et al.*, Safety, activity, and immune correlates of anti-PD-1 antibody in cancer. *N Engl J Med* **366**, 2443-2454 (2012).

46. E. H. Romond *et al.*, Trastuzumab plus adjuvant chemotherapy for operable HER2-positive breast cancer. *N Engl J Med* **353**, 1673-1684 (2005).

47. A. R. Ahmed, Z. Spigelman, L. A. Cavacini, M. R. Posner, Treatment of pemphigus vulgaris with rituximab and intravenous immune globulin. *N Engl J Med* **355**, 1772-1779 (2006).

48. M. E. Weinblatt *et al.*, Adalimumab, a fully human anti-tumor necrosis factor alpha monoclonal antibody, for the treatment of rheumatoid arthritis in patients taking concomitant methotrexate: the ARMADA trial. *Arthritis Rheum* **48**, 35-45 (2003).

49. F. Vincenti *et al.*, Interleukin-2-receptor blockade with daclizumab to prevent acute rejection in renal transplantation. Daclizumab Triple Therapy Study Group. *N Engl J Med* **338**, 161-165 (1998).

50. Y. Q. Chen *et al.*, Influenza Infection in Humans Induces Broadly Cross-Reactive and Protective Neuraminidase-Reactive Antibodies. *Cell* **173**, 417-429 e410 (2018).

51. L. M. Walker *et al.*, Broad and potent neutralizing antibodies from an African donor reveal a new HIV-1 vaccine target. *Science* **326**, 285-289 (2009).

52. X. Wu *et al.*, Rational design of envelope identifies broadly neutralizing human monoclonal antibodies to HIV-1. *Science* **329**, 856-861 (2010).

53. Z. Shriver, J. M. Trevejo, R. Sasisekharan, Antibody-Based Strategies to Prevent and Treat Influenza. *Front Immunol* **6**, 315 (2015).

54. C. Wang *et al.*, A human monoclonal antibody blocking SARS-CoV-2 infection. *Nat Commun* **11**, 2251 (2020).

55. T. Noy-Porat *et al.*, A panel of human neutralizing mAbs targeting SARS-CoV-2 spike at multiple epitopes. *Nat Commun* **11**, 4303 (2020).

56. D. R. Burton, What Are the Most Powerful Immunogen Design Vaccine Strategies? Reverse Vaccinology 2.0 Shows Great Promise. *Cold Spring Harb Perspect Biol* **9**, (2017).

57. A. Lanzavecchia, A. Fruhwirth, L. Perez, D. Corti, Antibody-guided vaccine design: identification of protective epitopes. *Curr Opin Immunol* **41**, 62-67 (2016).

58. D. R. Burton, L. Hangartner, Broadly Neutralizing Antibodies to HIV and Their Role in Vaccine Design. *Annu Rev Immunol* **34**, 635-659 (2016).

59. R. Hai *et al.*, Influenza viruses expressing chimeric hemagglutinins: globular head and stalk domains derived from different subtypes. *J Virol* **86**, 5774-5781 (2012).

60. A. Impagliazzo *et al.*, A stable trimeric influenza hemagglutinin stem as a broadly protective immunogen. *Science* **349**, 1301-1306 (2015).

61. A. D. Iuliano *et al.*, Estimates of global seasonal influenza-associated respiratory mortality: a modelling study. *Lancet* **391**, 1285-1300 (2018).

62. W. Putri, D. J. Muscatello, M. S. Stockwell, A. T. Newall, Economic burden of seasonal influenza in the United States. *Vaccine* **36**, 3960-3966 (2018).

63. F. Prager, D. Wei, A. Rose, Total Economic Consequences of an Influenza Outbreak in the United States. *Risk Anal* **37**, 4-19 (2017).

64. F. Krammer *et al.*, Influenza. *Nat Rev Dis Primers* **4**, 3 (2018).

65. W. Weis *et al.*, Structure of the influenza virus haemagglutinin complexed with its receptor, sialic acid. *Nature* **333**, 426-431 (1988).

66. G. M. Air, Sequence relationships among the hemagglutinin genes of 12 subtypes of influenza A virus. *Proc Natl Acad Sci U S A* **78**, 7639-7643 (1981).

67. D. Hobson, R. L. Curry, A. S. Beare, A. Ward-Gardner, The role of serum haemagglutination-inhibiting antibody in protection against challenge infection with influenza A2 and B viruses. *J Hyg (Lond)* **70**, 767-777 (1972).

68. J. J. Skehel *et al.*, Changes in the conformation of influenza virus hemagglutinin at the pH optimum of virus-mediated membrane fusion. *Proc Natl Acad Sci U S A* **79**, 968-972 (1982).

69. P. A. Bullough, F. M. Hughson, J. J. Skehel, D. C. Wiley, Structure of influenza haemagglutinin at the pH of membrane fusion. *Nature* **371**, 37-43 (1994).

70. F. Krammer *et al.*, NAction! How Can Neuraminidase-Based Immunity Contribute to Better Influenza Virus Vaccines? *mBio* **9**, (2018).

71. M. R. Sandbulte *et al.*, Discordant antigenic drift of neuraminidase and hemagglutinin in H1N1 and H3N2 influenza viruses. *Proc Natl Acad Sci U S A* **108**, 20748-20753 (2011).

72. C. Henry *et al.*, Influenza Virus Vaccination Elicits Poorly Adapted B Cell Responses in Elderly Individuals. *Cell Host Microbe* **25**, 357-366 e356 (2019).

73. E. D. Kilbourne, B. E. Johansson, B. Grajower, Independent and disparate evolution in nature of influenza A virus hemagglutinin and neuraminidase glycoproteins. *Proc Natl Acad Sci U S A* **87**, 786-790 (1990).

74. H. E. Maier *et al.*, Pre-existing Antineuraminidase Antibodies Are Associated With Shortened Duration of Influenza A(H1N1)pdm Virus Shedding and Illness in Naturally Infected Adults. *Clin Infect Dis* **70**, 2290-2297 (2020).

75. M. McMahon *et al.*, Mucosal Immunity against Neuraminidase Prevents Influenza B Virus Transmission in Guinea Pigs. *mBio* **10**, (2019).

76. R. B. Couch *et al.*, Randomized comparative study of the serum antihemagglutinin and antineuraminidase antibody responses to six licensed trivalent influenza vaccines. *Vaccine* **31**, 190-195 (2012).

77. N. Sukeno *et al.*, Anti-nucleoprotein antibody response in influenza A infection. *Tohoku J Exp Med* **128**, 241-249 (1979).

78. R. Haaheim, Single-radial-complement-fixation: a new immunodiffusion technique. 2. Assay of the antibody response to the internal antigens (MP and NP) of influenza A virus in human sera after vaccination and infection. *Dev Biol Stand* **39**, 481-484 (1977).

79. S. Jegaskanda *et al.*, Induction of H7N9-Cross-Reactive Antibody-Dependent Cellular Cytotoxicity Antibodies by Human Seasonal Influenza A Viruses that are Directed Toward the Nucleoprotein. *J Infect Dis* **215**, 818-823 (2017).

80. D. A. Steinhauer, E. Domingo, J. J. Holland, Lack of evidence for proofreading mechanisms associated with an RNA virus polymerase. *Gene* **122**, 281-288 (1992).

81. A. Ishihama, K. Mizumoto, K. Kawakami, A. Kato, A. Honda, Proofreading function associated with the RNA-dependent RNA polymerase from influenza virus. *J Biol Chem* **261**, 10417-10421 (1986).

82. J. K. Taubenberger, The origin and virulence of the 1918 "Spanish" influenza virus. *Proc Am Philos Soc* **150**, 86-112 (2006).

83. G. D. Victora, P. C. Wilson, Germinal center selection and the antibody response to influenza. *Cell* **163**, 545-548 (2015).

84. S. J. Zost *et al.*, Contemporary H3N2 influenza viruses have a glycosylation site that alters binding of antibodies elicited by egg-adapted vaccine strains. *Proc Natl Acad Sci U S A* **114**, 12578-12583 (2017).

85. F. S. Dawood *et al.*, Interim Estimates of 2019-20 Seasonal Influenza Vaccine Effectiveness - United States, February 2020. *MMWR Morb Mortal Wkly Rep* **69**, 177-182 (2020).

86. M. F. Boni, Vaccination and antigenic drift in influenza. *Vaccine* **26 Suppl 3**, C8-14 (2008).

87. A. C. Tricco *et al.*, Comparing influenza vaccine efficacy against mismatched and matched strains: a systematic review and meta-analysis. *BMC Med* **11**, 153 (2013).

88. C. I. Paules, H. D. Marston, R. W. Eisinger, D. Baltimore, A. S. Fauci, The Pathway to a Universal Influenza Vaccine. *Immunity* **47**, 599-603 (2017).

89. C. J. Wei *et al.*, Author Correction: Next-generation influenza vaccines: opportunities and challenges. *Nat Rev Drug Discov* **19**, 427 (2020).

90. Y. H. Jang, B. L. Seong, The Quest for a Truly Universal Influenza Vaccine. *Front Cell Infect Microbiol* **9**, 344 (2019).

91. S. A. Valkenburg *et al.*, Stalking influenza by vaccination with pre-fusion headless HA mini-stem. *Sci Rep* **6**, 22666 (2016).

92. D. Angeletti *et al.*, Outflanking immunodominance to target subdominant broadly neutralizing epitopes. *Proc Natl Acad Sci U S A* **116**, 13474-13479 (2019).

93. J. P. Julien, P. S. Lee, I. A. Wilson, Structural insights into key sites of vulnerability on HIV-1 Env and influenza HA. *Immunol Rev* **250**, 180-198 (2012).

94. J. R. Whittle *et al.*, Broadly neutralizing human antibody that recognizes the receptor-binding pocket of influenza virus hemagglutinin. *Proc Natl Acad Sci U S A* **108**, 14216-14221 (2011).

95. D. C. Ekiert *et al.*, Cross-neutralization of influenza A viruses mediated by a single antibody loop. *Nature* **489**, 526-532 (2012).

96. D. D. Raymond *et al.*, Conserved epitope on influenza-virus hemagglutinin head defined by a vaccine-induced antibody. *Proc Natl Acad Sci U S A* **115**, 168-173 (2018).

97. F. M. Davenport, A. V. Hennessy, T. Francis, Jr., Epidemiologic and immunologic significance of age distribution of antibody to antigenic variants of influenza virus. *J Exp Med* **98**, 641-656 (1953).

98. D. N. Fisman *et al.*, Older age and a reduced likelihood of 2009 H1N1 virus infection. *N Engl J Med* **361**, 2000-2001 (2009).

99. I. Skountzou *et al.*, Immunity to pre-1950 H1N1 influenza viruses confers cross-protection against the pandemic swine-origin 2009 A (H1N1) influenza virus. *J Immunol* **185**, 1642-1649 (2010).

100. J. Lessler *et al.*, Evidence for antigenic seniority in influenza A (H3N2) antibody responses in southern China. *PLoS Pathog* **8**, e1002802 (2012).

101. S. L. Linderman *et al.*, Potential antigenic explanation for atypical H1N1 infections among middle-aged adults during the 2013-2014 influenza season. *Proc Natl Acad Sci U S A* **111**, 15798-15803 (2014).

102. C. J. Henry Dunand *et al.*, Preexisting human antibodies neutralize recently emerged H7N9 influenza strains. *J Clin Invest* **125**, 1255-1268 (2015).

103. K. M. Gostic, M. Ambrose, M. Worobey, J. O. Lloyd-Smith, Potent protection against H5N1 and H7N9 influenza via childhood hemagglutinin imprinting. *Science* **354**, 722-726 (2016).

104. B. Flannery *et al.*, Influence of Birth Cohort on Effectiveness of 2015-2016 Influenza Vaccine Against Medically Attended Illness Due to 2009 Pandemic Influenza A(H1N1) Virus in the United States. *J Infect Dis* **218**, 189-196 (2018).

105. S. G. Tangye, D. T. Avery, E. K. Deenick, P. D. Hodgkin, Intrinsic differences in the proliferation of naive and memory human B cells as a mechanism for enhanced secondary immune responses. *J Immunol* **170**, 686-694 (2003).

106. M. Auladell *et al.*, Recalling the Future: Immunological Memory Toward Unpredictable Influenza Viruses. *Front Immunol* **10**, 1400 (2019).

107. K. A. Pape, M. K. Jenkins, Do Memory B Cells Form Secondary Germinal Centers? It Depends. *Cold Spring Harb Perspect Biol* **10**, (2018).

108. C. Henry, A. E. Palm, F. Krammer, P. C. Wilson, From Original Antigenic Sin to the Universal Influenza Virus Vaccine. *Trends Immunol* **39**, 70-79 (2018).

109. K. M. Gostic *et al.*, Childhood immune imprinting to influenza A shapes birth year-specific risk during seasonal H1N1 and H3N2 epidemics. *medRxiv*, 19001834 (2019).

110. J. Cui, F. Li, Z. L. Shi, Origin and evolution of pathogenic coronaviruses. *Nat Rev Microbiol* **17**, 181-192 (2019).

111. Z. Abdelrahman, M. Li, X. Wang, Comparative Review of SARS-CoV-2, SARS-CoV, MERS-CoV, and Influenza A Respiratory Viruses. *Front Immunol* **11**, 552909 (2020).

112. N. Zhu *et al.*, A Novel Coronavirus from Patients with Pneumonia in China, 2019. *N Engl J Med* **382**, 727-733 (2020).

113. C. Huang *et al.*, Clinical features of patients infected with 2019 novel coronavirus in Wuhan, China. *Lancet* **395**, 497-506 (2020).

114. R. Wang *et al.*, Analysis of SARS-CoV-2 mutations in the United States suggests presence of four substrains and novel variants. *Commun Biol* **4**, 228 (2021).

115. Z. Wang *et al.*, mRNA vaccine-elicited antibodies to SARS-CoV-2 and circulating variants. *Nature*, (2021).

116. R. E. Chen *et al.*, Resistance of SARS-CoV-2 variants to neutralization by monoclonal and serum-derived polyclonal antibodies. *Nat Med*, (2021).

117. P. Wang *et al.*, Antibody Resistance of SARS-CoV-2 Variants B.1.351 and B.1.1.7. *Nature*, (2021).

118. N. C. Kyriakidis, A. Lopez-Cortes, E. V. Gonzalez, A. B. Grimaldos, E. O. Prado, SARS-CoV-2 vaccines strategies: a comprehensive review of phase 3 candidates. *NPJ Vaccines* **6**, 28 (2021).

119. L. A. Jackson *et al.*, An mRNA Vaccine against SARS-CoV-2 - Preliminary Report. *N Engl J Med* **383**, 1920-1931 (2020).

120. E. J. Anderson *et al.*, Safety and Immunogenicity of SARS-CoV-2 mRNA-1273 Vaccine in Older Adults. *N Engl J Med* **383**, 2427-2438 (2020).

121. L. R. Baden *et al.*, Efficacy and Safety of the mRNA-1273 SARS-CoV-2 Vaccine. *N Engl J Med* **384**, 403-416 (2021).

122. F. P. Polack *et al.*, Safety and Efficacy of the BNT162b2 mRNA Covid-19 Vaccine. *N Engl J Med* **383**, 2603-2615 (2020).

123. J. Sadoff *et al.*, Interim Results of a Phase 1-2a Trial of Ad26.COV2.S Covid-19 Vaccine. *N Engl J Med*, (2021).

124. J. Lan *et al.*, Structure of the SARS-CoV-2 spike receptor-binding domain bound to the ACE2 receptor. *Nature* **581**, 215-220 (2020).

125. R. Yan *et al.*, Structural basis for the recognition of SARS-CoV-2 by full-length human ACE2. *Science* **367**, 1444-1448 (2020).

126. J. Hansen *et al.*, Studies in humanized mice and convalescent humans yield a SARS-CoV-2 antibody cocktail. *Science* **369**, 1010-1014 (2020).

127. A. Baum *et al.*, Antibody cocktail to SARS-CoV-2 spike protein prevents rapid mutational escape seen with individual antibodies. *Science* **369**, 1014-1018 (2020).

128. P. Mertens *et al.*, Development and Potential Usefulness of the COVID-19 Ag Respi-Strip Diagnostic Assay in a Pandemic Context. *Front Med (Lausanne)* **7**, 225 (2020).

129. D. F. Robbiani *et al.*, Convergent antibody responses to SARS-CoV-2 in convalescent individuals. *Nature* **584**, 437-442 (2020).

130. Q. X. Long *et al.*, Clinical and immunological assessment of asymptomatic SARS-CoV-2 infections. *Nat Med* **26**, 1200-1204 (2020).

131. J. Perreault *et al.*, Waning of SARS-CoV-2 RBD antibodies in longitudinal convalescent plasma samples within 4 months after symptom onset. *Blood* **136**, 2588-2591 (2020).

132. J. M. Dan *et al.*, Immunological memory to SARS-CoV-2 assessed for up to 8 months after infection. *Science* **371**, (2021).

133. M. Sakharkar *et al.*, Prolonged evolution of the human B cell response to SARS-CoV-2 infection. *Sci Immunol* **6**, (2021).

134. C. Gaebler *et al.*, Evolution of antibody immunity to SARS-CoV-2. *Nature*, (2021).

135. L. B. Rodda *et al.*, Functional SARS-CoV-2-Specific Immune Memory Persists after Mild COVID-19. *Cell* **184**, 169-183 e117 (2021).

136. J. J. Guthmiller *et al.*, SARS-CoV-2 Infection Severity Is Linked to Superior Humoral Immunity against the Spike. *mBio* **12**, (2021).

137. K. Roltgen *et al.*, Defining the features and duration of antibody responses to SARS-CoV-2 infection associated with disease severity and outcome. *Sci Immunol* **5**, (2020).

138. C. B. Hansen *et al.*, SARS-CoV-2 Antibody Responses Are Correlated to Disease Severity in COVID-19 Convalescent Individuals. *J Immunol* **206**, 109-117 (2021).

139. Y. C. Bartsch *et al.*, Humoral signatures of protective and pathological SARS-CoV-2 infection in children. *Nat Med*, (2021).

140. W. F. Garcia-Beltran *et al.*, COVID-19-neutralizing antibodies predict disease severity and survival. *Cell* **184**, 476-488 e411 (2021).

141. C. Atyeo *et al.*, Distinct Early Serological Signatures Track with SARS-CoV-2 Survival. *Immunity* **53**, 524-532 e524 (2020).

142. B. Oliviero *et al.*, Expansion of atypical memory B cells is a prominent feature of COVID-19. *Cell Mol Immunol* **17**, 1101-1103 (2020).

143. M. C. Woodruff *et al.*, Extrafollicular B cell responses correlate with neutralizing antibodies and morbidity in COVID-19. *Nat Immunol* **21**, 1506-1516 (2020).

144. N. Kaneko *et al.*, The Loss of Bcl-6 Expressing T Follicular Helper Cells and the Absence of Germinal Centers in COVID-19. *SSRN*, 3652322 (2020).

145. S. B. Halstead, S. Rojanasuphot, N. Sangkawibha, Original antigenic sin in dengue. *Am J Trop Med Hyg* **32**, 154-156 (1983).

146. C. M. Midgley *et al.*, An in-depth analysis of original antigenic sin in dengue virus infection. *J Virol* **85**, 410-421 (2011).

147. A. L. Rothman, Immunity to dengue virus: a tale of original antigenic sin and tropical cytokine storms. *Nat Rev Immunol* **11**, 532-543 (2011).

148. T. F. Rogers *et al.*, Zika virus activates de novo and cross-reactive memory B cell responses in dengue-experienced donors. *Sci Immunol* **2**, (2017).

149. E. M. Anderson *et al.*, Seasonal human coronavirus antibodies are boosted upon SARS-CoV-2 infection but not associated with protection. *Cell*, (2021).

150. P. Nguyen-Contant *et al.*, S Protein-Reactive IgG and Memory B Cell Production after Human SARS-CoV-2 Infection Includes Broad Reactivity to the S2 Subunit. *mBio* **11**, (2020).

151. A. Sokal *et al.*, Maturation and persistence of the anti-SARS-CoV-2 memory B cell response. *Cell* **184**, 1201-1213 e1214 (2021).

152. K. W. Ng *et al.*, Preexisting and de novo humoral immunity to SARS-CoV-2 in humans. *Science* **370**, 1339-1343 (2020).

153. A. Grifoni *et al.*, Targets of T Cell Responses to SARS-CoV-2 Coronavirus in Humans with COVID-19 Disease and Unexposed Individuals. *Cell* **181**, 1489-1501 e1415 (2020).

154. S. Y. Fung, K. S. Yuen, Z. W. Ye, C. P. Chan, D. Y. Jin, A tug-of-war between severe acute respiratory syndrome coronavirus 2 and host antiviral defence: lessons from other pathogenic viruses. *Emerg Microbes Infect* **9**, 558-570 (2020).

155. J. A. Jaimes, N. M. Andre, J. S. Chappie, J. K. Millet, G. R. Whittaker, Phylogenetic Analysis and Structural Modeling of SARS-CoV-2 Spike Protein Reveals an Evolutionary Distinct and Proteolytically Sensitive Activation Loop. *J Mol Biol* **432**, 3309-3325 (2020).

156. L. C. Katzelnick *et al.*, Antibody-dependent enhancement of severe dengue disease in humans. *Science* **358**, 929-932 (2017).

157. E. M. Anderson *et al.*, Seasonal human coronavirus antibodies are boosted upon SARS-CoV-2 infection but not associated with protection. *medRxiv*, (2020).

158. H. L. Dugan, C. Henry, P. C. Wilson, Aging and influenza vaccine-induced immunity. *Cell Immunol* **348**, 103998 (2020).

159. D. Santesmasses *et al.*, COVID-19 is an emergent disease of aging. *Aging Cell* **19**, e13230 (2020).

160. V. Bajaj *et al.*, Aging, Immunity, and COVID-19: How Age Influences the Host Immune Response to Coronavirus Infections? *Front Physiol* **11**, 571416 (2020).

161. S. L. Klein *et al.*, Sex, age, and hospitalization drive antibody responses in a COVID-19 convalescent plasma donor population. *J Clin Invest* **130**, 6141-6150 (2020).

162. L. Grzelak *et al.*, Sex differences in the evolution of neutralizing antibodies to SARS-CoV-2. *J Infect Dis*, (2021).

163. H. L. Dugan *et al.*, Preexisting immunity shapes distinct antibody landscapes after influenza virus infection and vaccination in humans. *Sci Transl Med* **12**, (2020).

164. R. G. Webster, W. G. Laver, G. M. Air, G. C. Schild, Molecular mechanisms of variation in influenza viruses. *Nature* **296**, 115-121 (1982).

165. F. Krammer, P. Palese, Advances in the development of influenza virus vaccines. *Nature reviews. Drug discovery* **14**, 167-182 (2015).

166. S. E. Ohmit, J. G. Petrie, R. T. Cross, E. Johnson, A. S. Monto, Influenza hemagglutination-inhibition antibody titer as a correlate of vaccine-induced protection. *J Infect Dis* **204**, 1879-1885 (2011).

167. M. B. Doud, J. M. Lee, J. D. Bloom, How single mutations affect viral escape from broad and narrow antibodies to H1 influenza hemagglutinin. *Nat Commun* **9**, 1386 (2018).

168. N. S. Heaton, D. Sachs, C. J. Chen, R. Hai, P. Palese, Genome-wide mutagenesis of influenza virus reveals unique plasticity of the hemagglutinin and NS1 proteins. *Proc Natl Acad Sci U S A* **110**, 20248-20253 (2013).

169. M. B. Doud, J. D. Bloom, Accurate Measurement of the Effects of All Amino-Acid Mutations on Influenza Hemagglutinin. *Viruses* **8**, (2016).

170. E. Kirkpatrick, X. Qiu, P. C. Wilson, J. Bahl, F. Krammer, The influenza virus hemagglutinin head evolves faster than the stalk domain. *Sci Rep* **8**, 10432 (2018).

171. J. M. Fonville *et al.*, Antibody landscapes after influenza virus infection or vaccination. *Science* **346**, 996-1000 (2014).

172. J. J. Guthmiller, P. C. Wilson, Harnessing immune history to combat influenza viruses. *Curr Opin Immunol* **53**, 187-195 (2018).

173. S. L. Linderman, S. E. Hensley, Antibodies with 'Original Antigenic Sin' Properties Are Valuable Components of Secondary Immune Responses to Influenza Viruses. *PLoS Pathog* **12**, e1005806 (2016).

174. P. Arevalo, H. Q. McLean, E. A. Belongia, S. Cobey, Earliest infections predict the age distribution of seasonal influenza A cases. *Elife* **9**, (2020).

175. K. M. Gostic *et al.*, Childhood immune imprinting to influenza A shapes birth year-specific risk during seasonal H1N1 and H3N2 epidemics. *PLoS Pathog* **15**, e1008109 (2019).

176. C. Henry *et al.*, Monoclonal antibody responses after recombinant HA vaccine versus subunit inactivated influenza virus vaccine: a comparative study. *J Virol*, (2019).

177. X. S. He *et al.*, Distinct patterns of B-cell activation and priming by natural influenza virus infection versus inactivated influenza vaccination. *J Infect Dis* **211**, 1051-1059 (2015).

178. I. Margine *et al.*, H3N2 influenza virus infection induces broadly reactive hemagglutinin stalk antibodies in humans and mice. *J Virol* **87**, 4728-4737 (2013).

179. J. Wrammert *et al.*, Rapid cloning of high-affinity human monoclonal antibodies against influenza virus. *Nature* **453**, 667-671 (2008).

180. G. D. Appiah *et al.*, Influenza activity - United States, 2014-15 season and composition of the 2015-16 influenza vaccine. *MMWR Morb Mortal Wkly Rep* **64**, 583-590 (2015).

181. S. L. Davlin *et al.*, Influenza Activity - United States, 2015-16 Season and Composition of the 2016-17 Influenza Vaccine. *MMWR Morb Mortal Wkly Rep* **65**, 567-575 (2016).

182. R. Nachbagauer *et al.*, Age Dependence and Isotype Specificity of Influenza Virus Hemagglutinin Stalk-Reactive Antibodies in Humans. *mBio* **7**, e01996-01915 (2016).

183. M. Rajendran *et al.*, Analysis of Anti-Influenza Virus Neuraminidase Antibodies in Children, Adults, and the Elderly by ELISA and Enzyme Inhibition: Evidence for Original Antigenic Sin. *mBio* **8**, (2017).

184. C. Dreyfus *et al.*, Highly conserved protective epitopes on influenza B viruses. *Science* **337**, 1343-1348 (2012).

185. N. M. Ferguson, A. P. Galvani, R. M. Bush, Ecological and immunological determinants of influenza evolution. *Nature* **422**, 428-433 (2003).

186. R. B. Abreu, G. A. Kirchenbaum, E. F. Clutter, G. A. Sautto, T. M. Ross, Preexisting subtype immunodominance shapes memory B cell recall response to influenza vaccination. *JCI Insight* **5**, (2020).

187. S. E. Hensley *et al.*, Hemagglutinin receptor binding avidity drives influenza A virus antigenic drift. *Science* **326**, 734-736 (2009).

188. C. Gerdil, The annual production cycle for influenza vaccine. *Vaccine* **21**, 1776-1779 (2003).

189. H. Jacobsen *et al.*, Influenza Virus Hemagglutinin Stalk-Specific Antibodies in Human Serum are a Surrogate Marker for In Vivo Protection in a Serum Transfer Mouse Challenge Model. *mBio* **8**, (2017).

190. D. C. Ekiert *et al.*, Antibody recognition of a highly conserved influenza virus epitope. *Science* **324**, 246-251 (2009).

191. D. C. Ekiert *et al.*, A highly conserved neutralizing epitope on group 2 influenza A viruses. *Science* **333**, 843-850 (2011).

192. T. J. Wohlbold *et al.*, Hemagglutinin Stalk- and Neuraminidase-Specific Monoclonal Antibodies Protect against Lethal H10N8 Influenza Virus Infection in Mice. *J Virol* **90**, 851-861 (2016).

193. D. Stadlbauer *et al.*, Broadly protective human antibodies that target the active site of influenza virus neuraminidase. *Science* **366**, 499-504 (2019).

194. H. E. Maier *et al.*, Pre-existing anti-neuraminidase antibodies are associated with shortened duration of influenza A (H1N1)pdm virus shedding and illness in naturally infected adults. *Clin Infect Dis*, (2019).

195. S. Ng *et al.*, Novel correlates of protection against pandemic H1N1 influenza A virus infection. *Nat Med* **25**, 962-967 (2019).

196. R. B. Couch *et al.*, Antibody correlates and predictors of immunity to naturally occurring influenza in humans and the importance of antibody to the neuraminidase. *J Infect Dis* **207**, 974-981 (2013).

197. A. S. Monto *et al.*, Antibody to Influenza Virus Neuraminidase: An Independent Correlate of Protection. *J Infect Dis* **212**, 1191-1199 (2015).

198. M. J. Memoli *et al.*, Evaluation of Antihemagglutinin and Antineuraminidase Antibodies as Correlates of Protection in an Influenza A/H1N1 Virus Healthy Human Challenge Model. *MBio* **7**, e00417-00416 (2016).

199. Y. Fujimoto *et al.*, Cross-protective potential of anti-nucleoprotein human monoclonal antibodies against lethal influenza A virus infection. *J Gen Virol* **97**, 2104-2116 (2016).

200. K. A. Richards, J. J. Treanor, J. L. Nayak, A. J. Sant, Overarching Immunodominance Patterns and Substantial Diversity in Specificity and Functionality in the Circulating Human Influenza A and B Virus-Specific CD4+ T-Cell Repertoire. *J Infect Dis* **218**, 1169-1174 (2018).

201. R. Nachbagauer *et al.*, Defining the antibody cross-reactome directed against the influenza virus surface glycoproteins. *Nat Immunol* **18**, 464-473 (2017).

202. B. L. Tesini *et al.*, Broad Hemagglutinin-Specific Memory B Cell Expansion by Seasonal Influenza Virus Infection Reflects Early-Life Imprinting and Adaptation to the Infecting Virus. *J Virol* **93**, (2019).

203. S. Ranjeva *et al.*, Age-specific differences in the dynamics of protective immunity to influenza. *Nat Commun* **10**, 1660 (2019).

204. S. Ng *et al.*, Novel correlates of protection against pandemic H1N1 influenza A virus infection. *Nat Med*, (2019).

205. J. Lee *et al.*, Persistent Antibody Clonotypes Dominate the Serum Response to Influenza over Multiple Years and Repeated Vaccinations. *Cell Host Microbe* **25**, 367-376 e365 (2019).

206. B. R. Murphy, J. A. Kasel, R. M. Chanock, Association of serum anti-neuraminidase antibody with resistance to influenza in man. *N Engl J Med* **286**, 1329-1332 (1972).

207. W. He *et al.*, Broadly neutralizing anti-influenza virus antibodies: enhancement of neutralizing potency in polyclonal mixtures and IgA backbones. *J Virol* **89**, 3610-3618 (2015).

208. F. Krammer, N. Pica, R. Hai, I. Margine, P. Palese, Chimeric hemagglutinin influenza virus vaccine constructs elicit broadly protective stalk-specific antibodies. *J Virol* **87**, 6542-6550 (2013).

209. T. J. Wohlbold *et al.*, Vaccination with adjuvanted recombinant neuraminidase induces broad heterologous, but not heterosubtypic, cross-protection against influenza virus infection in mice. *mBio* **6**, e02556 (2015).

210. K. Smith *et al.*, Rapid generation of fully human monoclonal antibodies specific to a vaccinating antigen. *Nat Protoc* **4**, 372-384 (2009).

211. K. B. Westgeest *et al.*, Optimization of an enzyme-linked lectin assay suitable for rapid antigenic characterization of the neuraminidase of human influenza A(H3N2) viruses. *J Virol Methods* **217**, 55-63 (2015).

212. H. L. Dugan *et al.*, Profiling B cell immunodominance after SARS-CoV-2 infection reveals antibody evolution to non-neutralizing viral targets. *Immunity*.

213. X. Chen *et al.*, Human monoclonal antibodies block the binding of SARS-CoV-2 spike protein to angiotensin converting enzyme 2 receptor. *Cell Mol Immunol* **17**, 647-649 (2020).

214. C. Yi *et al.*, Key residues of the receptor binding motif in the spike protein of SARS-CoV-2 that interact with ACE2 and neutralizing antibodies. *Cell Mol Immunol* **17**, 621-630 (2020).

215. J. M. Dan *et al.*, Immunological memory to SARS-CoV-2 assessed for up to 8 months after infection. *Science*, (2021).

216. G. E. Hartley *et al.*, Rapid generation of durable B cell memory to SARS-CoV-2 spike and nucleocapsid proteins in COVID-19 and convalescence. *Sci Immunol* **5**, (2020).

217. V. A. Sosa-Hernandez *et al.*, B Cell Subsets as Severity-Associated Signatures in COVID-19 Patients. *Front Immunol* **11**, 611004 (2020).

218. B. Liu *et al.*, An entropy-based metric for assessing the purity of single cell populations. *Nat Commun* **11**, 3155 (2020).

219. A. Itoh-Nakadai *et al.*, The transcription repressors Bach2 and Bach1 promote B cell development by repressing the myeloid program. *Nat Immunol* **15**, 1171-1180 (2014).

220. J. B. Moroney, A. Vasudev, A. Pertsemlidis, H. Zan, P. Casali, Integrative transcriptome and chromatin landscape analysis reveals distinct epigenetic regulations in human memory B cells. *Nat Commun* **11**, 5435 (2020).

221. T. Patzelt *et al.*, Foxp1 controls mature B cell survival and the development of follicular and B-1 B cells. *Proc Natl Acad Sci U S A* **115**, 3120-3125 (2018).

222. M. Uhlen *et al.*, Proteomics. Tissue-based map of the human proteome. *Science* **347**, 1260419 (2015).

223. M. J. Frank *et al.*, Expression of sprouty2 inhibits B-cell proliferation and is epigenetically silenced in mouse and human B-cell lymphomas. *Blood* **113**, 2478-2487 (2009).

224. J. W. Said *et al.*, TCL1 oncogene expression in B cell subsets from lymphoid hyperplasia and distinct classes of B cell lymphoma. *Lab Invest* **81**, 555-564 (2001).

225. S. Axelsson *et al.*, A combination of the activation marker CD86 and the immune checkpoint marker B and T lymphocyte attenuator (BTLA) indicates a putative permissive activation state of B cell subtypes in healthy blood donors independent of age and sex. *BMC Immunol* **21**, 14 (2020).

226. J. Muller-Winkler *et al.*, Critical requirement for BCR, BAFF, and BAFFR in memory B cell survival. *J Exp Med* **218**, (2021).

227. C. C. Kim, A. M. Baccarella, A. Bayat, M. Pepper, M. F. Fontana, FCRL5(+) Memory B Cells Exhibit Robust Recall Responses. *Cell Rep* **27**, 1446-1460 e1444 (2019).

228. O. Dienz *et al.*, The induction of antibody production by IL-6 is indirectly mediated by IL-21 produced by CD4+ T cells. *J Exp Med* **206**, 69-78 (2009).

229. F. Schena *et al.*, Dependence of immunoglobulin class switch recombination in B cells on vesicular release of ATP and CD73 ectonucleotidase activity. *Cell Rep* **3**, 1824-1831 (2013).

230. T. Scholzen, J. Gerdes, The Ki-67 protein: from the known and the unknown. *J Cell Physiol* **182**, 311-322 (2000).

231. K. Basso *et al.*, Tracking CD40 signaling during germinal center development. *Blood* **104**, 4088-4096 (2004).

232. L. Krzyzak *et al.*, CD83 Modulates B Cell Activation and Germinal Center Responses. *J Immunol* **196**, 3581-3594 (2016).

233. M. Wohner *et al.*, Molecular functions of the transcription factors E2A and E2-2 in controlling germinal center B cell and plasma cell development. *J Exp Med* **213**, 1201-1221 (2016).

234. E. Gallagher *et al.*, Kinase MEKK1 is required for CD40-dependent activation of the kinases Jnk and p38, germinal center formation, B cell proliferation and antibody production. *Nat Immunol* **8**, 57-63 (2007).

235. K. G. Smith, G. J. Nossal, D. M. Tarlinton, FAS is highly expressed in the germinal center but is not required for regulation of the B-cell response to antigen. *Proc Natl Acad Sci U S A* **92**, 11628-11632 (1995).

236. M. Descatoire *et al.*, Identification of a human splenic marginal zone B cell precursor with NOTCH2-dependent differentiation properties. *J Exp Med* **211**, 987-1000 (2014).

237. T. L. Rothstein, D. O. Griffin, N. E. Holodick, T. D. Quach, H. Kaku, Human B-1 cells take the stage. *Ann N Y Acad Sci* **1285**, 97-114 (2013).

238. A. Macias-Garcia *et al.*, Ikaros Is a Negative Regulator of B1 Cell Development and Function. *J Biol Chem* **291**, 9073-9086 (2016).

239. K. Ochiai *et al.*, Chromatin Protein PC4 Orchestrates B Cell Differentiation by Collaborating with IKAROS and IRF4. *Cell Rep* **33**, 108517 (2020).

240. M. Villa *et al.*, Aryl hydrocarbon receptor is required for optimal B-cell proliferation. *EMBO J* **36**, 116-128 (2017).

241. N. A. Mabbott, D. Gray, Identification of co-expressed gene signatures in mouse B1, marginal zone and B2 B-cell populations. *Immunology* **141**, 79-95 (2014).

242. C. R. Smulski, H. Eibel, BAFF and BAFF-Receptor in B Cell Selection and Survival. *Front Immunol* **9**, 2285 (2018).

243. F. Chen, N. Tzarum, I. A. Wilson, M. Law, VH1-69 antiviral broadly neutralizing antibodies: genetics, structures, and relevance to rational vaccine design. *Curr Opin Virol* **34**, 149-159 (2019).

244. C. Atyeo *et al.*, Distinct Early Serological Signatures Track with SARS-CoV-2 Survival. *Immunity*, (2020).

245. N. Le Bert *et al.*, SARS-CoV-2-specific T cell immunity in cases of COVID-19 and SARS, and uninfected controls. *Nature* **584**, 457-462 (2020).

246. Y. Peng *et al.*, Broad and strong memory CD4(+) and CD8(+) T cells induced by SARS-CoV-2 in UK convalescent individuals following COVID-19. *Nat Immunol*, (2020).

247. H. Yao *et al.*, Molecular Architecture of the SARS-CoV-2 Virus. *Cell* **183**, 730-738 e713 (2020).

248. S. Lu *et al.*, The SARS-CoV-2 nucleocapsid phosphoprotein forms mutually exclusive condensates with RNA and the membrane-associated M protein. *Nat Commun* **12**, 502 (2021).

249. F. Amanat *et al.*, A serological assay to detect SARS-CoV-2 seroconversion in humans. *medRxiv*, (2020).

250. D. Stadlbauer *et al.*, SARS-CoV-2 Seroconversion in Humans: A Detailed Protocol for a Serological Assay, Antigen Production, and Test Setup. *Curr Protoc Microbiol* **57**, e100 (2020).

251. C. A. Nelson, A. Pekosz, C. A. Lee, M. S. Diamond, D. H. Fremont, Structure and intracellular targeting of the SARS-coronavirus Orf7a accessory protein. *Structure* **13**, 75-85 (2005).

252. C. A. Nelson, C. A. Lee, D. H. Fremont, Oxidative refolding from inclusion bodies. *Methods Mol Biol* **1140**, 145-157 (2014).

253. T. Stuart *et al.*, Comprehensive Integration of Single-Cell Data. *Cell* **177**, 1888-1902 e1821 (2019).

254. J. J. Bunker *et al.*, Natural polyreactive IgA antibodies coat the intestinal microbiota. *Science* **358**, (2017).

255. J. J. Guthmiller *et al.*, Polyreactive Broadly Neutralizing B cells Are Selected to Provide Defense against Pandemic Threat Influenza Viruses. *Immunity* **53**, 1230-1244 e1235 (2020).

256. M. J. Shlomchik, A. H. Aucoin, D. S. Pisetsky, M. G. Weigert, Structure and function of anti-DNA autoantibodies derived from a single autoimmune mouse. *Proc Natl Acad Sci U S A* **84**, 9150-9154 (1987).

257. E. S. Winkler *et al.*, Publisher Correction: SARS-CoV-2 infection of human ACE2-transgenic mice causes severe lung inflammation and impaired function. *Nat Immunol* **21**, 1470 (2020).

258. C. P. Arevalo *et al.*, Original antigenic sin priming of influenza virus hemagglutinin stalk antibodies. *Proc Natl Acad Sci U S A* **117**, 17221-17227 (2020).

259. S. Gouma *et al.*, Middle-aged individuals may be in a perpetual state of H3N2 influenza virus susceptibility. *Nat Commun* **11**, 4566 (2020).

260. K. R. McCarthy *et al.*, Memory B Cells that Cross-React with Group 1 and Group 2 Influenza A Viruses Are Abundant in Adult Human Repertoires. *Immunity* **48**, 174-184 e179 (2018).

261. C. A. DiazGranados *et al.*, High-dose trivalent influenza vaccine compared to standard dose vaccine in elderly adults: safety, immunogenicity and relative efficacy during the 2009-2010 season. *Vaccine* **31**, 861-866 (2013).

262. P. Tsang *et al.*, Immunogenicity and safety of Fluzone((R)) intradermal and high-dose influenza vaccines in older adults >/=65 years of age: a randomized, controlled, phase II trial. *Vaccine* **32**, 2507-2517 (2014).

263. H. M. Yassine *et al.*, Hemagglutinin-stem nanoparticles generate heterosubtypic influenza protection. *Nat Med* **21**, 1065-1070 (2015).

264. D. M. Carter *et al.*, Design and Characterization of a Computationally Optimized Broadly Reactive Hemagglutinin Vaccine for H1N1 Influenza Viruses. *J Virol* **90**, 4720-4734 (2016).

265. B. M. Giles *et al.*, A computationally optimized hemagglutinin virus-like particle vaccine elicits broadly reactive antibodies that protect nonhuman primates from H5N1 infection. *J Infect Dis* **205**, 1562-1570 (2012).

266. T. M. Wong *et al.*, Computationally Optimized Broadly Reactive Hemagglutinin Elicits Hemagglutination Inhibition Antibodies against a Panel of H3N2 Influenza Virus Cocirculating Variants. *J Virol* **91**, (2017).

267. S. Boyoglu-Barnum *et al.*, Quadrivalent influenza nanoparticle vaccines induce broad protection. *Nature*, (2021).

268. V. Shinde *et al.*, Improved Titers against Influenza Drift Variants with a Nanoparticle Vaccine. *N Engl J Med* **378**, 2346-2348 (2018).

269. E. J. Erbelding *et al.*, A Universal Influenza Vaccine: The Strategic Plan for the National Institute of Allergy and Infectious Diseases. *J Infect Dis* **218**, 347-354 (2018).

270. Y. Kato *et al.*, Multifaceted Effects of Antigen Valency on B Cell Response Composition and Differentiation In Vivo. *Immunity* **53**, 548-563 e548 (2020).

271. H. G. Kelly *et al.*, Self-assembling influenza nanoparticle vaccines drive extended germinal center activity and memory B cell maturation. *JCI Insight* **5**, (2020).

272. M. Sangesland, D. Lingwood, Antibody Focusing to Conserved Sites of Vulnerability: The Immunological Pathways for 'Universal' Influenza Vaccines. *Vaccines (Basel)* **9**, (2021).

273. M. Worobey, S. Plotkin, S. E. Hensley, Influenza Vaccines Delivered in Early Childhood Could Turn Antigenic Sin into Antigenic Blessings. *Cold Spring Harb Perspect Med* **10**, (2020).

274. P. Meade *et al.*, Influenza Virus Infection Induces a Narrow Antibody Response in Children but a Broad Recall Response in Adults. *mBio* **11**, (2020).

275. R. B. Belshe *et al.*, Live attenuated versus inactivated influenza vaccine in infants and young children. *N Engl J Med* **356**, 685-696 (2007).

276. C. S. Ambrose, M. J. Levin, R. B. Belshe, The relative efficacy of trivalent live attenuated and inactivated influenza vaccines in children and adults. *Influenza Other Respir Viruses* **5**, 67-75 (2011).

277. I. Shannon, C. L. White, J. L. Nayak, Understanding Immunity in Children Vaccinated With Live Attenuated Influenza Vaccine. *J Pediatric Infect Dis Soc* **9**, S10-S14 (2020).

278. S. Sasaki *et al.*, Comparison of the influenza virus-specific effector and memory B-cell responses to immunization of children and adults with live attenuated or inactivated influenza virus vaccines. *J Virol* **81**, 215-228 (2007).

279. I. Shannon, C. L. White, H. Yang, J. L. Nayak, Differences in influenza-specific CD4 T cell mediated immunity following acute infection versus inactivated vaccination in children. *J Infect Dis*, (2020).

280. S. Duchene *et al.*, Temporal signal and the phylodynamic threshold of SARS-CoV-2. *Virus Evol* **6**, veaa061 (2020).

281. F. Robson *et al.*, Coronavirus RNA Proofreading: Molecular Basis and Therapeutic Targeting. *Mol Cell* **80**, 1136-1138 (2020).

282. S. E. Galloway *et al.*, Emergence of SARS-CoV-2 B.1.1.7 Lineage - United States, December 29, 2020-January 12, 2021. *MMWR Morb Mortal Wkly Rep* **70**, 95-99 (2021).

283. L. Yurkovetskiy *et al.*, Structural and Functional Analysis of the D614G SARS-CoV-2 Spike Protein Variant. *Cell* **183**, 739-751 e738 (2020).

284. M. H. S. Paiva *et al.*, Multiple Introductions Followed by Ongoing Community Spread of SARS-CoV-2 at One of the Largest Metropolitan Areas of Northeast Brazil. *Viruses* **12**, (2020).

285. T. Burki, Understanding variants of SARS-CoV-2. *Lancet* **397**, 462 (2021).

286. B. Korber *et al.*, Tracking Changes in SARS-CoV-2 Spike: Evidence that D614G Increases Infectivity of the COVID-19 Virus. *Cell* **182**, 812-827 e819 (2020).

287. B. Zhou *et al.*, SARS-CoV-2 spike D614G variant confers enhanced replication and transmissibility. *bioRxiv*, (2020).

288. Y. J. Hou *et al.*, SARS-CoV-2 D614G variant exhibits efficient replication ex vivo and transmission in vivo. *Science* **370**, 1464-1468 (2020).

289. C. S. Kow, S. S. Hasan, Could it be that the B.1.1.7 lineage is more deadly? *Infect Control Hosp Epidemiol*, 1 (2021).

290. H. Liu *et al.*, The basis of a more contagious 501Y.V1 variant of SARS-COV-2. *bioRxiv*, (2021).

291. E. C. Sabino *et al.*, Resurgence of COVID-19 in Manaus, Brazil, despite high seroprevalence. *Lancet* **397**, 452-455 (2021).

292. W. F. Garcia-Beltran *et al.*, Multiple SARS-CoV-2 variants escape neutralization by vaccine-induced humoral immunity. *Cell*, (2021).

293. L. Stamatatos *et al.*, mRNA vaccination boosts cross-variant neutralizing antibodies elicited by SARS-CoV-2 infection. *Science*, (2021).

294. P. Supasa *et al.*, Reduced neutralization of SARS-CoV-2 B.1.1.7 variant by convalescent and vaccine sera. *Cell*, (2021).

295. N. L. Kallewaard *et al.*, Structure and Function Analysis of an Antibody Recognizing All Influenza A Subtypes. *Cell* **166**, 596-608 (2016).

296. L. B. King, J. C. Milligan, B. R. West, S. L. Schendel, E. Ollmann Saphire, Achieving cross-reactivity with pan-ebolavirus antibodies. *Curr Opin Virol* **34**, 140-148 (2019).

297. K. E. Stephenson, K. Wagh, B. Korber, D. H. Barouch, Vaccines and Broadly Neutralizing Antibodies for HIV-1 Prevention. *Annu Rev Immunol* **38**, 673-703 (2020).

298. T. N. Starr *et al.*, Prospective mapping of viral mutations that escape antibodies used to treat COVID-19. *Science* **371**, 850-854 (2021).

299. Y. Weisblum *et al.*, Escape from neutralizing antibodies by SARS-CoV-2 spike protein variants. *Elife* **9**, (2020).

300. R. E. Chen *et al.*, Resistance of SARS-CoV-2 variants to neutralization by monoclonal and serum-derived polyclonal antibodies. *Nat Med* **27**, 717-726 (2021).

301. L. Vangelista, M. Secchi, Prepare for the Future: Dissecting the Spike to Seek Broadly Neutralizing Antibodies and Universal Vaccine for Pandemic Coronaviruses. *Front Mol Biosci* **7**, 226 (2020).

302. C. O. Barnes *et al.*, SARS-CoV-2 neutralizing antibody structures inform therapeutic strategies. *Nature* **588**, 682-687 (2020).